DRYING INDUCED CHANGE IN MOLECULAR INTERACTION BETWEEN COAL AND WATER

by

Koyo NORINAGA

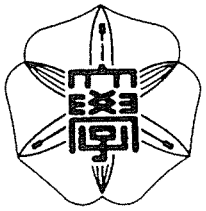

Thesis Submitted to the Graduate School of Engineering
for the Degree of Doctor of Engineering

Hokkaido University

March, 1999

CONTENTS

CHAPTER 1

General Introduction

1.1. BACKGROUND

Lignite or brown coal which generally has a moisture content between 30 and 70%, a low heat value (as mined) from about 6 to 16 MJ/kg and a higher oxygen content than bituminous coals. Lignites also tend to have a higher volatiles content. Substantial quantities of lignite and brown coal occur near the surface in the many parts of the world where it can provide a low-cost fuel and raw material. The details of the deposit are shown in Table 1.1.[12] The countries with the biggest reserves are Russia, Australia, Germany, and America. In addition, there are substantial reserves in other parts of eastern Europe. Countries with important reserves include Greece, Turkey and India.

In the context of this thesis, the words lignite and brown coal are used interchangeably, based on principally on the common usage in the country being referred to. Over 70% of lignite is used for power generation. It is generally regarded as uneconomic to transport lignite over long distances because of the high moisture content and hence low specific energy content. In Figure 1.2,[3] lower heat value, LHV and moisture content of coals of various ranks are given. In order to utilize lignite as a fuel with a higher specific energy or calorific value, water must be removed. So far, a considerable amount of research and development effort have been directed to the study on the drying of lignite owing to not only interest but also to practical importance. In the following section, the fundamental studies are briefly reviewed with restricting the attention to the works that seem to be auxiliary to the development of the present study.

1.2. REVIEW OF PREVIOUS STUDIES

1.2.1. Water in coal

Allardice and Evans[4, 5] constructed isotherms relating the equilibrium moisture content and the water vapor pressure, up to the saturation water vapor pressure at the isotherm temperature for a Yallourn brown coal by a vacuum microbalance method. They determined desorption isotherm starting with a bed moist coal while adsorption (or readosorption) is determined from the dry coal state. As illustrated in Figure 1.2, the shape of the isotherm is sigmoid. The sigmoid isotherm were generally observed for water sorption on coals over a wide range of ranks.[6-8] More generally, the sigmoid isotherm shape is also typical of physical adsorption of condensable vapors on porous adsorbents.[9] The generally accepted interpretation of sigmoid shaped isotherms with water as sorbate is as follows:

(i) The water removed at close to the saturation vapor pressure (above 0.96 p/p_0) in the nearly vertical part of the isotherm is free or bulk water admixed with the coal and contained in macropores and interparticles.

(ii) In the convex part of the curve from about 0.96 to 0.5 p/p_0 the water is desorbed from capillaries, and the depression in vapor pressure can be explained by a capillary meniscus effect.

(iii) Below relative vapor pressures of 0.5, the Kelvin equation[10] predicts pore sizes in the order of a few molecular diameters, and the concept of a meniscus loses its meaning. In this region desorption is attributed to the loss of water sorbed from multilayers on the walls of the pores. The monolayer sorption occurs in the region below the "knee" in the isotherm (below about 0.1 p/p_0) and multilayer sorption on top of the monolayer in the nearly linear region above this "knee".

The equilibrium isosteres, i.e., curves showing the variation of vapor pressure with temperature at constant moisture content were constructed based on the measurements of isotherms at several temperatures (303 - 333 K).[5] Application of the Clausius-Clapeyron equation to the isosteres permits the isosteric heat of sorption of water on the coal at any particular moisture content as illustrated in Figure 1.3. In the bulk and capillary water regions,

the isosteric heat of sorption of water is equivalent to the latent heat of condensation of bulk water (2.43 MJ/kg). The heat of sorption increases progressively up to 3.4 MJ/kg over the multilayer and monolayer regions, which is of the order expected for hydrogen bonding of water in the monolayer. This pattern of behavior has also been reported for other types of coals.[6, 11] Table 1.2 compares the characteristics of the water sorbed in the different regions of the sorption isotherms described above for Yallourn brown coal.[5, 12] It can be seem that most of the water in the bed moist coal has the properties of normal liquid water even in the interparticles and capillaries, without complex bonding mechanism. The bonding of the water in the monolayer is discussed by several workers. The monolayer capacities can be quantified by applying the BET equation[13] to the isotherm. Iyengar and Lahiri[14] demonstrated that the water in the sorbed monolayer on coals is bonded to hydrophilic sites on the coal surface. These sites were identified as oxygen-containing functional groups. This has been confirmed for a wide range of coal ranks.[6, 15, 16] The values of the isosteric heats of sorption for water on brown coals indicate that the attachment to the hydrophilic sites is via hydrogen bonds. Mazumdar et al.[17] noted that the acetylation of low rank coals resulted in a decrease in the water content proportional to the extent of acetylation of hydroxyl groups. It was postulated that the monolayer capacity provides an indication of the number of hydrophilic sites on the surface and not the physical extent of the surface.[14] An indication of the proportion of the physical surface covered by the hydrophilic sites can be obtained by assuming that the water molecules in the monolayer have cross-sectional areas equivalent to the packing density in normal liquid water, and comparing the area occupied by the monolayer water with the total internal surface area determined by physical adsorption of carbon dioxide. Mahajan and Walker[6] showed in this way that the proportion of the internal surface areas occupied by hydrophilic sites increased with decreasing coal rank, from 12% for a low volatile bituminous coal to 60% for a high volatile bituminous coal. Extending this approach to Yallourn brown coal, water sorption isotherms gave a water monolayer area of 280 m^2/g while carbon dioxide areas for a suite of Yallourn coals averaged 260 m^2/g indicating that in these low rank coals, the surface is essentially

completely covered by hydrophilic sites.

Schafer[15] showed that for a range of eleven low rank coals, the carboxylic acid groups, particularly in the carboxylate salt form, were the most important hydrophilic site, with the phenolic hydroxyl having a lesser effect. He also established through controlled ion exchange that the cations associated with the carboxylate groups contribute to the hydrophilic character of the coal in the order $Fe^{++} > Mg^{++} > Ca^{++} > Cu^{++} > Ba^{++} > Al^{+++} > = Fe^{+++} = Na^{+} > K^{+}$, which approximately parallels the degree of hydration of the cation in aqueous solution.

A significant feature of the isotherms for brown coals in the substantial hysteresis observed between the adsorption and desorption curves, which persists to very low relative vapor pressures. The desorption curve always follows a higher trajectory than the adsorption curve, as illustrated in Figure 1.2. At relative vapor pressures above 0.5, the hysteresis can be explained by the normal capillary condensation mechanism with vapor pressure lowering according to the Kelvin equation.[18] It is generally attributed to a difference in adsorption and desorption mechanisms, associated with swelling and shrinkage effects, and the irreversible collapse of capillaries on drying. The subject on the irreversible nature of brown coal will be discussed in the next section. However, there is still no generally accepted mechanism to explain the persistence of the hysteresis loop in the multilayer and monolayer region of the isotherms.

There have been some results to support that the water in coal can be distinguished into two major types, namely freezable and nonfreezable waters based on the freezing or melting characteristics of water. The former is identical to bulk or surface water and the latter is represented by pore water. Mraw and O'Rourke measured the low temperature heat capacity of naturally occurring water in Wyodak coal.[19, 20] They found more than two thirds is nonfreezable and the remainder is freezable water which is indicative of a phase transition. Vorres et al.[21, 22] measured the drying kinetics of a lignite and subbitunimous coals at several isothermal temperatures. They found that there are two segments in the dehydration kinetics; the first includes about 80-85% of the water loss and the second involves most of the remaining

water and concluded the initial water loss corresponds to freezable water, while the later loss corresponds to nonfreezable water. Wroblewski et al.[23] measured the time-dependent extraction of water in the presence of a large excess of five polar solvents and some reagents by means of ^{31}P-NMR. They found that 89% of the water extracted from Beulah Zap lignite by dioxane or dimetoxyethane within 15 min and termed this fraction of water as 'very loosely bound (surface) water'.

Liquid-solid transition accompanies with both the release of latent heat and the freezing of molecular mobilities. The former can be detected by calorimetric measurement and the latter by proton nuclear magnetic (^{1}H NMR) resonance spectroscopy. Mraw and O'Rourke[20] measured low temperature heat capacities of three coals in rank from lignite to bituminous and porous ceramic which were prepared to have different water content. They found that the fusion enthalpies of absorbed water in subbitunimous coal and lignite varied with water content, while that in ceramic having relatively narrow range of pore diameter from 4.5 nm to 6.0 nm could be represented a value of 234 J/g. Then they concluded that the differential enthalpy of fusion had directly reflect pore size distributions of the particular absorbent. The freezing point temperature and congelation (or fusion) enthalpy depend on the size of space which they are condensed and they are not observed when the size is smaller than a critical value.[24] The distribution of water types elucidated by DSC may give informations on the size distribution of assemblies of water molecules.

The NMR spin-spin relaxation can distinguish molecular structures/lattices on the basis of whether the molecular reorientation rates are below or above $\sim 10^5$ Hz.[25] Such molecular structures are termed rigid or mobile, respectively. The molecular reorientation rates of ice are of the order of 10^5 Hz,[26] which means that ice is considered to be a rigid structure in the NMR sense, whereas liquid water is characterized by molecular reorientation rates of $\sim 10^{10}$ Hz.[27] Therefore, the freezing of free and bound waters is expected to be detected in proton NMR relaxation measurements as mobile protons represented by exponential decays changing into "rigid protons" with

Gaussian decays. NMR has been adopted to determine the water content in coals.[28-32] Lynch et al.[33-37] measured the freezing and melting properties of water in coal by ^{1}H NMR. These works confirmed that the most of the water (that above about 0.25 kg/kg dry coal) in Yallourn brown coal is mobile at temperatures above 273 K and not bonded to the coal surface. Below 0.25 kg/kg of dry coal, the water interacts with the coal surface, occupying a continuous distribution of state rather than physically discrete classes. The properties of the water vary with changes in moisture content below 0.25 kg/kg.

1.2.2. Effect of drying on physical structure of coal

During desorption of water from the bed moist state the coals shrink and on readsorption of water they swell. When dried coals re-exposed to water it swells but it does not regain its original volume.[38, 39] Evans[40] examined the change in volume of the cylindrical lumps of Yallourn brown coal with drying. (Figure 1.4) It was shown that the initial stages of drying, water is removed from the macropores and owing to the rigidity of the coalified vegetable macrostructure little shrinkage occurs, i.e., rapid development of macroporosity results. As more water is removed the shrinkage increases; in the capillary water region the differential shrinkage rises from about 0.7 to 1.9 cm^3/cm^3. As the pore diameter decreases water removal results in pore collapse and at a diameter of about 30 nm the volumetric shrinkages equal to the volume of water removed. In the multilayer water region the differential shrinkage apparently shows maximum value, i.e. the colloidal gel collapses. It was reasoned that the removal of the lyosphere water permitted, shorter, stronger, hydrogen bond bridges and that these caused the structure to collapse. As the monolayer is approached the differential shrinkage drops to zero and may possibly become negative, i.e. swelling may occur in the monolayer region. The loss of monolayer water would entiled the formation of less stable linkage between coal macromolecules and thus they expanded. Deevi and Suuberg[38] examined change in volume and pore structure of four different types of lignites upon drying. The shrinkage induced by drying was always irreversible, even when drying was relatively incomplete; only ~80% of original volume

was regained upon reswelling in water. Nitrogen adsorption revealed that the drying reduced surface area and porosity in pores of radius approximately 1.5-10 nm. On the other hand the CO_2 surface area showed the opposite trend. This can be understood in terms of the different pore sizes examined by the two gases. It is likely that the transitional pores are collapsed by drying as opposed to the emptying microporosity.

Miura et al.[41] examined the interaction between brown coal and water by a combination of FTIR and DSC. They evaluated the changes in the total enthalpy including the contributions from dissociation of the hydrogen bonds between water and coal, evaporation of water, and the rearrangement of hydrogen bonds between coal macromolecules by DSC during heating up to 473 K. The enthalpy changes related to the changes of hydrogen bondings were also estimated based on the strength distributions of hydrogen bondings as evaluated by FTIR. They suggested that the importance of the rearrangement of hydrogen bonds in coal in the low water content region.

The collapse of the gel structure upon drying can limit mass transfer into the lignite matrix.[42, 43] Gorbaty[42] reported that the amount of the adsorption of nickel sulphate by subbitunimous coal reduced by drying as shown in Figure 1.5. Suuberg et al.[43] examined the effect of drying on the pyridine swellability of coal. The drying has no effects on the amount of pyridine uptake but significantly suppress the swelling rate.(Figure 1.6)

For thermal and catalytic liquefaction, several groups have examined the effects of drying on coal conversion.[21, 44-51] Some experiments have shown that drying of coal has negative impact on its conversion reactivity,[44, 46, 45] while there is also evidence to the contrary in noncatalytic liquefaction.[21] It has been indicated that drying can cause an irreversible change in the pore structure such as collapse of pores which could limit accessibility of the reacting components during liquefaction and thus limit the rate of reaction.

Table 1.1. Lignite Resources and Use World-Wide. [1, 2]

country	proved amount in place [Mt]	Recent annual production [Mt]	Quantity used for: power generation [Mt]	industry [Mt]	upgrading [Mt]	domestic [Mt]
Australia	39300	35	33	-	2	-
Austria	177	2.9	2.2	0.2	-	0.5
Bulgaria	4418	32	23.5	3.2	4.5	1.0
Canada	2839	10	9.2	0.5	-	0.3
China	126500	30	22	-	-	8
Czechoslovakia	7220	103	55	29	4	15
Germany	102000	423	295	8	120	-
Greece	5312	32.5	31.5	0.5	0.5	-
Hungary	5465	7.1	5.6	0.5	0.5	-
India	1581	7.7	6.9	-	0.8	-
Indonesia	18018	-	-	-	-	-
Italy	15	1.2	1.1	-	-	-
Japan	175	-	-	-	-	-
Mongolia	12000	4.6	2.1	-	-	2.5
New Zealand	1634	-	-	-	-	-
Poland	13200	50.4	49.3	0.6	0.3	0.2
Romania	1110	35	26.6	1.1	1.3	6.0
Russia	105000	122	76.8	24	13.8	7.4
Spain	315	17.4	17.4	-	-	-
Turkey	5292	22	12.4	2.2	0.4	7.0
UK	400	-	-	-	-	-
USA	40886	57	53.5	3.3	-	0.2
Yugoslavia	16000	65	47.2	4.3	4.3	9.2

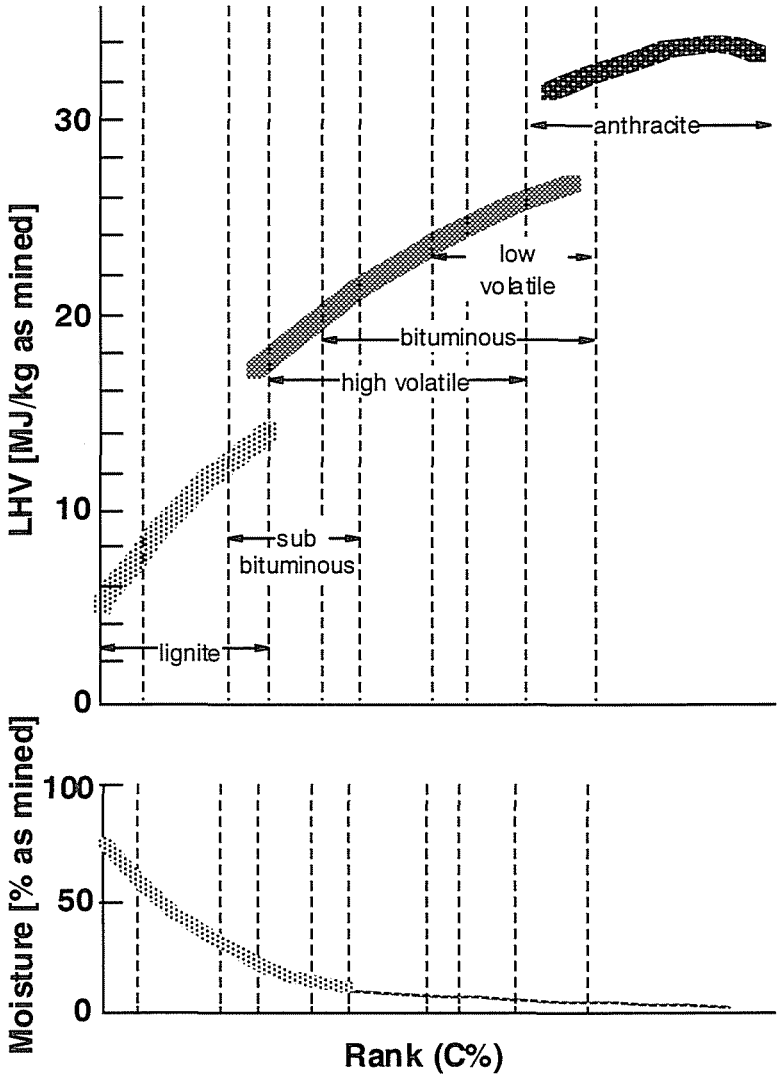

Figure 1.1. LHV and moisture content of coals of various ranks.[1]

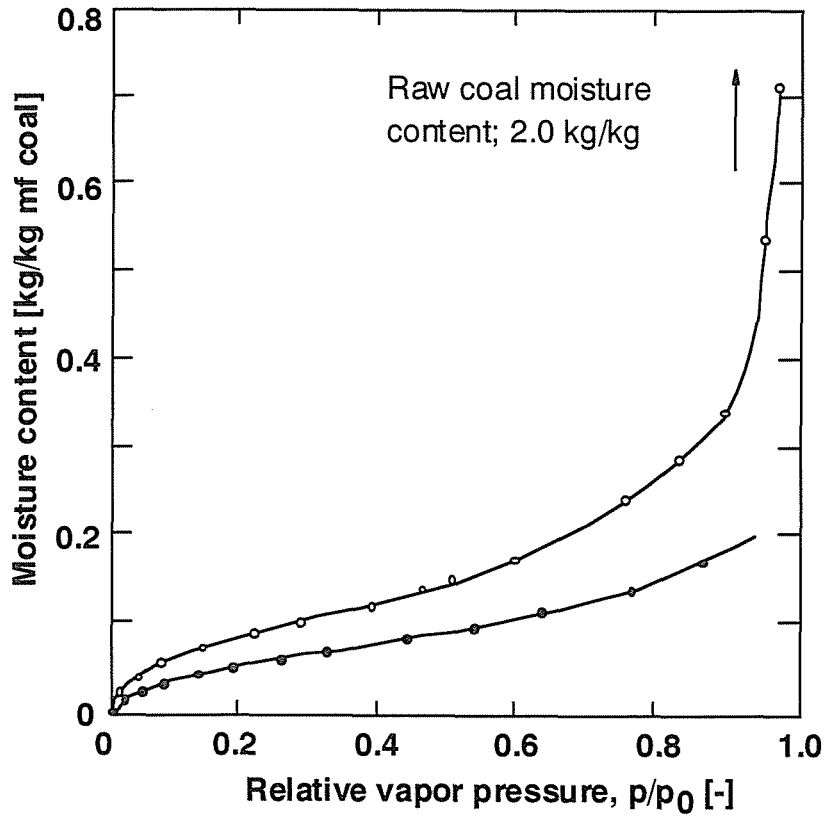

Figure 1.2. Water sorption isotherms on Yallourn brown coal at 303 K.[5]

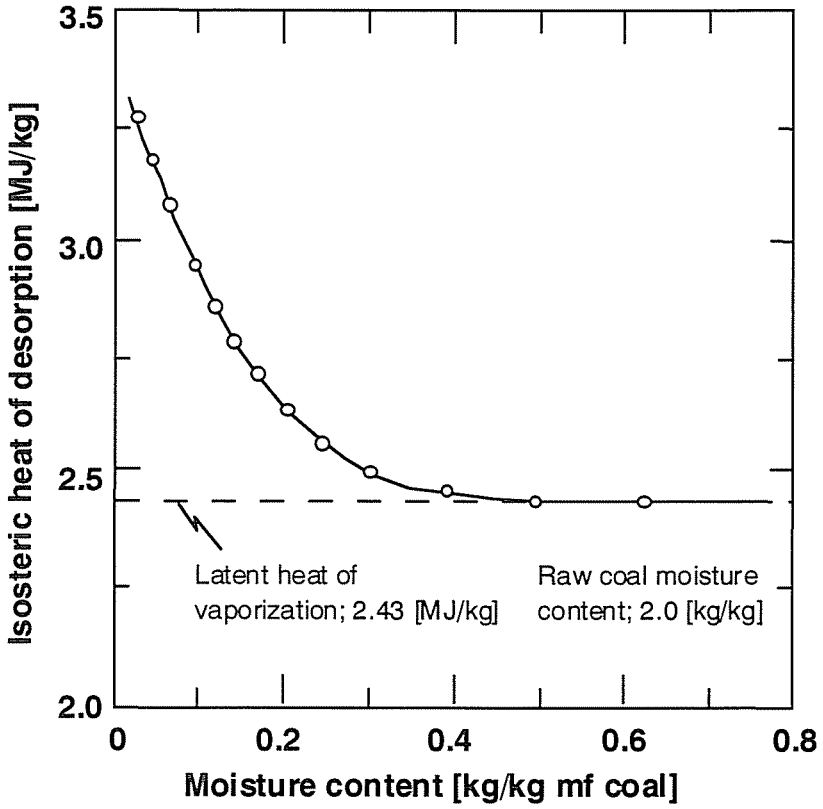

Figure 1.3. Isosteric heat of desorption of water on Yallourn brown coal as a function of moisture content.[5]

Table 1.2. Properties of Water in Yallourn Brown Coal.[12]

Water type	Moisture range of isotherm sorption regions dry coal basis [kg/kg]	Total water content of isotherm region [kg/kg]	Relative vapor pressure range [p/p_0]	Isosteric heat of desorption [MJ/kg]	Description
Bulk	2.0 to 0.725	1.275	1.0 to 0.96	2.43	Normal liquid water condensed in voids
Capillary	0.725 to 0.175	0.550	0.96 to 0.5	2.43 to 2.7	Water condensed in capillaries with slightly abnormal thermodynamics in the small capillaries
Multilayer	0.175 to 0.080	0.095	0.5 to 0.1	2.7 to 2.9	Weakly hydrogen bonded water on top of monolayer
Monolayer	0.080 to 0	0.080	0.1 to 0	2.9 to 3.4	Water hydrogen bonded to oxygen containing functional groups on the coal surface

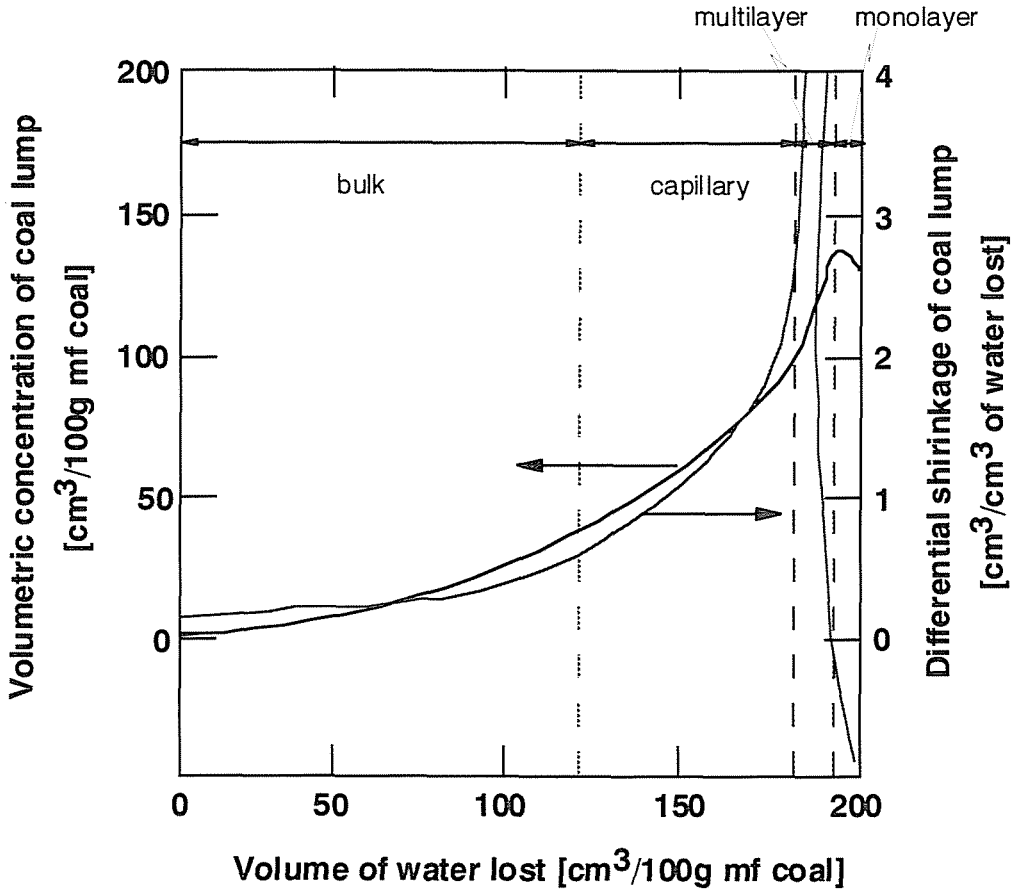

Figure 1.4. Volume losses as a function of volume of water removed from Yallourn coal.[40]

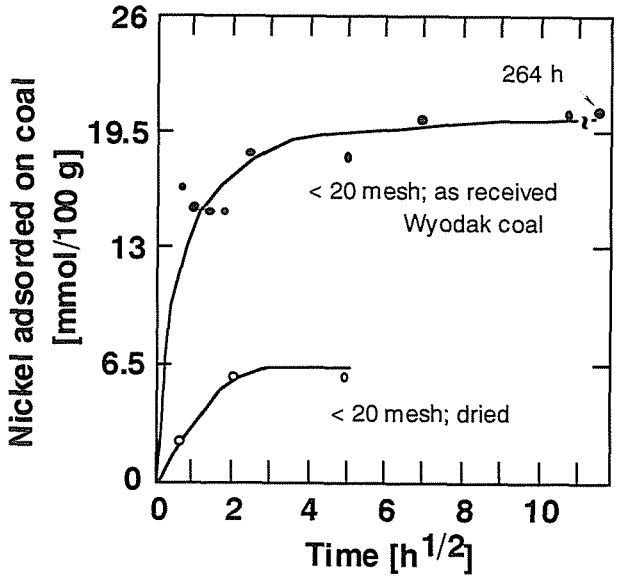

Figure 1.5. Adsorption of nickel sulphate by Wyodak coal.[42]

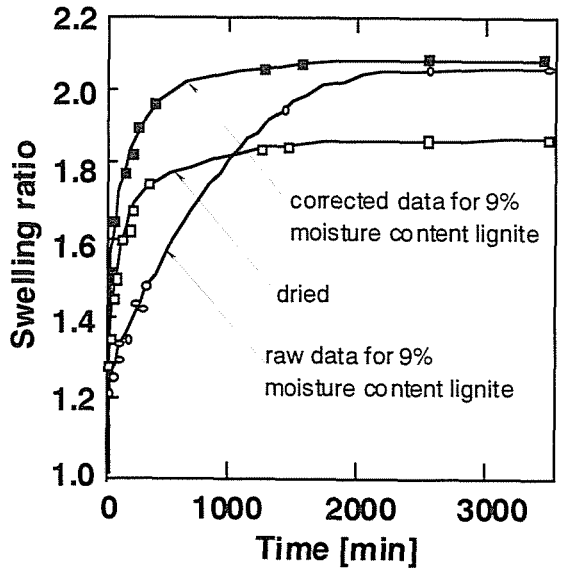

Figure 1.6. Volumetric swelling ratios in pyridine of Texas lignite at 298 K.[43]

1.3. PURPOSE AND SCOPE OF THE THESIS

Much of the relevant research in this area has been conducted on brown coals and lignites in which moisture is a major constituent as mined. The subject has been further complicated by the variety of terms used to describe the nature of the water in coal. Terms such as free, bulk, surface, equilibrium, capillary, adherent, inherent, or bound water have been used with little or no attempt at rigorous definition. Further, little effort has been made to correlate the macromolecular properties of brown coals and lignites with the nature of water therein. Although relatively much attention has been paid on the change in pore structure upon drying, the changes have seldom been characterized quantitatively. The Kelvin equation was often employed to consider what size of pores were involved in the change induced by drying. Nevertheless, the applicability of this equation below the relative vapor pressures of 0.5 is questionable because the concept of a meniscus loses its meaning where the pore sizes in the order of a few molecular diameters. The establishment of an alternative method to evaluate the pore size distributions in micro or meso pore region of moist coal should be, therefore, needed. It has been also suggested that the drying would alter the situation of noncovalent interactions in coal such as hydrogen bonding. The change in physical structure induced by drying are not explained only in terms of macroscopic phenomena such as porosity but also molecular interactions between water and coal matrix. However such molecular interactions have hardly ever been characterized experimentally. The ^{1}H NMR technique may help to determine the nature of these molecular interactions. The measured ^{1}H NMR relaxation signals can distinguish molecular structures on the basis of the molecular reorientation rates, i.e., molecular mobility.

The aims of present work are given as follows:

(1) To classify the types of water with a proper definition and to relate systematically the macromolecular structure to the properties of water therein.

(2) To establish an alternative techniques to characterize pore structure of coal quantitatively by using its containing water as a probe molecule.

(3) To evaluate the change in molecular mobility of coal macromolecules induced by drying.

The thesis is structured into six chapters and the outline of each chapter is given in the following:

CHAPTER 1: General Introduction:

A general introduction was given on lignite and brown coals. The relevant works in this area have been briefly reviewed. The purpose and construction of the present thesis were also described.

CHAPTER 2: Simulation of Interaction between a Model Molecule of Brown Coal and Water System by a Computer Aided Molecular Design Technique:

A computer aided molecular design (CAMD) technique was applied to a model molecule of brown coal and water systems. The changes in the conformation and noncovalent interaction energy during moisture release process were examined.

CHAPTER 3: Classification of Water Sorbed in Coal on the Basis of Congelation Characteristics:

Water sorbed in eight coals of different ranks was analyzed by a differential scanning calorimetry (DSC) over a temperature range from 123 to 293 K. On the basis of its congelation characteristics, the water was classified into three types; free water that is identical with bulk water, bound water that freezes at a lower temperature than free water, and non-freezable water that never freezes in the present temperature range. The contents of the free and bound waters were experimentally determined from their respective heats of congelation and the non-freezable water was then calculated by difference. The congelation of the freezable water was also observed using proton nuclear magnetic resonance (^{1}H NMR) as the conversion of the slowly-decaying into Gaussian components at 213-273 K. The fraction of freezable water as determined by the ^{1}H NMR was in good agreement with that by the DSC. The non-freezable water was also found to have some mobility and thus gave

exponential decays even at 213 K.

CHAPTER 4: Evaluation of Effect of Predrying on Porous Structure of Water Swollen Coal Based on Freezing Property of Pore Condensed Water.

The effect of the extent of pre-drying on the porous structure of water swollen coal was examined. Three kinds of as received coals (Yallourn (YL), Beulah Zap (BZ), and Illinoi #6 (IL)) were used as the samples. They were pre-dried at 303 K to different extents. Upon the pre-drying, the coal samples released water in the following order; free water identical to bulk water, bound water that froze at around 226 K, finally, nonfreezable water that never froze even at 123 K. Pre-dried samples were swollen in water at 303 K and subjected to ^{1}H NMR measurements to characterize the freezing property of water retained in pores in the temperature range from 170 to 294 K. The total volume of pores filled with water (V_p) was defined as the amount of water that was not frozen at 260 K. Removal of nonfreezable water from YL coal by the drying resulted in decrease of V_p while that of the other types of water little changed V_p. Complete pre-drying of the other coals also reduced V_p of which extent was smaller than that for YL coal. The freezing point distribution (FPD) was obtained by the NMR for pore condensed water that froze at 213 - 260 K and also numerically simulated using a Gaussian function. A modified Gibbs-Thompson equation, which relates the freezing point depression to the pore dimension, was applied to the conversion of FPD into pore size distribution (PSD) employing a cyrindrical shaped pore model. PSD was found to be in the range from 1 to 3 nm as pore radius and suggested that the reduction of V_p for YL coal was mainly owing to the collapse or shrinkage of pores with radii around 2 nm, abundant in the coal without pre-drying.

CHAPTER 6: Evaluation of Drying Induced Changes in the Molecular Mobility of Coal by Means of Pulsed Proton NMR:

Drying induced changes in the molecular properties of six different as-received coals with water contents ranging from 8 to 60 wt% of their wet

weight were investigated, on the basis of the mobility of the coal hydrogen and the distribution of different types of water. When dried at 303 K, a brown coal releases water in the following order; free water identical to bulk water, bound water that froze at around 226 K, finally, non-freezable water that never froze even at 123 K. According to ^{1}H NMR criteria, a portion of the coal hydrogen was found to be mobile. The amount of the mobile coal hydrogen (C_{MH}) varied inversely with the amount of the non-freezable water, while the release of the free and the bound water had little effect on the reduction of C_{MH} . For coals with water contents of up to 32 wt%, C_{MH} in the as-received samples agreed well with the hydroxylic hydrogen content, C_{DH}, which was determined by a hydrogen-deuterium exchange technique. However, in coals with higher water content, C_{MH} was approximately twice as great as C_{DH}.

CHAPTER 6: Summary of Findings

The results of the investigations and findings of the thesis are summarized.

References

(1) Couch, G. R. *Lignite resources and characteristics. IEA CR/13.* London, UK, IEA Coal Research **1988**.

(2) Couch, G. R. *Lignite upgrading. IEA CR/23.* London, UK, IEA Coal Research **1990**.

(3) *IEA Coal Research* **1983**.

(4) Allardice, D. J.; Evans, D. G. *Fuel* **1971**, *50*, 201.

(5) Allardice, D. J.; Evans, D. G. *Fuel* **1971**, *50*, 236.

(6) Mahajan, O. P.; Walker, P. L. *Fuel* **1971**, *50*, 308.

(7) Toei, R.; Tamon, H.; Vehara, K.; Matsumiya, S. *Ind. Eng. Chem. Process Design and Devlopment* **1986**, *25*, 168.

(8) Barton, W. A.; Mccutcheon, A. L. *Proceedings of 7th Australian Coal Conference* Gippsland, 1996, p 513.

(9) Brunauer, S.; Deming, L. S.; Deming, W. E.; Teller, E. *J. Am. Chem.Soc.* **1940**, *82*, 1723.

(10) Thompson, W. L. K. *Philos. Mag.* **1871**, *42*, 448.

(11) Staszczuk *Fuel Science Thechnology International* **1988**, *6*, 381.

(12) Allardice,D.J. *The Science of Victorian Brown Coal*; Durie, R. A., Ed.; Butterworth-Heinemann Ltd.: Oxford, 1991; p 103

(13) Brunauer, S.; Emmett, P. H.; Teller, E. *J. Am. Chem.Soc.* **1938**, *60*, 309.

(14) Iyengar, M. S.; Lahiri, A. *Fuel* **1957**, *36*, 286.

(15) Schafer, H. N. S. *Fuel* **1972**, *51*, 4.

(16) Kaji, R.; Muranaka, Y.; Otsuka, K.; Hishimuma, Y. *Fuel* **1986**, *65*, 288.

(17) Mazumdar, B. K.; Bhangale, E.; Lahiri, A. *Fuel* **1957**, *36*, 254.

(18) Lavine, I.; Gauger, A. W. *Ind. Eng. Chem.* **1930**, *22*, 1226.

(19) Mraw, S. C.; Naas-O'Rourke, D. F. *Science* **1979**, *205*, 901.

(20) Mraw, S. C.; Naas-O'Rourke, D. F. *J. Colloid Interface Sci.* **1982**, *89*, 268.

(21) Vorres, K. S.; Wertz, D. L.; Malhotra, V.; Dang, Y.; Joseph, J. T.; Fisher, R. *Fuel* **1992**, *71*, 1047.

(22) Vorres, K. S. *Energy Fuels* **1994**, *8*, 320.

(23) Wroblewski, A. E.; Reinartz, K.; Verkade, J. G. *Energy Fuels* **1991**, *5*, 786.

(24) Sheng, P.; Cohen, R. W.; Schrieffer, J. R. *J. Phys. C:Solid State Phys.* **1981**, *14*, 565.

(25) Lynch, L. J.; *Magnetic Resonance and Biology*: Cohen, J. S., Ed.: John Willey & Sons, New York, 1983, p 248.

(26) Bloembergen, N.; Purcell, E. M.; Pound, R. N. *Phys. Rev.* **1948**, *73*, 679.

(27) Krynicki, K. *Physica* **1966**, *32*, 167.

(28) Gerstein, B. C.; Chow, C.; Pembleton, R. G.; Wilson, R. C. *J. Phys. Chem.* **1977**, *81*, 565.

(29) Cutmore, N. G.; Sowerby, B. D.; Lynch, L. J.; Webster, D. S. *Fuel* **1986**, *65*, 34.

(30) Graebert, R.; Michel, D. *Fuel* **1990**, *69*, 826.

(31) Yang, X.; Garcia, A. R.; Larsen, J. W.; Silbernagel, B. G. *Energy Fuels* **1992**, *6*, 651.

(32) Rosa, L. D.; Pruski, M.; Gerstein, B. C. Quantitation of Protons in the Argonne Premium Coals by Solid State ^{1}H-NMR; In *Magnetic Resonance in Carbonaceous Solids*; Botto, C. E., Sanada, Y., Eds.; Advances in Chemistry; American Chemical Society: Washington, DC, **1993**, *229*, 359.

(33) Lynch, L. J.; Webster, D. S. *Fuel* **1979**, *58*, 429.

(34) Lynch, L. J.; Webster, D. S. *J. Magn. Reson.* **1980**, *40*, 259.

(35) Lynch, L. J.; Webster, D. S. *Fuel* **1982**, *61*, 271.

(36) Lynch, L. J.; Barton, W. A.; Webster, D. S. *Proceedings of Sixteenth Biennial Low-Rank Fuels Symposium*; Groenewold, G. H., Ed.; Energy and Environmental Research Center: Montana, 1991, p 187.

(37) Barton, W. A.; Lynch, L. J. *Proceedings of 6th Australian Coal Science Conference* Newcastle, 1994, p 65.

(38) Deevi, S. C.; Suuberg, E. M. *Fuel* **1987**, *66*, 454.

(39) Woskoboenko, F.; Stacy, W. O.; Raisbeck, D. *The Science of Victorian Brown Coal*; Durie, R. A., Ed.; Butterworth-Heinemann Ltd.: Oxford, 1991; p 152

(40) Evans, D. G. *Fuel* **1973**, *52*, 186.

(41) Miura, K.; Mae, K.; Morozumi, F. *Proceedings of 9th Int. Conf. Coal. Sci.*

1997, *I*, pp 191.

(42) Gorbaty, M. L. *Fuel* **1978**, *57*, 796.

(43) Suuberg, E. M.; Otake, Y.; Yun, Y.; Deevi, S. C. *Energy Fuels* **1993**, *7*, 384.

(44) Neavel, R. **1976**, *55*, 237.

(45) Cronauer, D. C.; Ruberto, R. G.; Silver, R. S.; Jenkins, R. G.; Davis, A.; Hoover, D. S. *Fuel* **1984**, *63*, 77.

(46) Atherton, L. E. *Proceedings Int. Conf. Coal Sci.* 1985, pp 553.

(47) Ruether, J. A.; Mima, J. A.; Kornosky, R. M.; Ha, B. C. *Energy Fuels* **1987**, *1*, 198.

(48) Serio, M. A.; Solomon, P. R.; Kroo, E.; Bassilakis, R.; Malhotra, R.; McMillen, D. *Am. Chem. Soc. Div. Fuel Chem. Prepr.* **1990**, *35(1)*, 61.

(49) Okuma, O., Masuda, K., Murakoshi, K., Yanai, S-i., and Matsumura, T. *Nenryoukyoukaishi (in Japanese)* **1990**, *69*, 259.

(50) Song, C.; Saini, A. K.; Schobert, H. H. *Energy Fuels* **1994**, *8*, 301.

(51) Miknis, F. P.; Netzel, D. A.; Turner, T. F.; Wallace, J. C.; Butcher, C. H. *Energy Fuels* **1996**, *10*, 631.

CHAPTER 2

Simulation of Interaction between a Model Molecule of Brown Coal and Water by a Computer Aided Molecular Design Technique

2.1. INTRODUCTION

With the development of molecular modeling software,[1] it has become possible not only to visualize molecular structures in three dimensions on the computer screen, but also to calculate energetically favorable structural conformation using molecular mechanics and molecular dynamics methods. Molecular modeling techniques are being used widely today to provide insight in to the structure, properties and interactions of biomolecules (e.g., enzymes, proteins, inhibitors)[2] in order to guide the design and synthesis of pharmaceuticals. Recently, in the area of fuel science, variations of these techniques have been applied to visualize asphaltene structures[3] and to construct average molecular representations of kerogen macromolecules[4] and bituminous coals[5-12] based on analytical data. Carlson[7] firstly proposed the most probable conformation of each model molecule of bituminous coal previously reported by Given,[13] Wiser,[14] Solomon,[15] or Shinn[16] by utilizing CAMD technique. These studies demonstrated the importance of van der Waals interactions and hydrogen bonding in the formation and stabilization of the coal macromolecular structure. It was also found that physical densities and microporosities calculated for the simulated coal structures were in good agreement with those observed experimentally. Several similar works, so far, have been accumulated with some modifications. CAMD would help to determine whether the proposed chemical structures are sterically acceptable, what conformations are most probable, and to understand the nature of several

types of noncovalent bonding interactions between the coal macromolecules. It would be also useful to predict what happen in the coal molecules in a given conditions. The results could give some suggestions on the subsequent experimental work in the following chapter.

In this chapter , CAMD was applied to a model molecule of brown coal and water systems to predict the change in the conformation and noncovalent interaction energy during its moisture release process.

2.2. SIMULATION

2.2.1. Model molecule for a brown coal

Two types of unit structure of brown coal were constructed based on the data from elemental composition and solid state ^{13}C NMR of Yallourn coal,[17] and depicts in Figure 2.1. Yallourn brown coal has a moisture content of 59.3wt% on wet basis, an ash content of 1.1wt% on dry basis and the following elemental composition on dry-ash-free weight basis;

C; 62.6%, H; 4.6%, N; 0.7%, S; 0.3% and O; 31.6% (by difference)

A heptamer composed of unit structures A was assumed as a model molecule for a brown coal having a molecular weight of 1922. Two associated molecule of a pentamer and a tetramer of unit structures B was also used as model molecule in order to predict the excluded volume of the model molecules. Hereafter, the model molecule composed of unit structures A will be referred to as Model-A and that of unit structures B as Model-B, respectively.

2.2.2. Computer and software

TITAN 750V graphic work station (Kubota Computer Inc.) and Polygraf (version 3.21, Molecular simulation Inc.) were used as the hardware on computer and the software program for CAMD, respectively. The software allows the construction of relatively large molecular structure containing up to 20 000 atoms and the subsequent manipulation of these structures using molecular mechanics and dynamics techniques to determine the most probable

structure. Polygraf supports AMBER, MM2 and DREIDING force fields. In the present study, DREIDING force field was employed.

2.2.3. Calculation

The procedure for the calculation is shown in Figure 2.2. The energy for model molecule, E, was evaluated from the sum of forces of bonded interactions (bond (E_b), angle (E_θ), torsion (E_ϕ), inversion (E_i)), and forces of nonbonded interactions (van der Waals (E_{vdW}), electrostatic (E_{el}), hydrogen bond (E_{hb})), as written by

$$E = E_b + E_\theta + E_\phi + E_i + E_{vdW} + E_{el} + E_{hb} \qquad (2.1)$$

Initially about 200 water molecules were generated around Model-A, while Model-B was surrounded by about 360 water molecules. The minimum-energy conformation (MEC) for the model including water molecules was determined after the molecular mechanics (MM) and molecular dynamics (MD) calculations. The number of nonbonding interactions and potential energies were calculated. Then, a certain number of water molecules were taken away from the force field and MEC was determined again by MM and MD calculations. These procedures were repeated along with decreasing the number of water molecules towards 0. Readsorption of water onto the dried model molecule was simulated in the same manner by increasing the number of water molecules around the model molecule.

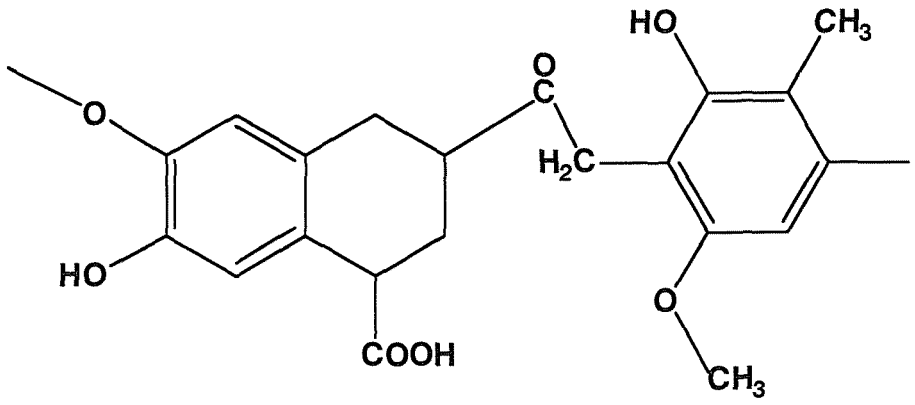

Model A

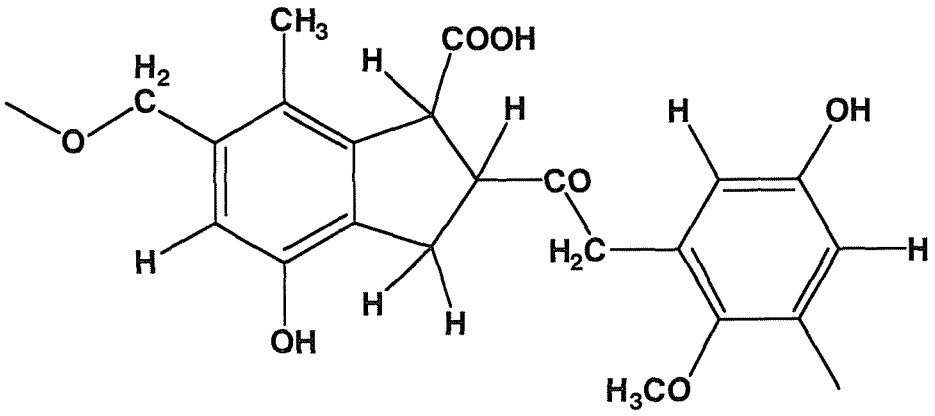

Model B

Figure 2.1. Unit structures of Model A and Model B.

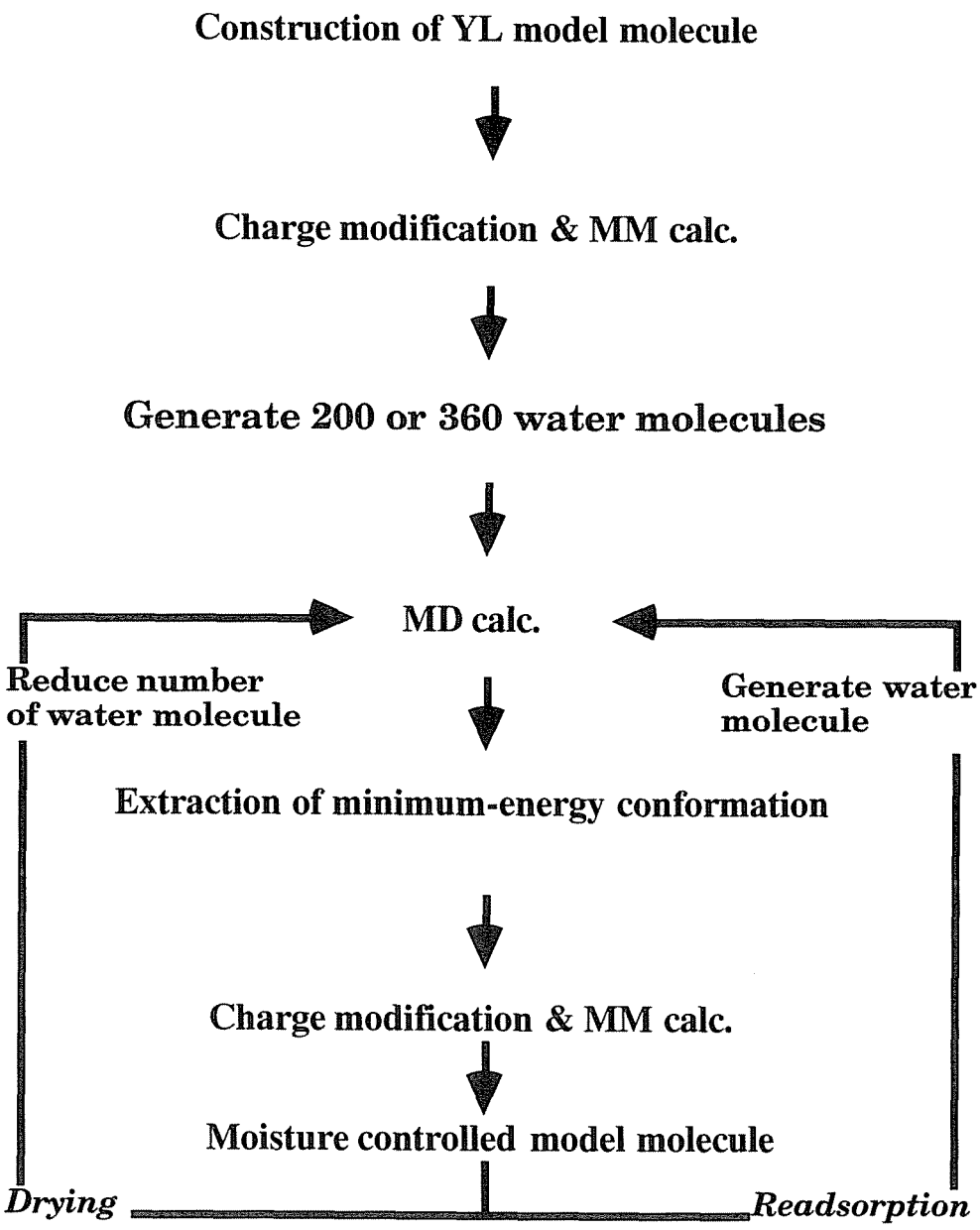

Figure 2.2. Flow chart of calculation procedure.

2.3. RESULTS AND DISCUSSION

2.3.1. Conformational change with drying

Figure 2.3 shows changes in MEC of Model-A with moisture release. MEC was determined after 50 picosecond molecular dynamics calculation. The conformational shape of Model-A changes from an expanded to a contracted state with a decrease in the number of water molecules. It was also found that after the complete removal of water molecules, Model-A can never return to its initial shape, even when again surrounded by the same number of water molecules as demonstrated in Figure 2.4. The number of intramolecular hydrogen bonds in Model-A increased from 4 to 10 during drying process. In the readsorption process, however, the number of intramolecular hydrogen bonds remained to be 10.

2.3.2. Energy change with drying

The total energy of the system, E_s, the model molecule, E_c, and water molecules, E_w, were calculated respectively by integrating the forces of bonded and nonbonded interactions. These energy terms at a given water content are listed in Table 2.1. E_{c-w} is the total energy for interaction between the model and water molecules as given by.

$$E_{c\text{-}w} = E_s - (E_c + E_w) \qquad (2.2)$$

E_s increases with the extent of drying, while E_c decreases. The decrease of E_c indicates the stabilization of Model-A induced by drying. E_w and E_{c-w} always show negative values regardless of water content. They are divided by the number of water molecules and the normalized values are also listed in Table 2.1. The normalized values of E_w, E'_w, are smaller than that of E_{c-w}, E'_{c-w}, when the number of water molecules are larger than 70. With further decreasing the number of water molecules E'_w become larger than E'_{c-w}. This suggests the interaction between Model-A and water molecules become more significant than that between water molecules in lower water content.

E_c is divided into two interaction energy terms, i.e., bonding, E_c(b),

and nonbonding, E_c (nb). Figure 2.5 represents variation of E_c(b) and E_c (nb) for Model-B as a function of water removal. E_c (nb) keeps almost constant values in the extent of water removal up to 80%, by further removal of water, it drops significantly. In contrast, E_c(b) keeps a steady value over the range of water content. Accordingly the decrease in E_c, i.e., stabilization of the model molecule is brought about by the reduction of E_c (nb). It is also found that E_c (nb) never regain its original value even when again surrounded by the same number of water molecules. The nonbonding energy term was further divided into three energy terms, i.e., E_c (vdW) arisen from van der Waals interactions, E_c (el) from electrostatic interactions, and E_c (hb) from hydrogen bonding interactions. As shown in Figure 2.6, all the energy terms decreases in the region of water removal larger than 80%. The difference of the energy terms between original and completely dried Model-B are 90 kcal/mol for E_c (hb) , 70 kcal/mol for E_c (el) , and 40 kcal/mol for E_c (vdW). The hydrogen bonding interaction contributes to the conformational stabilization much more extent than the electrostatic and van der Waals interactions.

2.3.3. Change in excluded volume with drying

The excluded volumes of Model-B alone, V_m and whole system including water molecules and Model-B, V_s, were evaluated by using water as a probe molecule. V_m and V_s were plotted in Figure 2.7 as a function of water removal. V_s decreased monotonously with water removal. On the other hand, V_m is almost unchanged up to 80% of water removal, V_m decreases rapidly by further removal of water. Finally it reached 80% of the initial volume. Note that V_m is unchanged even when again surrounded by water molecules. This trend well corresponds to the change in E_c (nb) as shown in Figure 2.5. The shrinking of Model-B accompanies the reduction of nonbonding energy.

Table 2.1. Relationship Between Number of H_2O and Energy Terms.

Number of H_2O	Energy (kcal)				Normalized energy (kcal/mol)	
	E_s	E_c	E_w	$E_{c\text{-}w}$	E'_w	$E'_{c\text{-}w}$
199	-2738.0	348.6	-2407.5	-679.1	-12.1	-3.4
70	-757.4	319.3	-646.0	-430.7	-9.2	-6.2
38	-327.8	313.5	-301.1	-340.2	-7.9	-9.0
17	2.7	300.0	-99.2	-198.0	-5.8	-11.6
8	146.9	284.6	-22.4	-115.3	-2.8	-14.4
0	267.6	267.6	0.0	0.0		

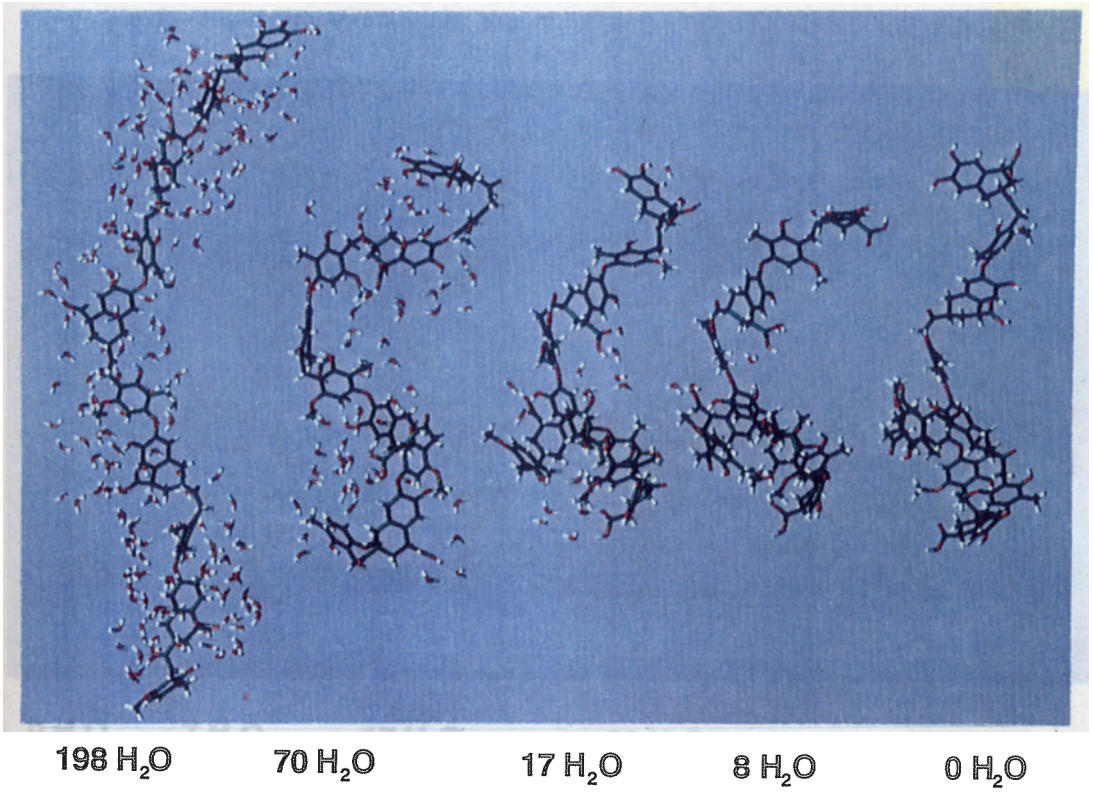

Figure 2.3. Change in conformation of Model-A along with drying.

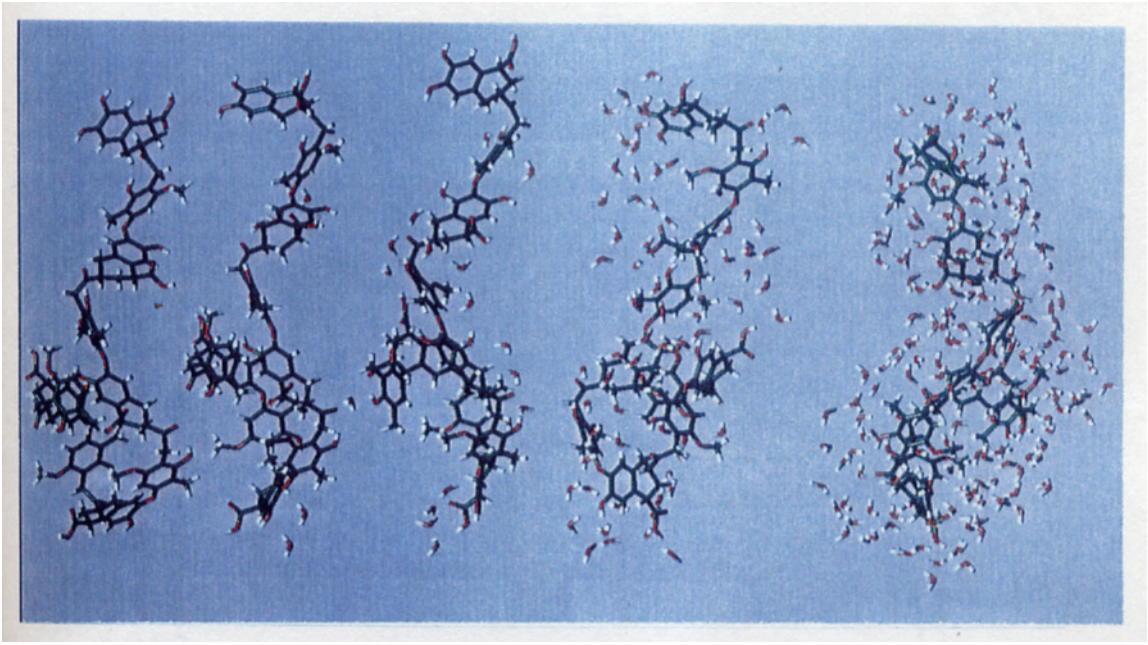

Figure 2.4. Change in conformation of Model-A along with water readsorption.

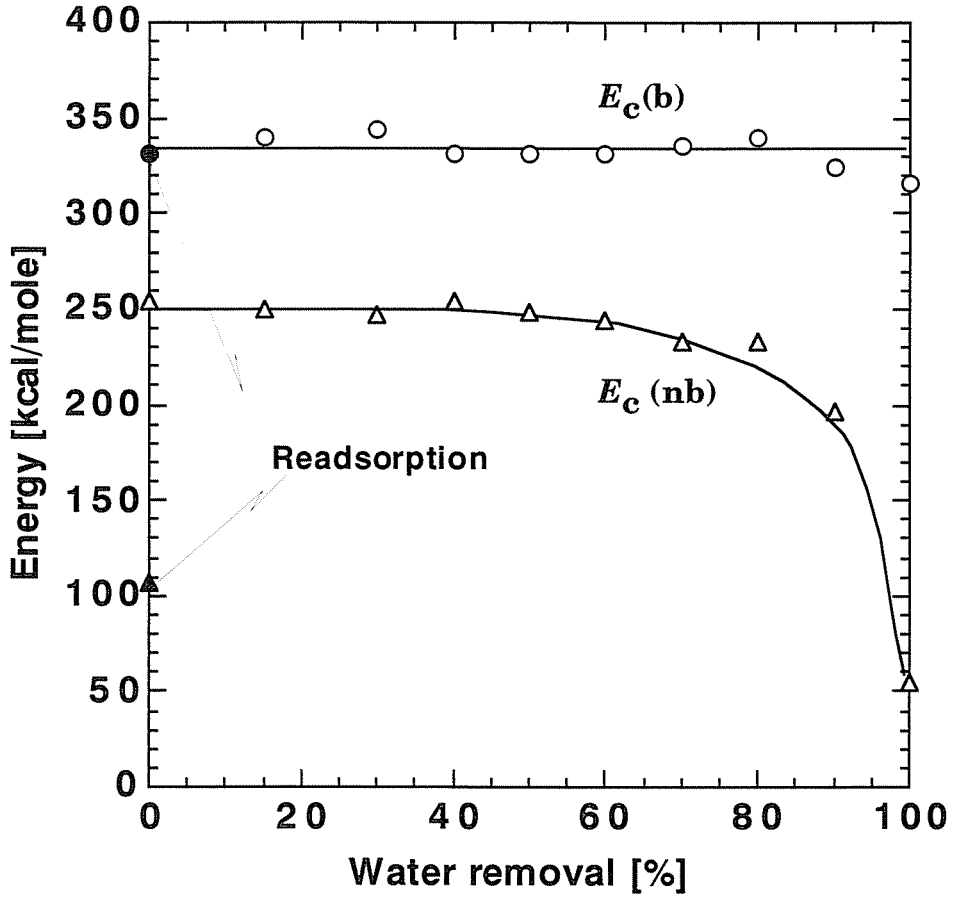

Figure 2.5. Variation of E_c(b) and E_c (nb) for Model-B with water removal.

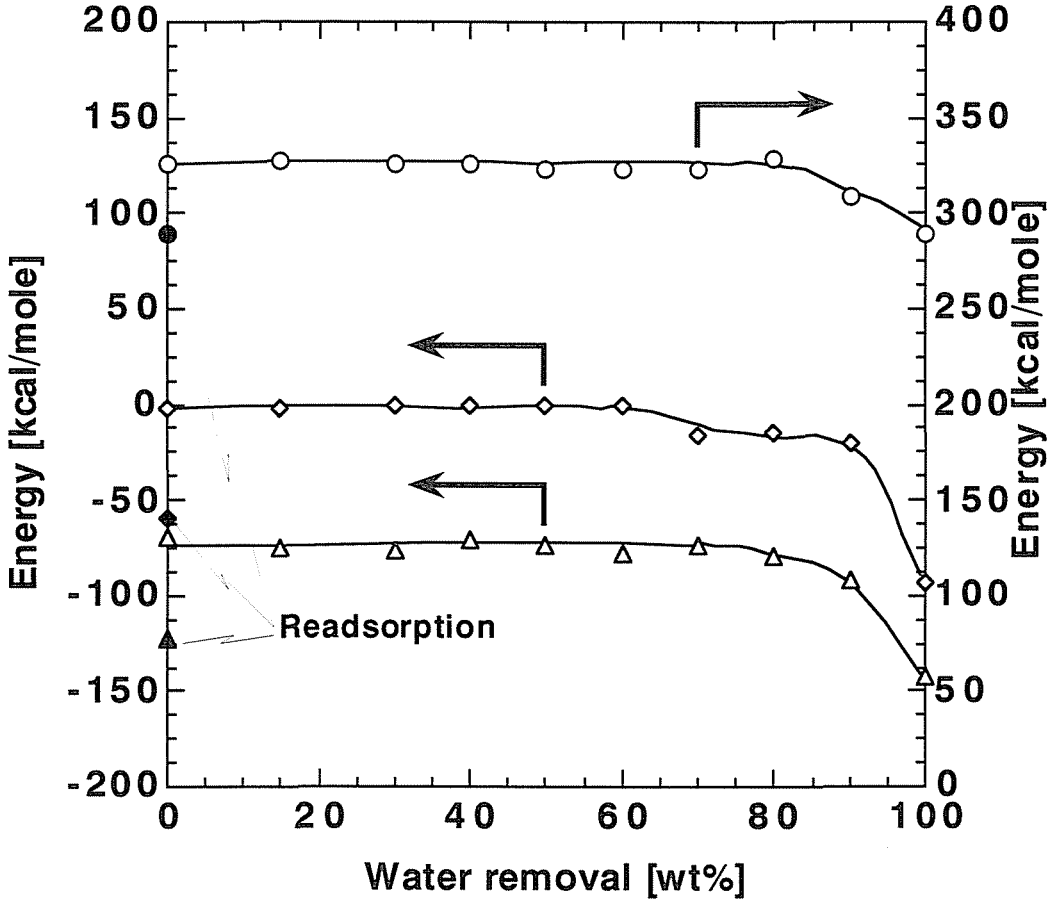

Figure 2.6. Variation of E_c (vdW), E_c (el), and E_c (hb) for Model-B with water removal.

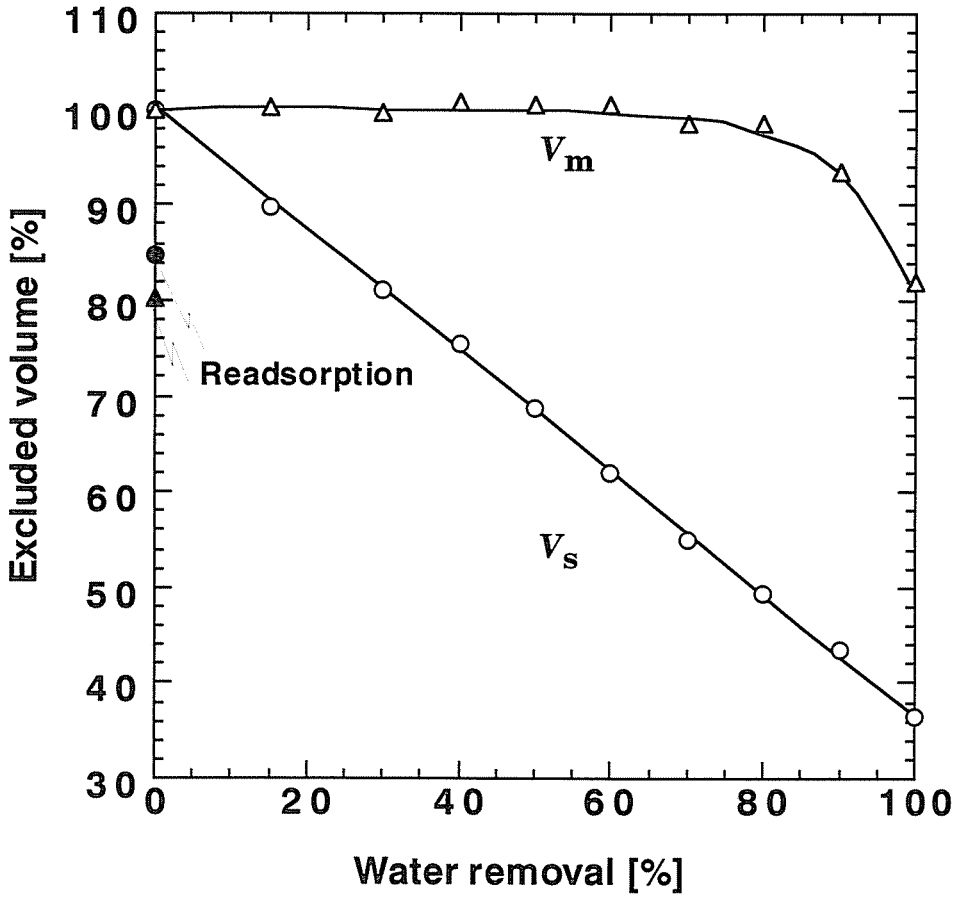

Figure 2.7. Changes in V_m and V_s with water removal.

2.4. CONCLUSIONS

CAMD technique was utilized to evaluate the change in conformation of a model molecule of brown coal along with a progress of moisture release. Based on the simulative studies, following conclusions were made:

(1) The interaction between model molecule and water molecules become more significant than that between water molecules in lower water content.

(2) E_c (nb) and V_m drop significantly when the water removal exceeds 80% and it never regain their original values even when again surrounded by the same number of water molecules.

(3) The hydrogen bonding interaction contributes to the conformational stabilization much more extent than the electrostatic and van der Waals interactions.

References

(1) Fruhbenis, H.; Klein, R.; Wallmeir, H. *Angew. Chem., Int. Ed. Engl.* **1987**, *26*, 403.

(2) Bajorath, J.; Kraut, J.; Li, Z.; Kitson, D. H.; Hagler, A. T. *Proc. Natl. Acad. Sci.* **1991**, *88*, 6423.

(3) Robinson, K. K. *Proceedings of the Electric Power Research Institute Conference on Coal Structure, Palo Alto, CA*; EPRI, **1987**, pp 3-1-3-11.

(4) Faulon, J. L.; Vandenbroucke, M.; Drappier, J. M.; Behar, F.; Romero, M. *Adv. Org. Geochem.* **1990**, *16*, 981.

(5) Carlson, G. A. *Prepr. Am. Chem. Soc., Div. Fuel Chem.* **1989**, *34(3)*, 780.

(6) Carlson, G. A.; Granoff, B. *Coal Science II* **1991**, Shorbert, H. H., Bartle, K. D., Eds.; ACS Symposium Series 461; American Chemical Society: Washington, DC, 1991; pp159.

(7) Carlson, G. A. *Energy Fuels* **1992**, *6*, 771.

(8) Nomura, M.; Matsubayashi, K.; Ida, T.; Murata, S. *Fuel Process. Technol.* **1992**, *31*, 169.

(9) Nakamura, K.; Murata, S.; Nomura, M. *Energy Fuels* **1993**, *7*, 347.

(10) Faulon, J. L.; Carlson, G. A.; Hatcher, P. G. *Fuel Process. Technol.* **1993**, *34*, 277.

(11) Faulon, J. L.; Carlson, G. A.; Hatcher, P. G. *Energy Fuels* **1993**, *7*, 1062.

(12) Nakamura, K.; Takanohashi, T.; Iino, M.; Kumagai, H.; Sato, M.; Yokoyama, S.; Sanada, Y. *Energy Fuels* **1995**, *9*, 1003.

(13) Given, P. H. *Fuel* **1960**, *39*, 147.

(14) Wiser, W. H. *NATO ASI Ser. C* **1983**, *124*, 325.

(15) Solomon, P. R. *New Approaches in Coal Chemistry;* ACS Symposium Series 169; American Chemical Society: Washington, DC, 1981; pp 61.

(16) Shinn, J. H. *Fuel* **1981**, *63*, 1187.

(17) Yoshida, T.; Nakata, Y.; Toshida, R.; Ueda, S.; Kanda, N.; Maekawa, Y. *Fuel* **1982**, *61*, 824.

CHAPTER 3

Classification of Water Sorbed in Coal on the Basis of Congelation Characteristics

3.1. INTRODUCTION

As-received coals hold more or less residual water. In particular, low-rank coals contain a number of oxygen functional groups resulting in material with hydrophilicity, and this is the primary reason for their water content being as much as 30-60 wt% on a wet basis. Such substantial water content necessitates drying prior to use. It is a widely recognized fact that the coals have gellike structures that can shrink and swell in response to water loss and uptake, respectively.[1-4] The extent of drying is therefore an important measure for the reactivity of the coals in subsequent conversions that are dependent on their initial physical properties.[5-10] The above also implies that a portion of sorbed water interacts with oxygen functionalities via hydrogen bonds and thereby contributes to the three-dimensional structure of the macromolecular coal network.

In Chapter 2, the effects of drying on the physical structure of coal was examined at the molecular scale, using a computer-aided molecular design technique.[11] A simulation was performed for a model molecule of a brown coal, which was initially surrounded by about 200 water molecules. A heptamer composed of unit structures was assumed as the model molecule having a molecular weight of 1922. The conformational shape of the molecule was found to change from an expanded to a contracted state with a decrease in the number of water molecules. The contraction was mainly due to an increasing number of intramolecular hydrogen bonds with the removal of water molecules that directly interacted with the coal molecule. The simulation also

demonstrated that after the complete removal of water molecules, the macromolecule can never return to its initial shape, even when again surrounded by the same number of water molecules. Such an irreversible process was actually observed in the variation in swellability of a brown coal in water with regard to the extent of drying. Furthermore, Suuberg et al. [4] pointed out the swellability of coal changes depending not only on the extent of drying but also on drying method. These results reflect the importance of evaluating the distribution of water of different types with different properties and of determining the concentration of water that is in close contact with the macromolecules of coal.

There have been some results published that support the idea that water retained in coal can be divided into two major types, freezable and nonfreezable, on the basis of the characteristic phase transition, i.e., fusion or congelation.[12] A liquid-to-solid transition is accompanied by evolution of latent heat as well as by reduction of molecular mobility. The former can be detected by calorimetry and the latter by proton nuclear magnetic resonance (^{1}H NMR) spectroscopy. Differential scanning calorimetry (DSC) has been adopted to evaluate the freezing/fusion characteristics of water sorbed in polymers[13], coals[12, 14, 15] and other solids.[16-18] Nakamura et al.[13] employed this technique to study the properties of water contained in a poly(hydroxystyrene). When the water content reached a critical level, the authors observed two exothermic peaks due to the congelation of water, one centered at 273 K and the other at 235 K. One peak arose from a type of water identical with bulk water, called "free water" and the other from water retained by molecular interactions within the porous system of the polymer, termed "freezable bound water". Their results also suggest the presence of another type of water, which they named "nonfreezable water". Congelation of this type of water is, however, undetectable, and its concentration must therefore be estimated by difference. It has been confirmed for pore-condensed water that heat of fusion and fusion-point temperature become smaller and lower, respectively, as the size of the space where the water is condensed decreases, and, ultimately, no fusion is observed when the space size is smaller than a certain value.[19]

Quantitative classification of freezable water is possible only when the heat of congelation or fusion of all types of water can be detected and accurately determined. The heat of fusion of bound water, which is found in a variety of porous solid materials, has been determined experimentally from the dependency of the latent heat on the water content.[12, 14] Mraw and O'Rourke[12] evaluated the heat of fusion of water retained in some coals by measuring the quantity of heat absorbed by its fusion as a function of the water content. This technique is applicable to rigid porous solids materials as ceramics, but its applicability to gellike macromolecular solids, such as coal, is questionable. As mentioned earlier, coal can shrink in response to loss of water, and this behavior might then lead to the transition of one type of water into another within the coal matrix. Although some of the disadvantages of DSC are pointed out above, calorimetry is still useful in the quantification of freezable water present in coal, in particular when combined with complementary analysis using another technique that allows validation of the classification of water in coal.

The NMR spin-spin relaxation can distinguish molecular structures/lattices on the basis of whether the molecular reorientation rates are below or above ~10^5 Hz. Such molecular structures are termed rigid or mobile, respectively. The molecular reorientation rates of ice are of the order of 10^5 Hz, which means that ice is considered a rigid structure in the NMR sense, whereas liquid water is characterized by molecular reorientation rates of ~10^{10} Hz.[20] Therefore, the congelation of free and bound waters is expected to be detected in proton NMR relaxation measurements as mobile protons represented by exponential decays changing into "rigid protons" with Gaussian decays. Furthermore, non-freezable water would be observed separately from the other types of water, if its liquid-like mobility is maintained at temperatures where the others are frozen. NMR has been adopted to determine the water content in coals.[21-25] Lynch et al.[15,20,26] measured the relaxation characteristics of water in coals with a range of water contents during temperature cycling between 300 and 220 K. They observed a Gaussian-exponential transition for water at around 273 K, and from this they estimated the content of free water. Measurement of the proton relaxation characteristics by NMR thus

enable us to distinguish and quantify the three types of water discussed above. However, few previous NMR studies have resulted in a quantitative distribution of different types of water in coal that is directly comparable with that evaluated by DSC. Furthermore, no studies have evaluated such distribution of water in coal in the wide range of ranks and as-received state.

The present study aims first to quantify the free, bound, and nonfreezable waters sorbed in various coals (ranging from lignite to bituminous), on the basis of the congelation characteristics of the sorbed water as measured by DSC. The second objective is to measure the three types of water using a proton NMR and then to compare these results with the DSC data.

3.2. EXPERIMENTAL SECTION

3.2.1. Coal samples

Four Argonne PCSP (Premium Coal Sample Program) coals and four brown coals were used for the present study. Lumps of the brown coals were supplied from the Nippon Brown Coal Liquefaction Co. Ltd., Japan, and the Coal Corp. of Victoria, Australia. They were stored in gastight drums during transportation to prevent evaporation of water. The coals other than PCSP coals were pulverized in a globe bag filled with nitrogen gas saturated with water vapor. The elemental compositions and ash and water contents of the coal samples are listed in Table 1. The brown coals, the particle sizes of which were finer than 150 μm, were stored for 2 weeks prior to use at 293 K in a gastight vessel filled with nitrogen gas saturated with water vapor. The water contents of the brown coals was determined from the fractional mass release observed upon drying at 380 K under a nitrogen gas flow for 2 h in a thermobalance (TG-2000S, Mac Science Co. Ltd.). Literature values[27] were used for the water content of the PCSP coals. The PCSP coals were analyzed immediately after opening the ampules. Samples with different water contents were prepared from the individual coals by allowing them to lose water slowly at ambient temperature under a nitrogen atmosphere, prior to the DSC analysis. The water content of the partially dried samples was determined as described above.

3.2.2. DSC

DSC measurements were made employing a calorimeter (DSC 200, Seiko Co. Ltd.) equipped with a liquid nitrogen cooling accessory. Typically about 5 mg of sample was placed in an aluminum pan and cooled from 293 K to 123 K at a rate of 8 K/min and then heated to 293 K at 8 K/min under 80 mL/min nitrogen gas flow. The quantity of heat given off by the sample was determined from the area between the peak in the heat evolution rate and a straight baseline drawn from 213 to 263 K. In preliminary experiments it was confirmed that the quantity of heat evolved was independent of the cooling rate in the range from 2 to 8 K/min. Several measurements were made for the individual coal samples. The quantities of heat given off by the samples were reproducible to about ± 5 % on the same conditions.

3.2.3. Proton NMR

A proton magnetic resonance method was adopted to measure the spin-spin relaxation characteristics of the coal samples. The relaxation measurements were carried out using a JEOL Mu-25 spectrometer operated at 25 MHz. A $90°_x$-τ-$90°_y$ solid-echo pulse sequence[28, 29] was used to obtain the entire free induction decays (FID). Typical values for the pulse width, pulse spacing, repetition time, and number of scans were 2.0 μs, 8.0 μs, 6 s, and 32, respectively. About 0.3 g of the samples were transferred to 10-mm (o.d.) NMR tubes. The FID was measured at temperature intervals of 2-5 K, while cooling from 293 to 213 K. The signal at each temperature was recorded under temperature equilibration. The outline of the design and operation of a low-temperature probe for ^{1}H NMR spectroscopy was shown in Figure 3.1. The probe employed was made of poly(tetrafluoroethylene), which is a proton-free material. The probe was heated at 373 K prior to all the measurements, and dried-air was continuously supplied to the probe throughout the experiments to reject the background proton signal that arises from water sorbed on the probe.

Table 3.1. Properties of Coals.

coal	(symbol)	C	H	N	S	O[a]	ash	moisture
		[wt.%-daf[b] coal]					[wt.%-mf[c] coal]	[wt.%-sample]
Yallourn	(YL)	65.0	4.6	0.6	0.2	29.6	1.6	57.5
Loy Yang	(LY)	62.8	4.6	0.6	0.3	31.7	2.5	56.7
Morwell	(MW)	66.3	4.7	0.6	0.3	28.2	2.3	55.5
South Banko	(SB)	72.8	5.9	1.1	0.4	19.9	2.9	31.5
Beulah Zap	(BZ)	72.9	4.8	1.2	0.7	20.3	9.7	32.2
Wyodak	(WY)	75.0	5.4	1.1	0.5	18.0	8.8	28.1
Illinois#6	(IL)	77.7	5.0	1.4	2.4	13.5	15.5	8.0
Blind Canyon	(BL)	80.7	5.8	1.6	0.4	11.6	4.7	4.6

[a] by difference. [b] dry-ash-free. [c] moisture-free.

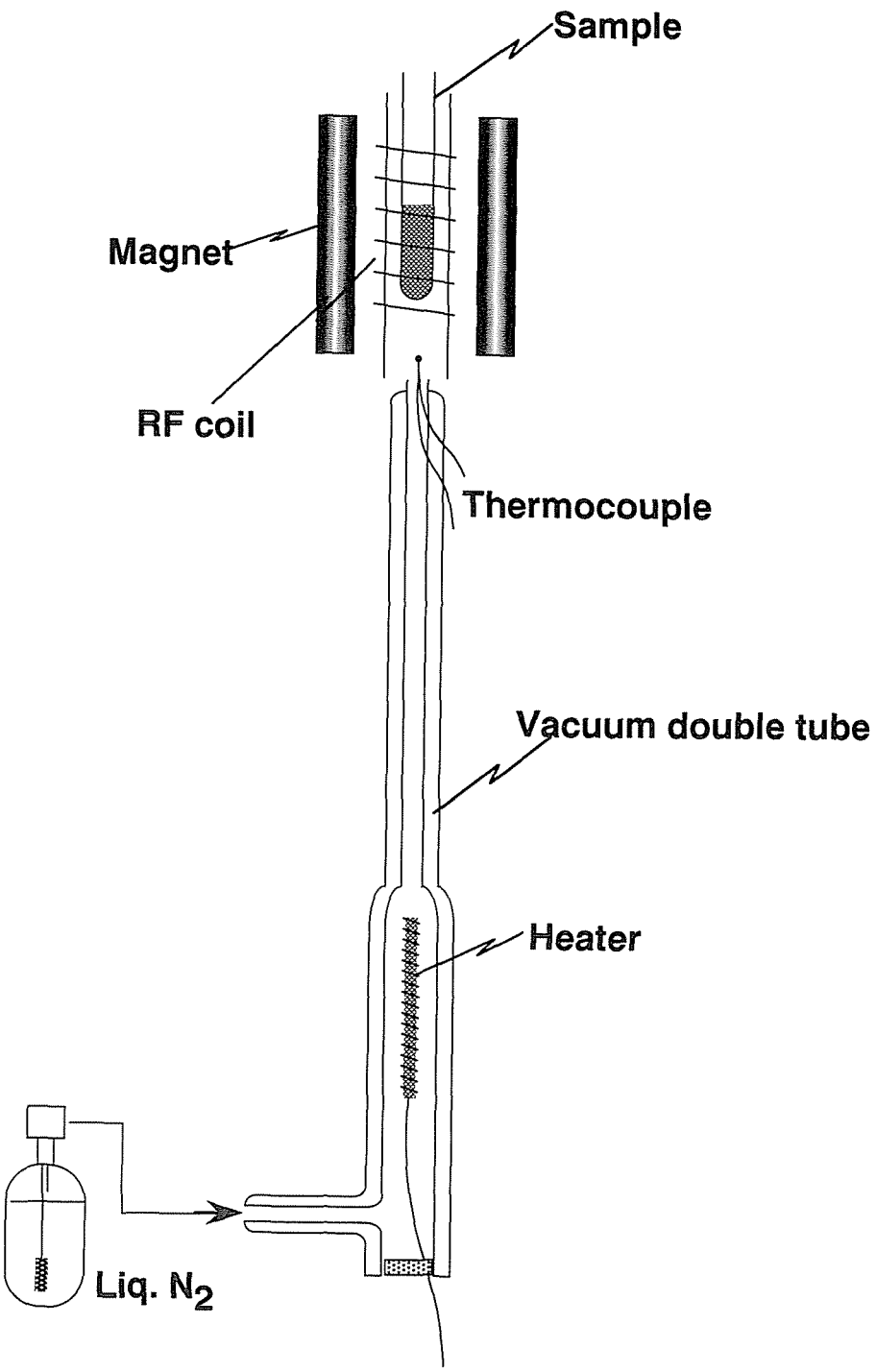

Figure 3.1. Overview of the low temperature NMR probe.

3.3. RESULTS AND DISCUSSION

3.3.1. DSC results

Figure 3.2 shows the DSC curves for pure water and the coal samples under cooling. Negligible weight change was detected during the analyses. The positive peaks appearing in the thermograms are the result of exothermic processes. Since such peaks were never observed for the coals dried at 380 K, these peaks arise from the phase transition of the water sorbed in the coal into ice, i.e., congelation. For each of LY, MW, and YL coals, peaks are seen around 258 and 226 K. Since the peaks at 226 K are much smaller than the peak at 258 K, different heat evolution rate scales are used in this figure. Note that the peak centered at 258 K is for pure water. Peaks at the latter temperature are also found for the other coals and are probably indicative of the congelation of water condensed in capillaries with diameters less than several micrometers.[30] In addition, for BZ and SB coals, the peaks at 226 K overlap with those at 235 and 248 K, respectively. While two exothermic peaks are detectable in DSC thermograms for YL, MW, and LY during cooling, only a single broad endothermic peak centered at around 273 K was observed during heating. A similar phenomenon also appeared in the DSC thermogram for water sorbed on poly(hydroxystyrene).[13] Thus, the thermograms obtained in cooling stage reveal that the coals hold at least two distinct types of freezable water. Therefore, discussion will be made of the results obtained from the cooling process.

From the thermograms shown in Figure 3.2, the water in the coals can be classified into two or more types, each with different congelation characteristics. The DSC analysis was then carried out for the original and partially dried samples of the individual coals in order to measure the quantity of heat, ΔH, as a function of water content. The results for selected coals are shown in Figure 3.3(a), (b). For YL coal, ΔH decreases linearly with decreasing water content in its range between 1.3 to 0.6 g/g of coal on a dry basis. The peak at 258 K became smaller and finally disappeared, while the peak at 226 K remained unchanged. In this range the decrease in ΔH per unit reduction of water mass is 333 J/g of water and is in good agreement with the congelation

heat of bulk water into ice having a type-I polymorphic form, i.e., 334 J/g of water.[31] Type-I is the only form possible under the present conditions. Thus, the peaks at 258 K is ascribed to water having no interaction with the coal, which is hereafter referred to as "free water". For water contents ranging from 0.6 to 0.3 g/g of coal, and where the peak at 226 K diminished with the extent of drying, ΔH decreases with a slope of 188 J/g of water. The peaks are therefore due to the congelation of another type of water freezing at a lower temperature and having a lower congelation heat than free water. The congelation heat of capillary-condensed water is generally less than that of bulk water.[12] This freezable water is then referred to as "bound water" according to Nakamura et al.[13] For the other coals, the amount and congelation heat of bound water can be derived from the relationship between the water content and ΔH shown in Figure 3.3(b). Two types of bound water are found for SB coals, corresponding to the two peaks that are clearly seen at 228 and 248 K in the thermogram shown in Figure 3.2.

Table 3.2 summarizes the congelation heats and the percentages of free and bound waters in the coals. It should be noted that the sum of the two types of water accounts for only 35-78% of the total water content of the coals examined. This indicates the presence of another type of water in which congelation is not observed, namely, "non-freezable water". The fraction of nonfreezable water is estimated by difference and is also given in the table. Sheng et al.[19] theorized that water becomes nonfreezable when the molecular cluster is too small; specifically, when the number of water molecules involved in the molecular cluster is less than a critical value of around 10. If the nonfreezable water is in such an environment, it is likely to be dispersed on a molecular scale, i.e., condensed in micropores and/or bound to specific sites via specified interactions such as hydrogen bonds.

In Figure 3.4 the relative molar abundance (with respect to oxygen and nitrogen atoms) of the non-freezable water is plotted versus the sum of the oxygen and nitrogen molar contents per unit mass of coal on a dry basis. It demonstrates that the former ranges from 0.4 for IL coal to 1.4 for BZ. Although the indicated values are averages, they are sufficiently small to support the idea that water molecules interact directly with oxygen- and

nitrogen-containing groups in the coal matrix.

The above DSC results reveal that the coals contain freezable water, which is classified into free and bound waters with different congelation properties. They also indicate the presence of nonfreezable water. Even with these data, there is still considerable uncertainty as to the percentage of each type of water. It is possible that drying shrinks the coal matrix, thereby inducing the transition of one type of water into another. In addition, the amount of nonfreezable water was calculated rather than measured. Thus, the NMR relaxation measurements were made in order to examine the validity of the above classification methods. The congelation of the bound water as well as that of the free water can be directly observed as the conversion of the slowly decaying into Gaussian components in the proton NMR signal that arises from the water. Moreover, if the nonfreezable water is still in a mobile state at temperatures where the other types of water are frozen, then it can be observed as a slowly decaying component and can be distinguished from the others, which are observed as Gaussian components.

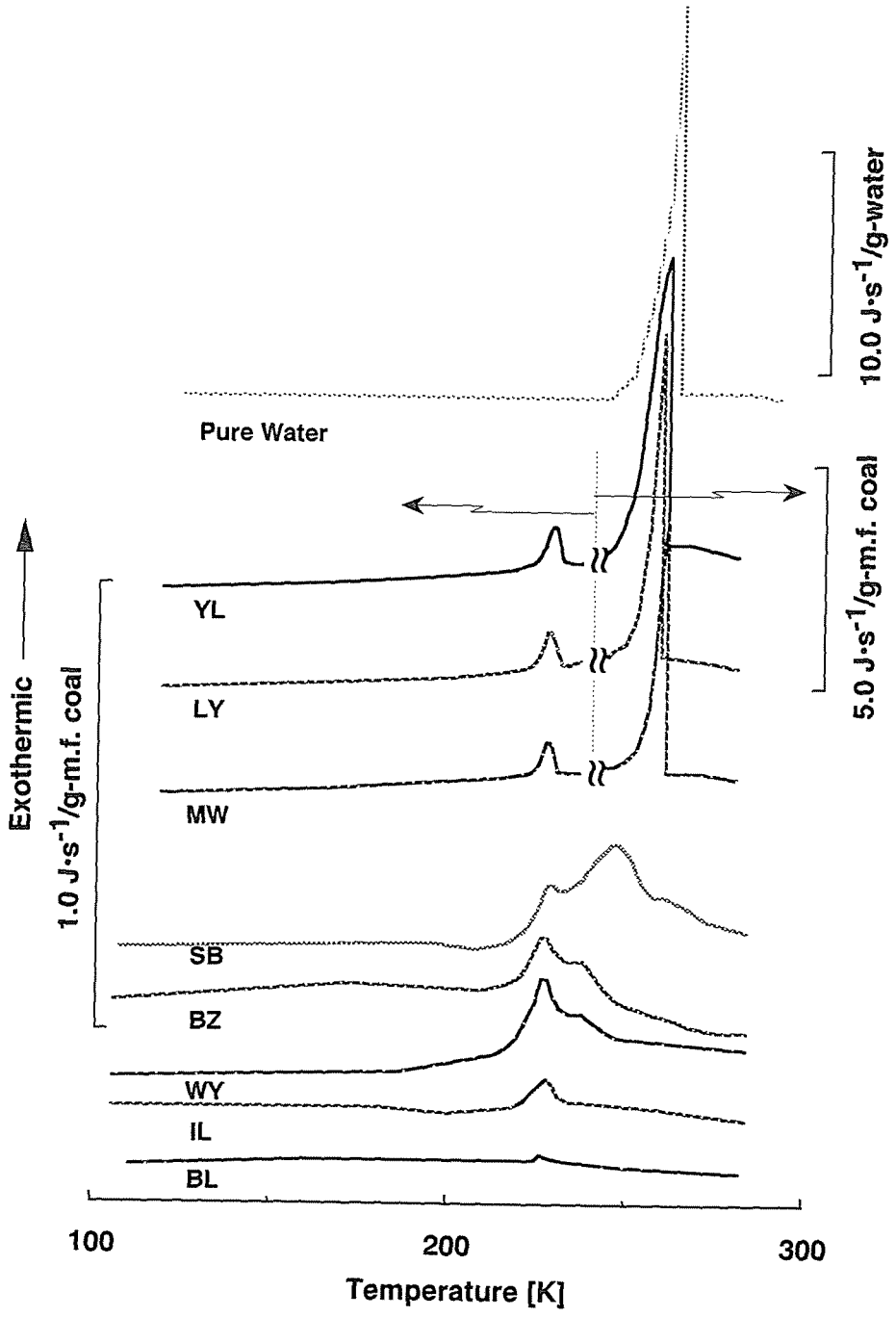

Figure 3.2. DSC thermograms of the coal samples and pure water.

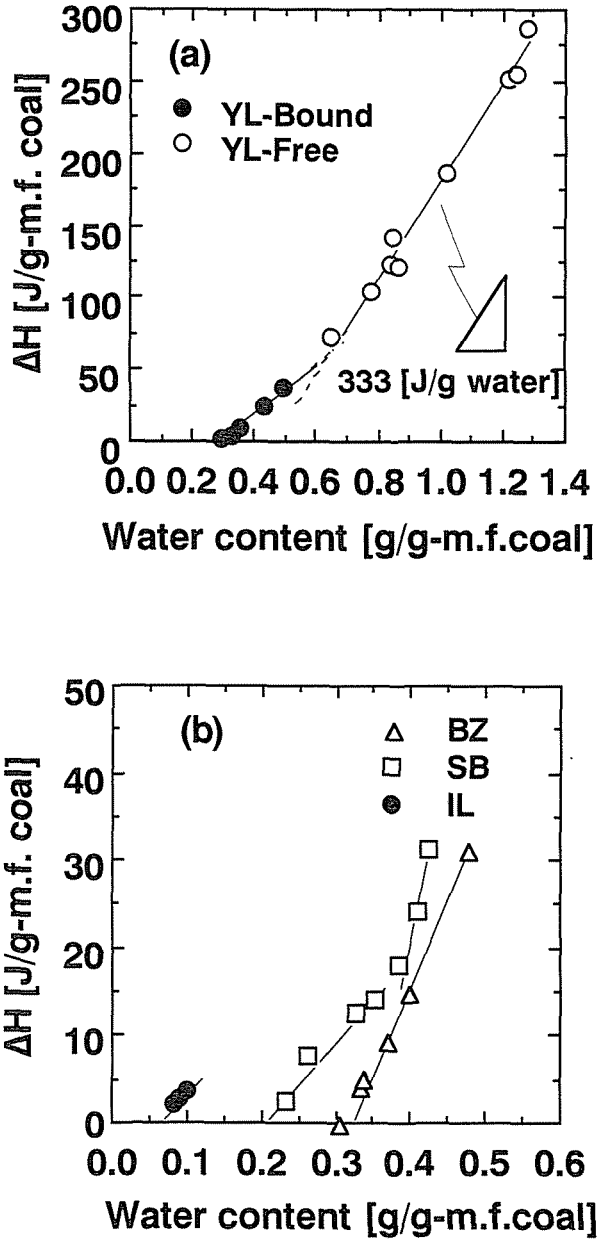

Figure 3.3. Quantity of heat generated by the congelation as a function of water content. (a) YL, (b) BZ, SB and IL.

Table 3.2. Summary of DSC Results.

coal	peak temperature [K] higer	peak temperature [K] lower	congelation-enthalpy [J/g-water]	water type [g/g-mf coal] free	bound	non-freezable[a]
YL	258.5	226.3	333, 188	0.70(52)	0.35(26)	0.30(22)
LY	258.4	227.1	-	-	-	-
MW	257.9	227.0	-	-	-	-
SB	-	248.1, 227.6	315, 90	0 (-)	0.26(56)	0.20(44)
BZ	-	226.4	186	0 (-)	0.17(35)	0.31(65)
WY	-	227.6	141	0 (-)	0.15(38)	0.24(62)
IL	-	227.0	74	0 (-)	0.05(50)	0.05(50)
BL	-	226.2	n.d.	0 (-)	n.d. (-)	- (-)

[a] by difference. Values in parentheses; % of total water.

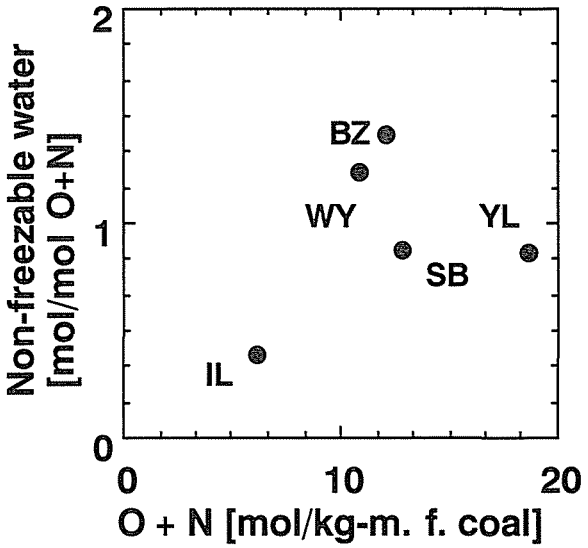

Figure 3.4. Relationship between molar content of non-freezable water normalized to that of coal oxygen and nitrogen and molar content of coal oxygen and nitrogen.

3.3.2. NMR results

The FID curve was analyzed by using a sequential linear-least-squares fitting method, which is commonly employed for deconvoluting the total FID into two Gaussian and one exponential functions with different specific relaxation times, i.e., T_2.[24] The following equations were used to fit the FID signal.

$$I(t) = I_L(t) + I_G(t) \quad (3.1)$$

$$I_L(t) = I_L(0) \exp [-t/T_{2L}] \quad (3.2)$$

$$I_G(t) = I_{G1}(0) \exp [-t^2/2T_{2G1}^2] + I_{G2}(0) \exp [-t^2/2T_{2G2}^2] \quad (3.3)$$

where $I(t)$ and $I_i(t)$ are the observed intensity at time t, and that attributed to component i , respectively. In Figure 3.5 the log of FID intensities for YL, BZ, and WY coals at 293 K are plotted versus the decay times. The slowly decaying component appearing after 50 μs for each coal is described by an exponential function. After the slowly-decaying component was fit by eq 3.2 to determine $I_L(0)$ and T_{2L} and then $I_L(t)$ was subtracted from $I(t)$, the rest of the data, i.e., $I(t)$-$I_L(t)$ was further described by eq 3.3 to obtain $I_{G1}(0)$, $I_{G2}(0)$, T_{2G1}, and T_{2G2}.

In Figure 3.6 is shown the relationship between the amount of hydrogen assigned to the slowly decaying component at 293 K and that of hydrogen as water sorbed in the coals. The former, given as $I_L(0)/I(0)$ multiplied by the total amount of hydrogen in the water-containing coals, is always larger than the latter, suggesting that a portion of the coal hydrogen has the mobility characteristic of that found in a liquid environment. Under the assumption that all of the hydrogen present as water can be attributed to the slowly decaying component at 293 K, the fraction of coal hydrogen having this mobility is 9-38% of the total, as indicated. The fraction of mobile hydrogen seems to increase with a decrease in coal rank. This result agrees well with the findings of Lynch et al.[20] who observed mobile coal hydrogen thought to be located in a part of the coal structure plasticized by its interaction with water. Nakamura et al. reported that the glass transition temperature of a

poly(hydroxystyrene) decreases with increasing amount of sorbed water and estimated that water molecules act as hydrogen-bond breakers, thereby plasticizing the polymer.[17] Yang et al.[32], who studied the proton relaxation characteristics of dried and pyridine-swollen high-volatile bituminous coals by means of a spin-echo NMR technique, found that the fraction of the slowly-decaying component in the coals increases from 0 to 70-80% owing to the swelling. Thus the results shown in Figures 3.6 are not surprising. However, an another factor would contribute to this inequality. Lynch et al.[33] pointed out that there is some deviation of the solid-echo signal from a true representation of the transverse relaxation. The solid-echo signal component that arises from structures with lesser degrees of molecular mobility (Gaussian component) is attenuated as a result of multiple proton dipolar interactions producing irreversible dephasing of the transverse magnetization. The extent of the attenuation of is very sensitive to the ratio $\tau / T_2(\tau$; pulse spacing). Barton et al.[34] have verified experimentally that the ^{1}H NMR transverse relaxation signals resulting from the solid-echo sequence with τ=6 μs are almost identical to those produced by a single 90° pulse for coal samples whose structure possesses various degrees of molecular mobility. It was also examined the relationship between the amount of hydrogen in the sample and the initial intensity of the FID obtained by solid-echo sequence at room temperature by employing polystyrene, polyethylene, dried coal, and wet coal. Although the samples have different distributions of rapidly and slowly decaying components, the solid-echo peak amplitude was proportional to the amount of hydrogen in the specimen as shown in Figure 3.7. Therefore, it is judged that the attenuation of the Gaussian components in solid-echo signals is negligible under the present conditions.

Figure 3.8 presents the amount of hydrogen demonstrating the exponential decay, H_L, as a function of temperature (ranging from 293 to 213 K). H_L has been normalized by the amount of hydrogen present as water and therefore can be directly compared with the fractions of three types of waters listed in Table 3.2. Values of H_L greater than 100% are, as stated above, due to a portion of the coal hydrogen that is involved in the exponential component. For YL coal, H_L decreases rapidly from 116% to 60% in a narrow temperature

range from 273 to 263 K and then decreases more slowly at lower temperatures reaching 35% at 213 K. Though not shown, similar profiles were obtained for LY and MW coals. Considering that such a rapid reduction in H_L in the same temperature range is not observed for the other coals, it can be attributed in this case to the congelation of free water. On the other hand, the slower decrease in the latter temperature range certainly involves a transition due to the congelation of the bound water and, in addition, may also be due to other transitions for hydrogen as non-freezable water and/or coal hydrogen. The total loss of H_L is thus expected to be equivalent to, or larger than, the amount of hydrogen present as the sum of the free and bound waters, respectively, in a case where the initial liquidlike mobility of the nonfreezable water and coal hydrogen is maintained over the temperature range examined, or in the other case where a portion of the nonfreezing water or coal hydrogen loses the mobility. Figure 3.9 shows T_{2L} of the four different coals as s function of temperature. Although there is a wide variation in the temperature dependence of T_{2L} with the coals, the relaxation time seems to reach a value of 60 μs at 213 K for the all coals. Such a coal-independent relaxation time implies that the slowly decaying components observed for the different coals at the temperature, which consist mainly of the nonfreezable water, have similar mobilities.

Table 3.3 summarizes the decrease of H_L in the temperature range of 213-293 K for the different coals. For YL coal, the extent of H_L reduction in the ranges of 263-273 K and 213-263 K, i.e., 56% and 25%, coincides quite well with the fractions of the free (52%) and bound waters (26%), respectively. For the coals containing no free water, the total H_L reduction also agrees well with the fraction of the bound water. The reduction of H_L is 39, 36, and 52% for WY, BZ, and SB coals, respectively; these values are nearly equivalent to their respective fractions of the bound water, i.e., 38, 35, and 56%. Thus, the NMR results confirm the validity of the measurements of the bound water as determined by DSC. A close agreement is seen between the reduction in H_L during cooling from 293 to 213 K and the proportion of bound water as measured by DSC, and this suggests that the non-freezable water remains mobile and that the extent of coal plasticization is maintained over this

temperature range.

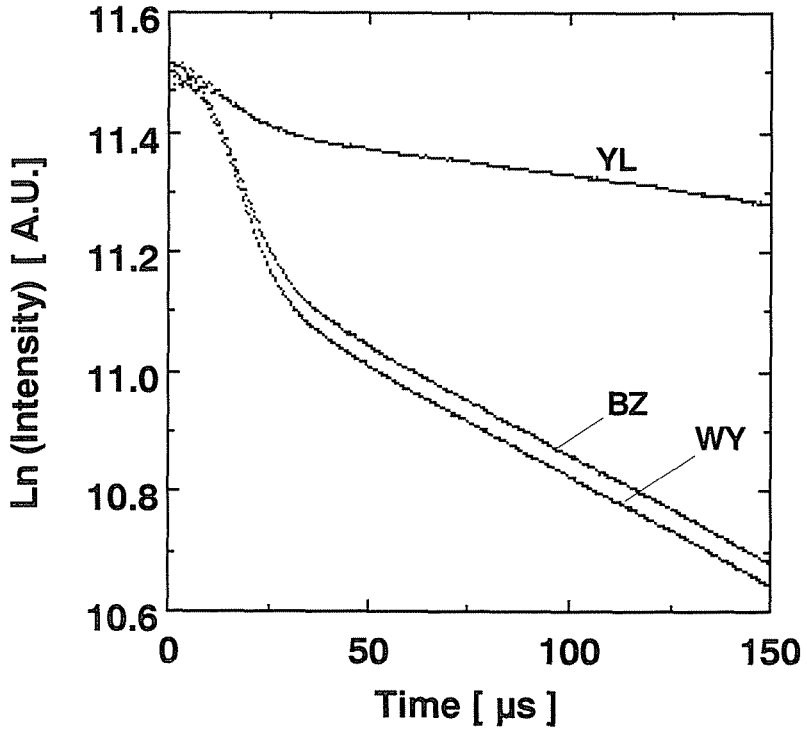

Figure 3.5. Natural logarithm of FID intensity versus decay time at 293 K for YL, BZ, and WY coals.

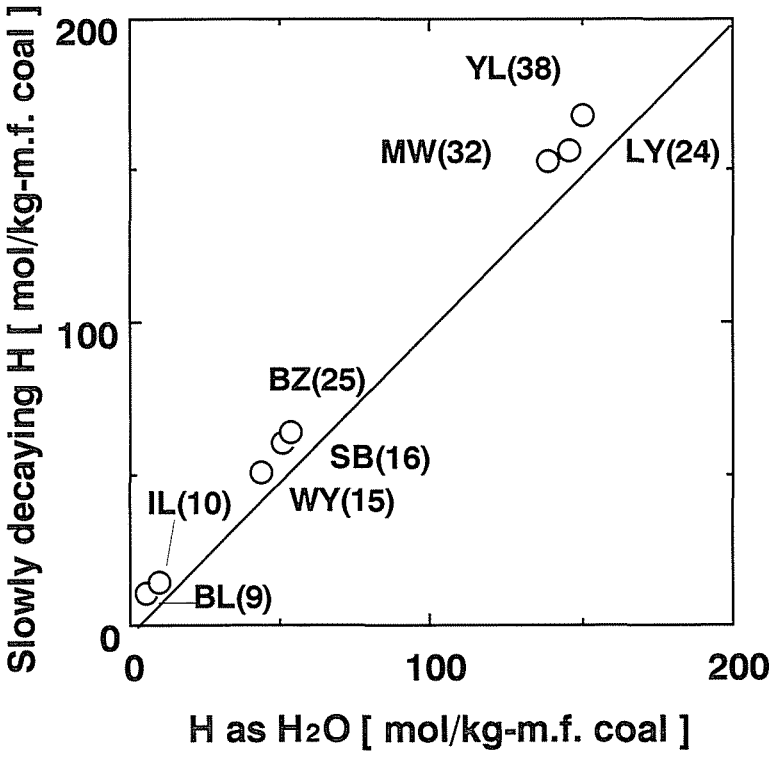

Figure 3.6. Amount of hydrogen belonging to the slowly decaying component as a function of that as water sorbed in different coals. Values in parentheses: % fractions of coal hydrogen belonging to the slowly decaying component to total.

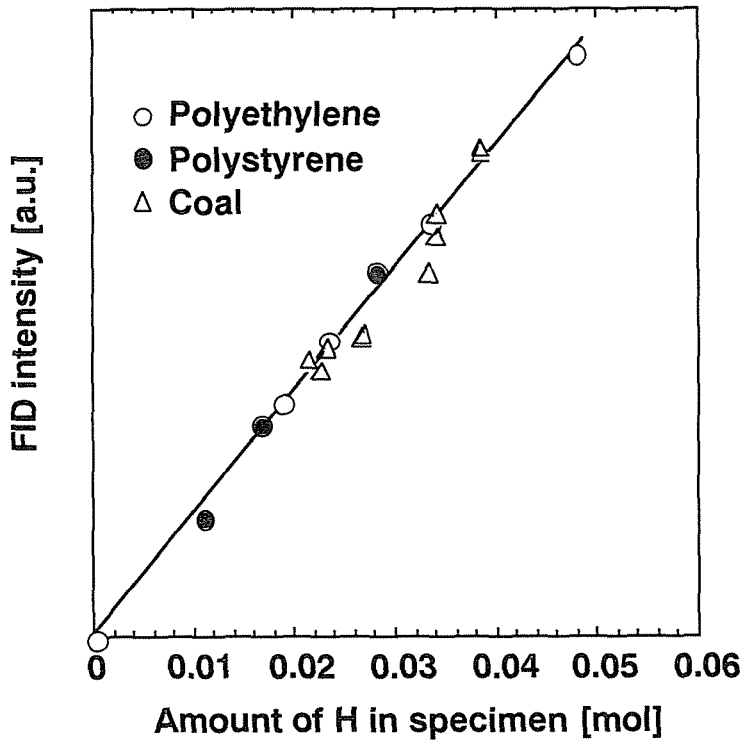

Figure 3.7. Relationship between the amount of hydrogen in the sample and initial intensity of the FID obtained by solid-echo sequence.

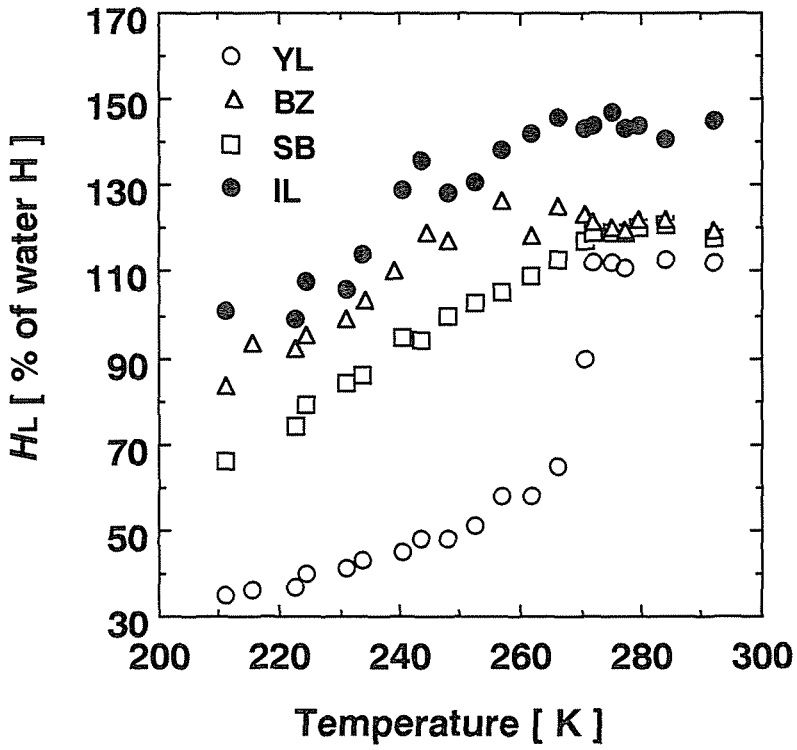

Figure 3.8. Temperature-dependent changes of H_L.

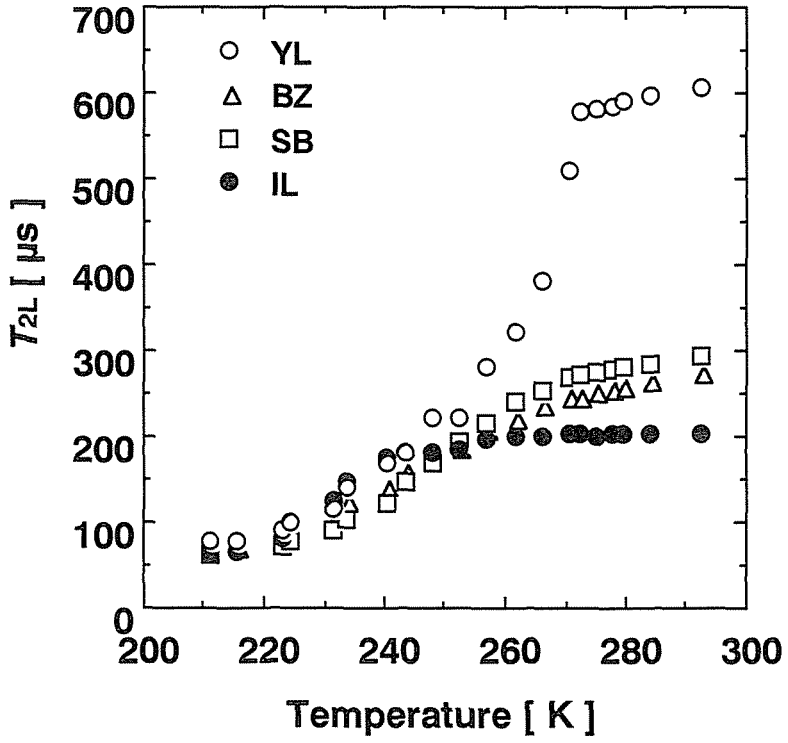

Figure 3.9. Temperature-dependent changes of T_{2L}.

Table 3.3. H_L at 293 and 213 K and Their Difference.

coal	H as H_2O [mol/kg-dried coal]	H_L [%] 293 K (1)	213 K (2)	(1)-(2)
YL	138.7	112	35	76
LY	145.5	108	36	72
MW	150.6	111	41	70
SB	51.1	118	66	52
BZ	52.9	120	84	36
WY	43.4	117	78	39
IL	9.6	145	101	44
BL	5.4	196	181	15

3.4. CONCLUSIONS

The eight different coals were subjected to DSC and NMR analyses in order to characterize and classify the water sorbed in their matrices on the basis of its congelation characteristics. Within the limits of the present experimental conditions, the following conclusions were made:

(1) Two different types of freezable water, namely, free water and bound water were found in DSC, and these two types were quantified from their experimental heat of congelation. Their fractions account for 35-78% of the total, with the balance defined as nonfreezable water.

(2) The congelation of freezable water was also observed in NMR, as the conversion of the slowly decaying components into Gaussian one at 213-273 K. The amounts of the freezable water determined by NMR were in good agreement with those determined by DSC.

(3) The nonfreezable water was determined to be mobile in the NMR sense, i.e., with molecular reorientation rates above 10^5 Hz even at 213 K, and it was thus observed independently from the other types of water.

References

(1) Evans, D. G. *Fuel* **1973**, 52, 186.

(2) Gorbaty, M. L. *Fuel* **1978**, 57, 796.

(3) Deevi, S. C.; Suuberg, E. M. *Fuel* **1987**, 66, 454.

(4) Suuberg, E. M.; Otake, Y.; Yun, Y.; Deevi, S. C. *Energy Fuels* **1993**, 7, 384.

(5) Okuma, O.; Masuda,K.; Murakoshi,K.; Yanai, S-i.; and Matsumura,T. *Nenryoukyoukaishi (in Japanese)* **1990**, 69, 259.

(6) Serio, M. A.; Solomon, P. R.; Kroo, E.; Bassilakis, R.; Malhotra, R.; McMillen, D. *Am. Chem. Soc. Div. Fuel Chem. Prepr.* **1990**, 35(1), 61.

(7) Vorres, K. S.; Wertz, D. L.; Malhotra, V.; Dang, Y.; Joseph, J. T.; Fisher, R. *Fuel* **1992**, 71, 1047.

(8) Song, C.; Saini, A. K.; Schobert, H. H. *Energy Fuels* **1994**, 8, 301.

(9) Gale, T. K.; Fletcher, T. H.; Bartholomew, C. H. *Energy Fuels* **1995**, 9, 513.

(10) Miknis, F. P.; Netzel, D. A.; Turner, T. F.; Wallace, J. C.; Butcher, C. H. *Energy Fuels* **1996**, 10, 631.

(11) Kumagai, H.; Nakamura, K.; Sasaki, M.; Yoneda, J.; Sanada, Y. *Proceedings of International Conference on Coal Science,* Banff, Canada: 1993, Vol. I, p. 136.

(12) Mraw, S. C.; O'Rourke, D. F. *J. Colloid Interface Sci.* **1982**, 89, 268.

(13) Nakamura, K.; Hatakeyama, T.; Hatakeyama, H. *Polymer* **1983**, 24, 871.

(14) Mraw, S. C.; Naas-O'Rourke, D. F. *Science* **1979**, 205, 901.

(15) Barton, W. A.; Lynch, L. J. *Proceedings of 6th Australian Coal Science Conference* Newcastle, **1994**, p 65.

(16) Rennie, G. K.; Clifford, J. *J. Chem. Soc. Faraday Trans.* **1977**, 73 I, 680.

(17) Nakamura, K.; Hatakeyama, T.; Hatakeyama, H. *Polymer* **1981**, 22, 473.

(18) Nakamura, K.; Hatakeyama, T.; Hatakeyama, H. *Text. Res. J.* **1983**, 53, 682.

(19) Sheng, P.; Cohen, R. W.; Schrieffer, J. R. *J. Phys. C:Solid State Phys.*

1981, 14, 565.

(20) Lynch, L. J.; Barton, W. A.; Webster, D. S. *Proceedings of the 16th Biennial Low-Rank Fuels Symposium*; Groenewold, G. H., Ed.; Energy and Environmental Reseach Center: Montana, **1991**, p 187.

(21) Gerstein, B. C.; Chow, C.; Pembleton, R. G.; Wilson, R. C. *J. Phys. Chem.* **1977**, 81, 565.

(22) Cutmore, N. G.; Sowerby, B. D.; Lynch, L. J.; Webster, D. S. *Fuel* **1986**, 65, 34.

(23) Graebert, R.; Michel, D. *Fuel* **1990**, 69, 826.

(24) Yang, X.; Garcia, A. R.; Larsen, J. W.; Silbernagel, B. G. *Energy Fuels* **1992**, 6, 651.

(25) *Quantitation of Protons in the Argonne Premium Coals by Solid State ^{1}H-NMR*; Rosa, L. D.; Pruski, M.; Gerstein, B. C., In *Magnetic Resonance in Carbonaceous Solids*; Botto, C. E., Sanada, Y., Eds.; Advances in Chemistry; American Chemical Society: Washington, DC, **1993**, *229*,359.

(26) Lynch, L. J.; Webster, D. S. *Fuel* **1979**, 58, 429.

(27) Vorres, K. S. *User's Handbook for the Argonne Premium Coal Sample Program*; Argonne National Laboratory, Argonne: IL, 1993.

(28) Solomon, I. *Phys. Rev.* **1958**, 110, 61.

(29) Powles, J. G.; Mansfield, P. *Phys. Lett.* **1962**, 2, 58.

(30) Thomas, D. G.; Stavely, L. A. K. *J. Chem. Soc.* **1952**, 5, 4569.

(31) Eisenberg, D.; Kauzmann, W. *The Structure and Properties of Water*; Oxford at the Clarendon Press: London, 1969.

(32) Yang, X.; Larsen, J. W.; Silbernagel, B. G. *Energy Fuels* **1993**, 7, 439.

(33) Lynch, L. J.; Webster, D. S.; Barton, W. A. *Adv. Magn. Reson.* **1988**, 12, 385.

(34) Barton, W. A.; Lynch, L. J.; Webster, D. S. *Fuel* **1984**, 63, 1262.

CHAPTER 4

Evaluation of Effect of Predrying on Porous Structure of Water Swollen Coal Based on Freezing Property of Pore Condensed Water

4.1. INTRODUCTION

When partially or completely dried brown coals or lignites are exposed to water, they swell but often do not regain their original volumes.[1, 2] Such an irreversible change induced by drying has been attributed partly to collapse of the colloidal gel[1, 3,4] accompanied by the formation of stronger and shorter hydrogen bond bridges between coal macromolecules. The gel collapse could limit the accessibility of organic solvents[5] and mass transfer in aqueous media.[4] Water sorption isotherm on bed moist brown coal[6] shows strong hysteresis between the desorption and re-adsorption curves, and the hysteresis persists to very low relative vapor pressures. At relative vapor pressures above 0.5, the hysteresis can be explained by the normal capillary condensation mechanism with vapor pressure lowering according to the Kelvin equation.[7] Although there is still no generally accepted mechanism to explain the persistence of the hysteresis loop in the multilayer and monolayer water region of the isotherms, the hysteresis would be attributed to difference in the mechanisms between adsorption and desorption, associated with swelling and shrinkage effects, and irreversible collapse or shrinkage of capillaries on the drying. The present study has been undertaken to understand the irreversible nature of the colloidal gel structure of coal in water removal and swelling cycle focusing on its porous structure.

Conventional techniques, such as gas adsorption/desorption and mercury porosimetry, which are utilized only for characterizing dry materials, can hardly be applied to pore structure analysis of the water containing systems. Because irreversible pore collapse and a considerable reduction in the internal porosity would be induced by the drying. Hence there is no choice other than using water itself as a probe molecule to investigate the porous structure of coal sorbing water. In general, water sorbed in or on solid materials, such as coal, has properties that differ from those of bulk water in its normal thermodynamic states.[8-14] Norinaga et al.[14] classified water sorbed in coals of various types on the basis of its freezing properties, which were evaluated by using a combination of differential scanning calorimetry (DSC) and proton magnetic resonance (^{1}H NMR) techniques. They found two different types of freezable water; free water identical to bulk water and bound water that freezes at around 226 K. These two types of water account for only 35-78 % of the total water content, leaving nonfreezable water. Bound water has lower freezing point temperatures and congelation enthalpy than bulk water. The difference in the freezing properties of bulk and bound water would be directly related to the size of a cluster of water molecules, that is, the size of the space in which they are condensed. The lowered melting or freezing temperature of solid or liquid in pores has frequently been ascribed to a very small cluster size in the pore[15, 16] and the large surface to volume ratio of material condensed in a capillary.[16] The thermodynamic stability of small crystals formed from liquid confined within pores has been treated by Gibbs,[17] who demonstrated that the melting transition temperature of pore material depends on surface curvature. A related theory was derived by Thompson[7] in terms of the effect of the curvature on vapor pressure of liquid droplets. The Gibbs and Thompson equations can be combined to relate the reduction in the transition temperature to the crystal dimensions. For a liquid confined within a pore in which a crystal is forming, assuming the contact angle between liquid, solid, and pore wall is 180°, the temperature reduction ΔT is given by the Gibbs-Thompson equation as $\Delta T=(2\gamma_{s,l}T_0/r\rho\Delta H)$, where $\gamma_{s,l}$ is the surface free energy at liquid-solid interface; T_0 is normal

bulk melting point; r is radius of the crystal; ΔH is the heat of fusion; and ρ is the density of the solid formed by the phase transition. It is thus possible to predict the pore size distribution from the freezing point distribution of water in pores by employing Gibbs-Thompson equation as a theoretical basis. So far, inorganic porous materials have been characterized on the basis of freezing or melting properties of water confined in the pores which were evaluated by ^{1}H NMR,[18-25] DSC,[26, 27] or combination of them.[28] The ^{1}H NMR technique is particularly suited to studying freezing phenomena. Because of the large reduction in the transverse relaxation time of water when it turns into ice, it is easy to measure the signals due to water remaining unfrozen in a sample. By following the signals during cooling of the sample we can see how much of the pore water is frozen at any particular temperature.

In the present study, we present the pore size distribution of the rewetted coal samples prepared from non-, partially and completely pre-dried coals. Three kinds of as-received coals ranging from brown to bituminous were used. The pore size distribution was estimated on the basis of the freezing property of water in the coal samples evaluated by ^{1}H NMR in the temperature range from 170 to 294 K. The effect of the extent of pre-drying and coal type on the pore structure of coal after rewetted is discussed.

4.2. EXPERIMENTAL SECTION

4.2.1. Coal samples

Two Argonne Premium Coal Sample Program (PCSP) coals[29] and a brown coal were studied. Lumps of the brown coal were supplied from the Nippon Brown Coal Liquefaction Co. Ltd., Japan and the Coal Corp. of Victoria, Australia. They were stored in gastight drums during transportation to prevent evaporation of water. The elemental compositions, ash and water contents of the coal samples are listed in Table 3.1. Yallourn (YL) coal was pulverized to sizes finer than 150 μm in a globe bag filled with nitrogen gas saturated with water vapor. Figure 4.1 presents the procedure of the sample preparation. Each coal sample was stored at 293 K in a gastight vessel filled with nitrogen gas saturated with water vapor for more than 2 weeks prior to

use. The water content of the coal samples was determined from the fractional mass release by drying at 380 K under a nitrogen gas flow for 2 h in a thermobalance (TG-2000S, Mac Science Co. Ltd.). For each coal, samples with different residual water contents were prepared at 303 K by varying the relative humidity in the closed container from 5 to 97% using aqueous solutions saturated with selected inorganic salts (Table 4.1).[1] The water content of the partially dried samples was determined in the same manner as described above. Hereafter, the water content will be referred to as w and indicated in the unit of g-water per gram of moisture free coal. The completely dried samples were prepared by drying under a pressure of 1 Pa at 303 K for 48 h, long enough to reach a constant weight. The amount of free, bound and nonfreezable water contained in the as received samples were determined by DSC as reported in the previous work.[14]

4.2.2. ^{1}H NMR

The coal sample was weighed and transferred to an NMR tube of 10 mm o.d.. The mass of the samples on a dry coal basis was 0.1 g for YL, 0.15 g for BZ, or 0.2 g for IL coal. A 5 ml aliquot of pure water was then added to the sample and the content was vigorously stirred with a thin rod to remove gas trapped in the slurry under nitrogen atmosphere. The tube was sealed and then stored in an air bath kept at 303 K over a week, long enough to equilibrate the swelling. After centrifuging the content, the excess water was removed via canular to let the mass of the water saturated samples approximately be 0.4 g for YL and 0.35 g for BZ, and 0.3 g for IL coal, respectively. The removal was done to minimize the inhomogeneity of magnetic field influencing the observed transverse relaxation. The water content of the swollen sample will be referred to as W and indicated in the unit of g-water per gram of moisture free coal. Since W of the sample is much larger than w of as received state, all the pores of coal samples are expected to be fulfilled with water. The free induction decays (FID) after a single 90 degree pulse were measured at temperature intervals of 2-5 K while cooling from 294 K to 170 K using a JEOL Mu-25 NMR spectrometer operating at 25 MHz proton

resonance frequency. The signal at each temperature was recorded under temperature equilibration. Typical values for the pulse width, repetition time, and number of scans were 2.0 μs, 6 s, and 16, respectively. Details of the NMR measurement were described elsewhere.[14] A particular procedure was adopted to measure the freezing process of water without significant supercooling. The preliminary observation showed that the temperature had to be lowered to about 258 K before spontaneous freezing of bulk water took place. Thus, the sample was cooled at 253 K for 10 min after measuring the FID at 274 K, and then warmed to 272 K. This procedure ensured that all the interparticle and bulk water was frozen out before the actual recording of the FID below 272 K was started.

4.2.3. Swelling and specific gravity measurements in water

The effect of pre-drying on volume of rewetted coal was examined by employing a conventional solvent swelling technique.[30] About 0.3 g of the coal sample with known w was put in a cylindrical glass tube. About 5 ml of water was added to the sample and the content was vigorously stirred under nitrogen atmosphere. The tube was sealed and stored at 303 K over a week. The content was then centrifuged and the height of the bed of water-swollen coal, H_w, was measured. Here, the height of the coal particle bed per unit mass of coal on a dry basis, $H_w{}^n$, is defined as,

$$H_w{}^n = \frac{H_w(1+w)}{m} \tag{4.1}$$

where, m is the mass of the coal samples. Under the assumption that the volumetric fraction of the swollen coal particles to the total bed volume is constant at any w, the volume of the swollen coal at w relative to that at the as-received state is given by $H_w{}^n / H_{wi}{}^n$ where wi indicates the w of the raw coal. The apparent densities of the nondried and completely dried coal samples were also measured by a pycnometry. Approximately 0.25 g of the sample and about 4 ml of water were introduced in a 5 cm^3 of Wadon type specific

gravity bottle and the content was vigorously stirred with a thin rod. The bottle placed in a vacuum desiccator and the pressure was gradually reduced to remove gas trapped in the slurry. The bottle was placed in an air bath kept at 303 K over a week, before levelling the water and weighing. The reproducibilities on the determinations of H_w^n / H_{wi}^n and the density were within ±2% and ±0.5%, respectively.

Table 4.1. Solutions Used for Controlled Humidity Atmospheres.

solute	relative humidity at 303 K [%]
None	100
K_2SO_4	97
KNO_3	91
KCl	84
NaCl	75
$Mg(NO_3)_2$	52
CH_3COOK	22
KOH	7
H_2SO_4 (conc.)	0

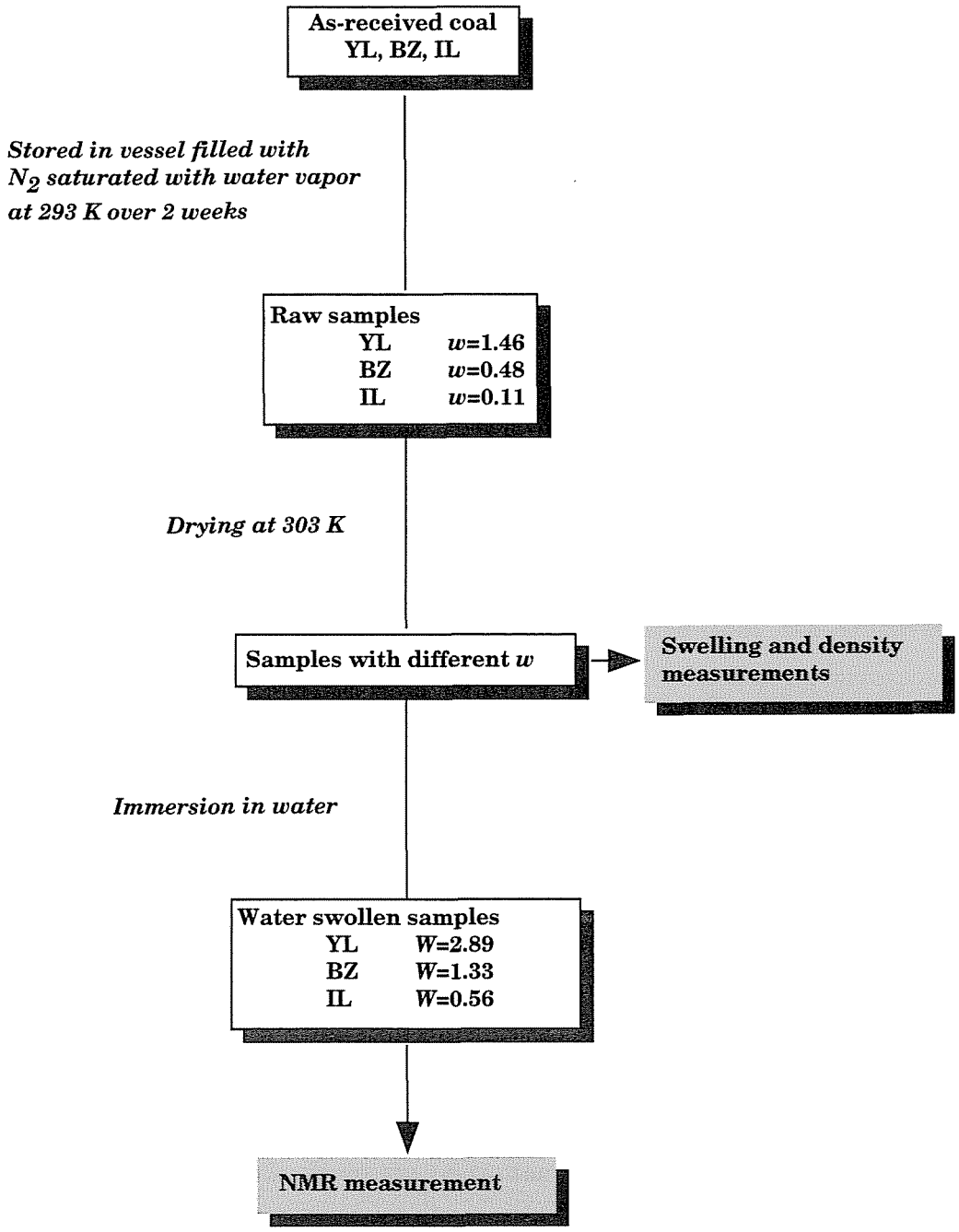

Figure 4.1. Procedure of sample preparation

4.3. RESULTS AND DISCUSSION

4.3.1. Volume of water condensed in coal pores

Figure 4.2 illustrates FIDs of YL with $w = 1.46$ at different temperatures. Each FID consists of two different decays; a rapid Gaussian decay arisen from "rigid" or "immobile" protons and a slow exponential decay from "mobile" protons. The mobile protons involve the water protons and a portion of coal protons, the latter of which are nearly identical with hydroxylic protons interacting with water as a plasticizing agent via hydrogen bonds.[31] The rigid protons can be attributed to ice protons at temperatures below the freezing point temperature of bulk water as well as rigid coal protons representing a major portion of coal protons. The spin-spin relaxation times of ice and rigid coal proton are known to be 6 μs[20] and less than 30 μs,[32] respectively. It is therefore reasonable to assume that the transverse magnetization at 40 μs at a given temperature, TK, defined as I_T, corresponds quantitatively to the amount of the mobile protons contained in the sample. The validity of this assumption will be discussed later. I_{256}, I_{221}, and I_{190} are definitely smaller than I_{294}, and this is primarily due to the transition of water into ice. I_T for the other samples also changed with temperature in the same manners as YL with $w = 1.46$. At 294 K where ice is never formed, I_{294} represents the sum of the amounts of water protons and mobile coal protons. Since W for YL with $w = 1.46$ is 2.89, the coal contains 0.32 mol of water protons and 0.015 mol of mobile coal protons[31] when the coal is exposed to excess amount of water at 294 K. Thus the percentage of the latters to total mobile protons is 4.5%, while the percentages for BZ and IL coals were 5.4% and 4.6%, respectively. Although the mobile coal protons can never be distinguished from the water protons, their fraction to the total mobile protons is small enough to consider I_{294} represents the amount of water protons for expedience. Based on the above discussion, the amount of water per unit mass of dry coal at T is here defined as $W(T)$, which can be expressed in the unit of g-water per gram of moisture free coal by

$$W(T) = W(294)\left(\frac{I_T}{I_{294}}\right) \tag{4.2}$$

$W(T)$ can be further converted into the volume of water, $V(T)$, in the unit of cm^3-water per gram of moisture free coal by assuming the density of water to temperature-independent and 1 cm^3/g.

$$V(T) = W(T) \tag{4.3}$$

Figure 4.3 shows $V(T)$ as a function of temperature for the previously nondried coals. In the course of cooling, the volumes for the all coals are seen to decrease sharply in the range from 273 K to 260 K, indicated as region I. The reduction is attributed to the freezing of bulk water, i.e., extrapore water. However Gibbs-Thompson equation predicts the radius if pores as 5 nm when water filling the pores freezes at 260 K. Thus a portion of bulk water may be confined in pores with sizes larger than the 5 nm. The changes in $V(T)$ in this region are rather continuous and therefore it is difficult to distinguish the freezing of water condensed in relatively large pores from that of extrapore water. The region II ranges from 260 K to 213 K where $V(T)$ decreases due to the freezing of "bound water" condensed in pores having radii smaller than 5 nm. The freezing of bound water is a phase transition of the water into ice, and detected by DSC as an exothermic process.[14] The diminution of $V(T)$ at temperatures lower than 213 K, defined as region III, is also assigned to a transition of pore water that is a non-exothermic process distinct from normal colligative freezing of water. Thus the decrease in the volume in this region would be caused by the reduction of mobility of "nonfreezable water", which should be recognized as an apparent phase transition as discussed extensively by Overloop et al..[20] The above discussion allows to determine the volumes of nonfreezable pore water (V_{nf}), freezable pore water (V_f), and bulk water (V_b) respectively as $V(213)$, decrement of $V(T)$ at 260 - 213 K, and that at 273 - 260 K. V_{nf}, V_f, and V_b are all indicated in the unit of cm^3-water per gram

moisture free coal and hence the sum of these equals to $V(294)$.

V_{nf} and V_f for the coals without the pre-drying are summarized in Table 4.2 and compared with the amounts of nonfreezable water ($W_{nf\text{-}dsc}$) and freezable bound water ($W_{f\text{-}dsc}$) determined previously,[14] respectively. V_{nf} and V_f for YL coal both agree well with the corresponding amounts and the agreement confirms the validity of the above-described procedure analyzing FID. Different from YL, V_f is somewhat larger than $W_{f\text{-}dsc}$ for the other coals. This would be brought about much larger W in the present NMR (1.33 for BZ and 0.56 for IL) than those in the DSC[14] where water contents of the samples were identical with w of raw coals (0.48 for BZ and 0.11 for IL). Considering that the DSC detected no bulk water in the as-received BZ and IL coals,[14] the amount of inherent water would not be enough to fill up and/or fully expand pores in these coals and therefore the significantly larger W could result in greater V_f of the coals.

The raw YL coal with w = 1.46 was partially or completely dried as described in Experimental section so as to let the coal have w ranging from 0 to 0.90. The dried samples were subjected to the DSC analysis and water remaining in the samples was classified into bulk water, freezable bound water and nonfreezable water. The analysis revealed that the drying removed water sorbed in the raw YL coal in the order of bulk, bound and nonfreezable waters as reported elsewhere.[31] The samples having different w were further analyzed by the NMR after swollen in water, and then V_b, V_f, and V_{nf} were determined. In Figure 4.4 are plotted the total volumes of freezable and nonfreezable pore waters, V_p, V_f, and V_{nf} of the samples against w. When w is 0.33 or larger at which bound and/or free water has been removed but nonfreezable water never done, V_p, V_f, and V_{nf} are all seen to remain unchanged. The volumes independent of w indicate that the volume of pores filled with water is not affected by the drying as far as w is greater than 0.33. This result also suggests that the porous structure of YL coal changes reversibly in the drying-swelling cycle unless nonfreezable water is removed. When nonfreezable water is removed by the drying beyond w of 0.33, V_p decreases from 0.64 to 0.53. The change in the volume of water-retaining pores thus

becomes irreversible due to the extensive drying. The reduction of V_p also seems to be caused by the decrease in V_f. Table 4.3 compares V_p, V_f, and V_{nf} for the raw BZ (w = 0.48) and IL (w = 0.11) with those for completely dried samples at w = 0. The complete drying of IL reduces V_f thereby decreasing V_p as observed in the drying of YL coal. The drying of BZ seems to decrease V_{nf} slightly as well as V_f while the reduction of the former is smaller. The results shown in Figure 4.4 and Table 4.3 prove that the irreversible volumetric shrinkage of the coals can be evaluated as the decrease in volume of pores, which is described quantitatively by the reduction of volume of pore condensed water. It is also demonstrated that the removal of inherent nonfreezable water is responsible for the irreversible change.

The irreversible volumetric shrinkage of coals was also examined by employing the conventional solvent swelling technique.[30] Table 4.4 presents V_p, volumetric recovery, H_w^n / H_{wi}^n, and the density measured in water, ρ_c, for the raw and the completely pre-dried coals which were subsequently immersed in water. For all the pre-dried coals, H_w^n / H_{wi}^n are smaller than unity, that implies an incomplete recovery of the volume at a swollen state, namely an irreversible volumetric shrinkage induced by the drying. H_w^n / H_{wi}^n becomes smaller as the coal rank decreases. On the other hand, the drying had little effect on the density as measured by the water pycnometry. This would means that the volume of dense part of the coal samples, i.e., the excluded volume of coal macromolecules is not altered irreversibly by the drying. The coal volume swollen by water, V_c, which include the volumes of dense and porous parts, can be expressed as

$$V_c = 1/\rho_c + V_p \qquad (4.4)$$

V_c of the swollen coal at w = 0 relative to that at the raw state is here defined as f_V and shown in Table 4.4. f_V becomes smaller as the coal rank decreases as H_w^n / H_{wi}^n does. Thus the irreversible decrease in H_w^n / H_{wi}^n upon drying can be partially attributed to the irreversible change in V_p which leads to the loss of moisture holding capacities. The collapse, shrinkage of pores, or both

of them induced by drying would contribute to the irreversible reduction of pore volume. f_V larger than ${H_w}^n / {H_{wi}}^n$ indicates that the irreversible change of the latter is due not only to the decrease in V_p but also to collapse of macropores ruled out from V_p or increase in packing efficiency of the particles due to changes in their shapes.

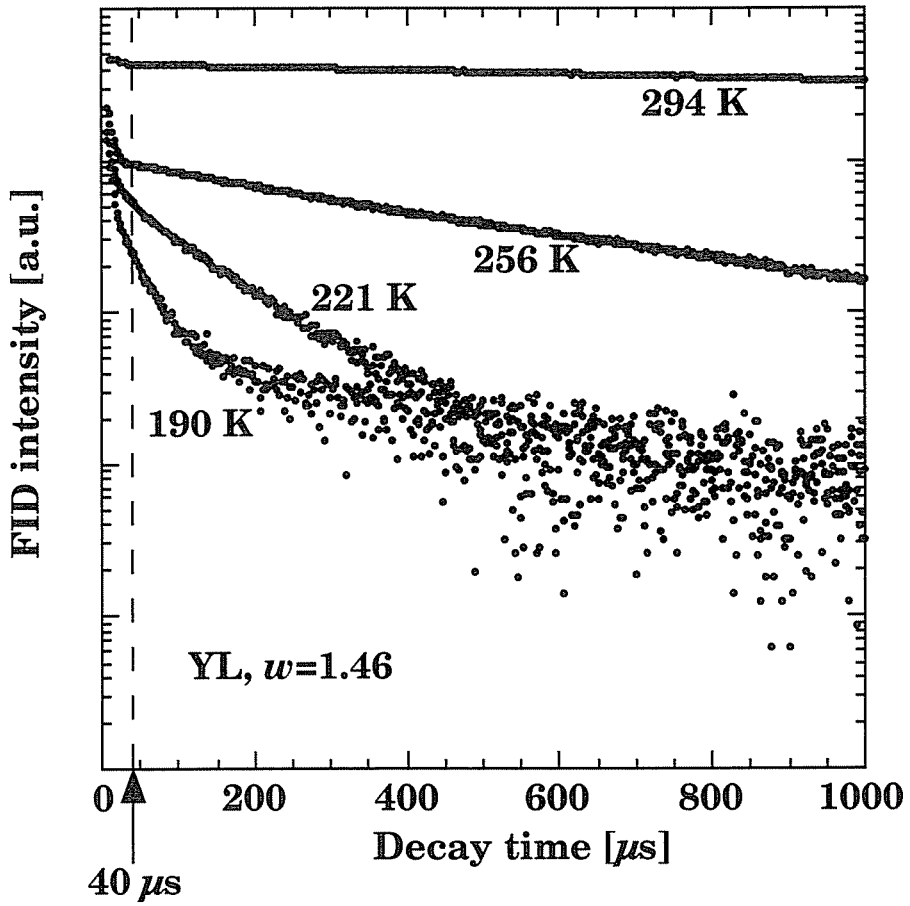

Figure 4.2. Temperature dependent changes of ^{1}H NMR transverse relaxation signals for YL coals. (w=1.46, W=2.89)

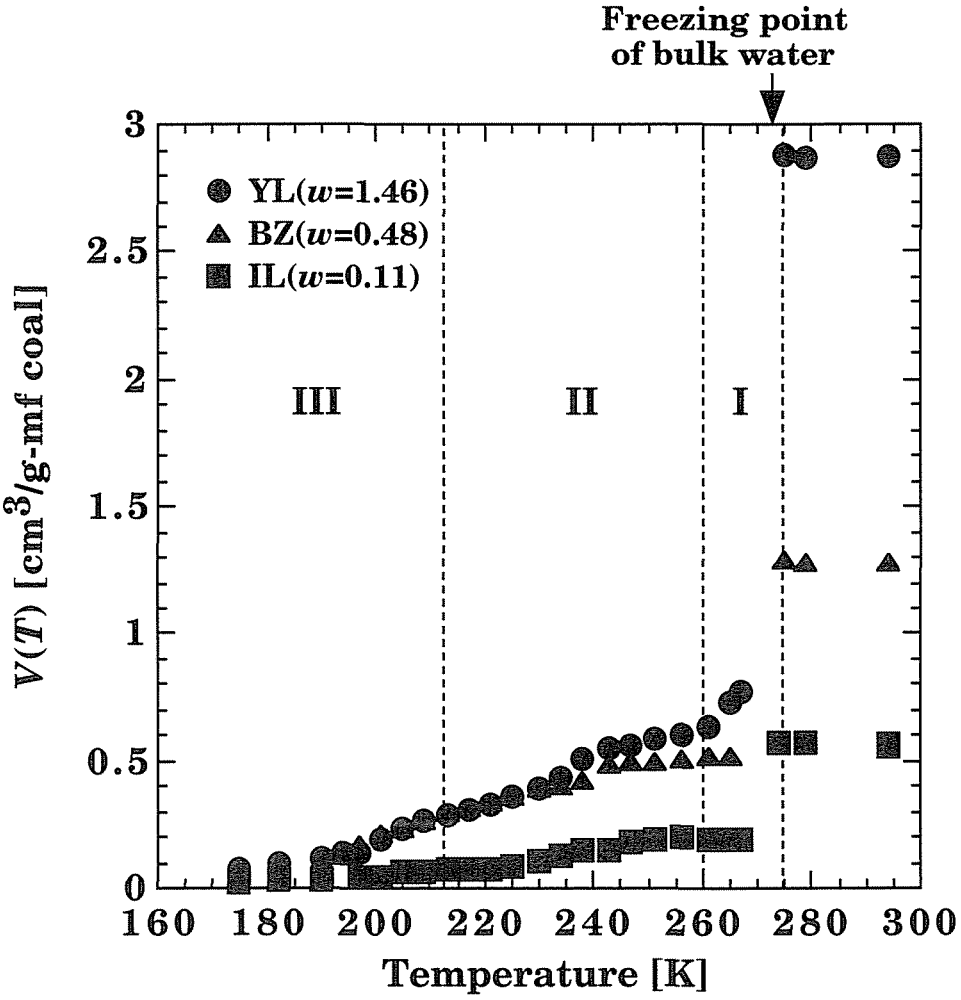

Figure 4.3. Change in V with temperature for the sample prepared from raw samples. Region I(273 - 260 K); freezing of bulk water, Region II(260 - 213 K); freezing of pore condensed water, Region III(less than 213 K); reduction of mobility of nonfreezable pore water

Table 4.2. Comparison of V_f, V_p, and V_{nf} with the Amount of Bound, Nonfreezable Water, and Sum of These Two Types Waters

	^{1}H NMR			DSC [a]		
coal [b]	V_f,	V_{nf}	V_p	$W_{f\text{-}dsc}$	$W_{nf\text{-}dsc}$	sum
	[cm^3/g-mf coal]			[cm^3/g-mf coal] [c]		
YL	0.32	0.32	0.64	0.35	0.30	0.65
BZ	0.24	0.27	0.51	0.17	0.31	0.48
IL	0.13	0.06	0.19	0.05	0.05	0.10

[a] ref. 14. [b] raw samples. [c] represented by volumetric unit by assuming the density of water as 1 g/cm^3.

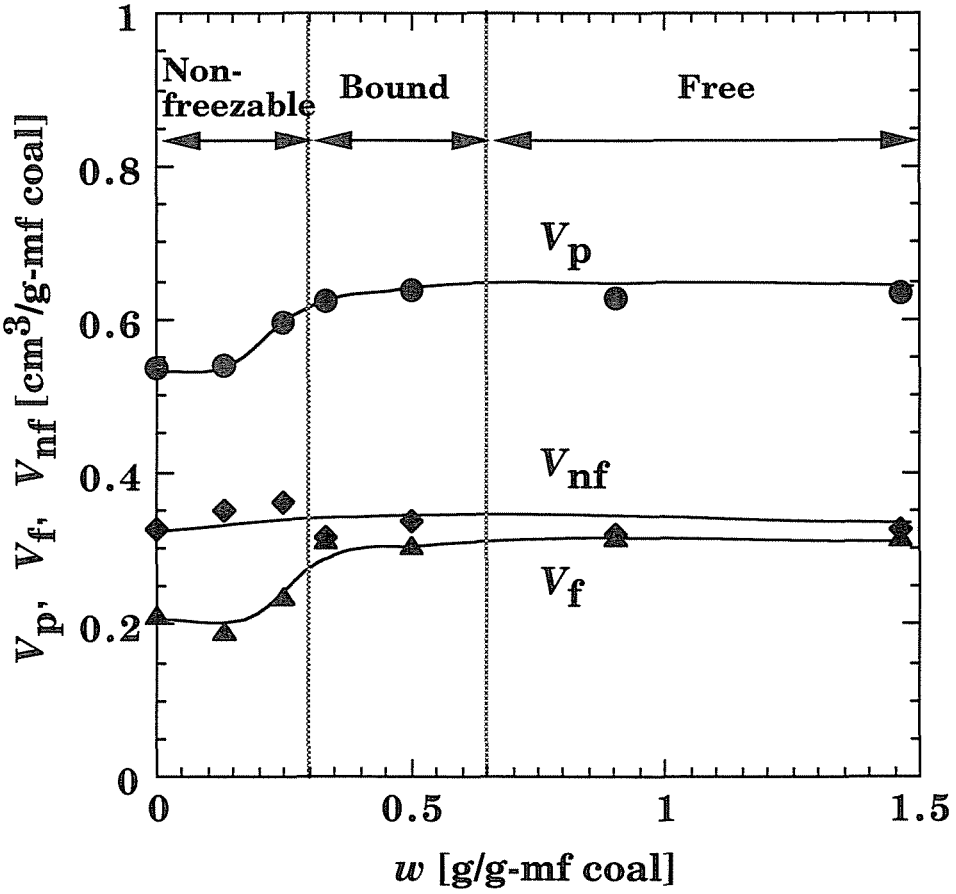

Figure 4.4. Change in V_f, V_{nf}, and V_p with w for YL coal .

Table 4.3. Comparison of V_p, V_f, and V_{nf} for Raw BZ and IL with Those for Completely Pre-Dried Samples.

coal	w [g/g-mf coal]	V_f, [cm^3/g-mf coal]	V_{nf}	V_p
BZ	0.48	0.24	0.27	0.51
BZ	0	0.17	0.24	0.41
IL	0.10	0.13	0.06	0.19
IL	0	0.10	0.06	0.16

Table 4.4. V_p, H_w^n / H_{wi}^n, ρ_c, and f_V of Raw and Completely Pre-Dried Coals Subsequently Immersed in Water.

coal	w [g/g-mf coal]	V_p [cm^3/g-mf coal]	H_w^n / H_{wi}^n [-]	ρ_c [g/cm^3-mf coal]	f_V [-]
YL	1.46	0.64	1.00	1.49	1.00
YL	0	0.53	0.75	1.51	0.91
BZ	0.48	0.51	1.00	1.53	1.00
BZ	0	0.41	0.80	1.52	0.92
IL	0.11	0.19	1.00	1.44	1.00
IL	0	0.16	0.93	1.46	0.96

4.3.2. Freezing point distribution of pore confined water

In order to estimate the size of pores which dominantly involved in the change in V_p, the freezing properties of the freezable pore water are further analyzed. It is well known that the freezing point temperature of pore condensed water is a function of the pore size. The distribution in size of pores retaining freezable water can be derived from that in the freezing point for the water. Figure 4.5 shows the volume of freezable water that has not yet been converted into ice, V, as a function of inversed temperature X(=1000/T) for the samples prepared from raw YL, BZ, and IL coals. $V(X)$ at upper limit of X at 3.85 (T = 260 K) and the lower limit at 4.69 (T = 213 K) are identical to V_p and V_{nf}, respectively. Each of solid lines drawn in the figure represents $V(X)$ given by an integrated Gaussian distribution function according to Schmidt et al. who analyzed the freezing properties of water confined in the mesoporous silica materials.[22]

$$V(X) = \frac{V_p}{\sqrt{\pi}} \int_0^{\frac{X-X_c}{\sqrt{2}\Delta}} \exp(-u^2)du + k = \frac{V_p}{2} \mathrm{erf}\left(\frac{X-X_c}{\sqrt{2}\Delta}\right) + k \qquad (4.5)$$

where X_c, Δ and k are X at the center of the distribution, the width of the distribution and a integral constant, respectively. These parameters were determined by fitting the calculated $V(X)$ to the observed one using a nonlinear least-squares method. Table 4.5 summarizes the combinations of X_c and Δ giving the best fit to $V(X)$ observed for the individual samples. The temperature at the center of distribution for the samples, T_c (=1000/X_c) , is in the range from 222 K to 233 K and the range agrees well with that where the DSC[14] detected exothermic peaks arisen from the congelation of freezable bound water, around 227 K. By differentiating eq 4.5 with respect to X, we obtain

$$\frac{dV}{dX} = \frac{V_p}{\sqrt{2\pi}\Delta} \exp\left(-\frac{X-X_c}{\sqrt{2}\Delta}\right)^2 \qquad (4.6)$$

Figure 4.5 presents dV/dX for the individual coals with different w as a function of X. The removal of nonfreezable water prior to swelling of YL coal, resulting in w less than 0.33, is seen to shift the freezing point distribution (FPD), toward larger X corresponding to lower T. The shift due to the decrease in w from 1.46 to 0.33 is smaller than the above. For the other coals, the FPD also shifts toward larger X by complete drying, although the changes are less significant than those for YL coal. According to Gibbs-Thompson equation, freezing of pore water at larger X is interpreted as pores smaller in size. Thus the results suggests an irreversible shrinkage of pores induced by drying.

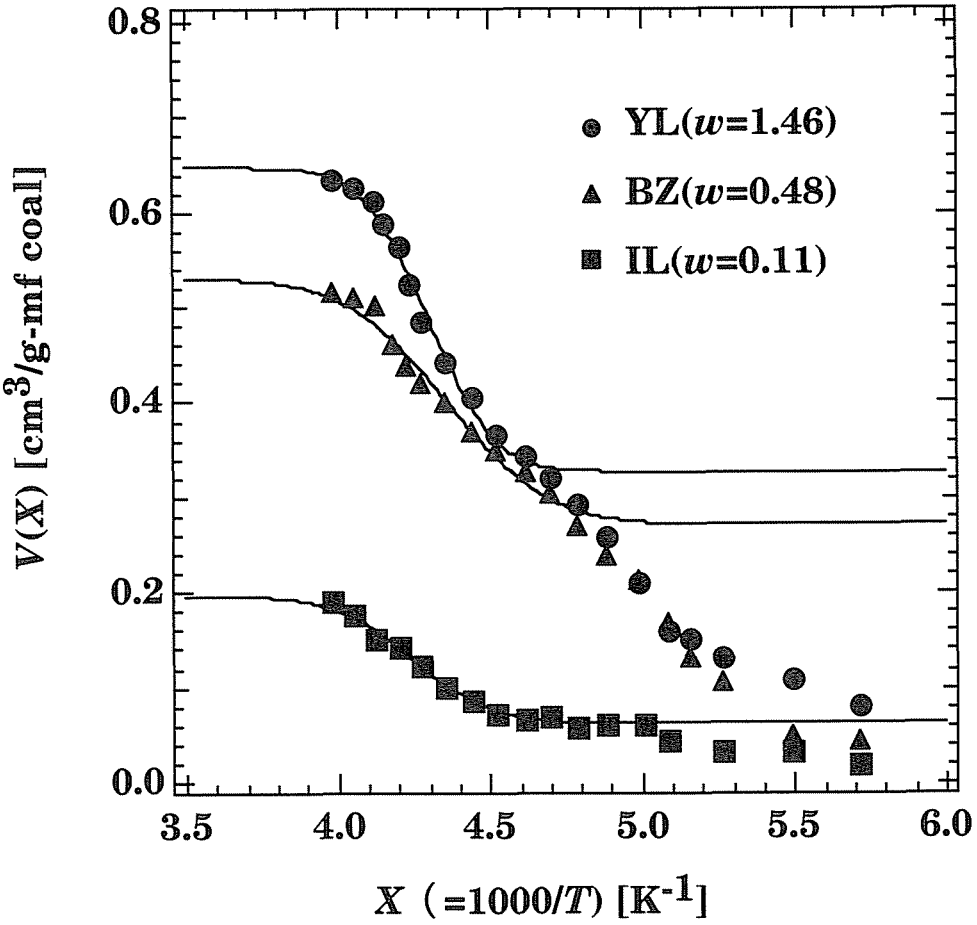

Figure 4.5. V versus inversed temperature X (=1000/T) for the samples prepared from as received YL, BZ, and IL coals. Solid lines represent nonlinear least-squares fit to eq 4.6.

Table 4.5. Values of the Analytical Fit of the Intensity versus Inversed Temperature Curves.

coal	w [g/g-mf coal]	X_c (T_c) [K^{-1}] ([K])	Δ
YL	1.46	4.30 (233)	0.17
YL	0.33	4.31 (232)	0.22
YL	0.25	4.35 (230)	0.16
YL	0.13	4.48 (223)	0.26
YL	0	4.50 (222)	0.28
BZ	0.48	4.36 (229)	0.27
BZ	0	4.38 (228)	0.25
IL	0.11	4.25 (235)	0.21
IL	0	4.30 (233)	0.13

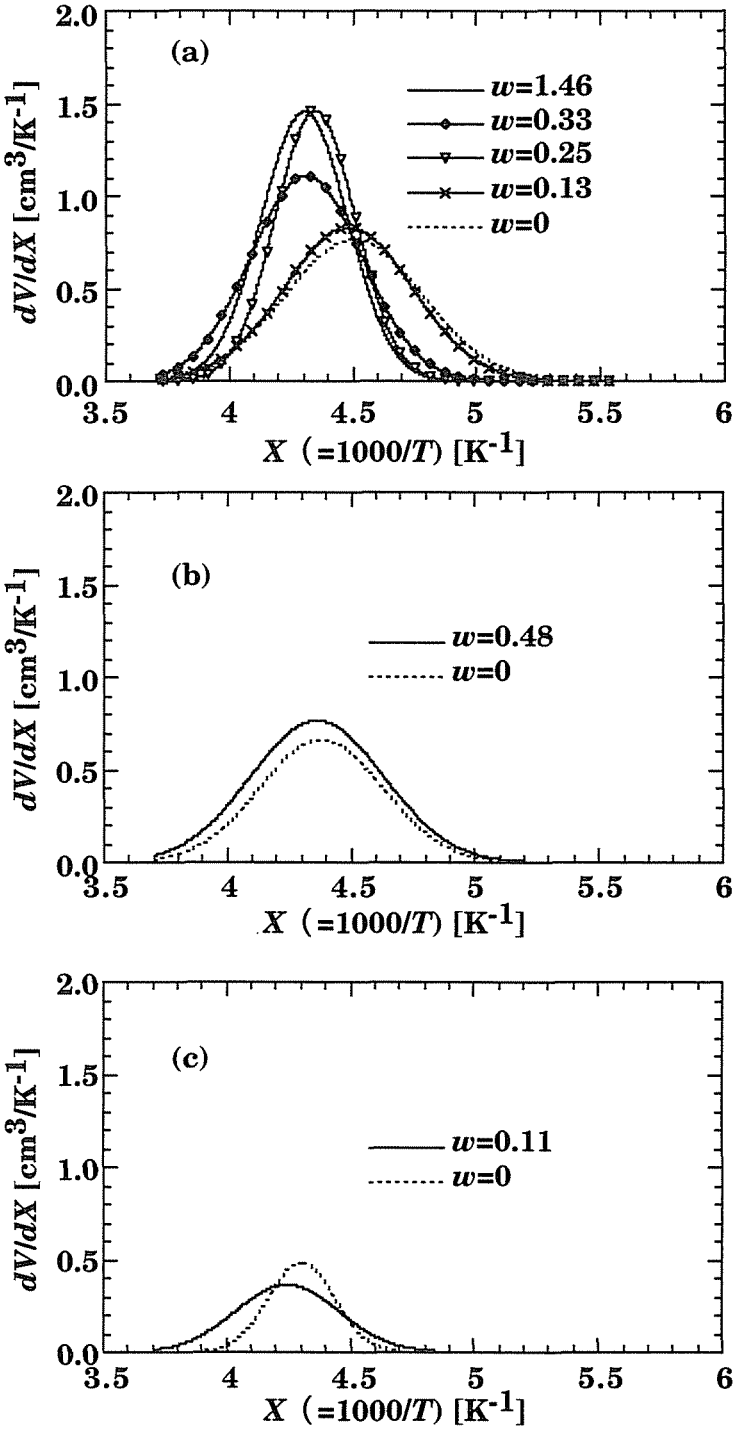

Figure 4.6. Freezing point distribution of freezable pore water for YL (a), BZ (b), and IL (c) coals.

4.3.2. Estimation of size distribution of pores retaining freezable and nonfreezable waters

A theoretical basis for the analysis of the FPD is Gibbs-Thompson equation which relates the freezing point depression (ΔT) of a liquid filling a pore to the pore dimension or radius, r. Assuming all the parameters in the equation to be independent of the temperature and pore dimension, this equation will take a simple form by

$$\Delta T = \frac{\alpha}{r} \tag{4.7}$$

The coefficient α is characteristic of the condensed liquid and will also depend on the interaction between the condensates and host materials. Presented in the form of Gibbs-Thompson equation, it is assumed that the parameters can be represented as those of the bulk liquid. However it is well known that the molar heats of fusion of a number of organic liquids confined in the pores of glasses decrease with decreasing pore radius smaller than 10 nm.[33] The lower heat of fusion of freezable bound water in coals than that of bulk water has been also reported.[8, 9, 14] Furthermore, many different values of the ice-water interfacial tension have been reported or assumed tacitly in the literature.[34-39] Accordingly, the inverse proportional coefficient α must be calculated based on a presumed model of pore structure of coal as described later. In addition to the above, eq 7 assumes r equivalent of the dimension of crystalline solid formed by phase transition. A portion of pore water in the present systems is nonfreezable as described above. This type of water may not be isolated from freezable water and would act as an interface shield between the solid coal matrix and the inner ice core as has been reported by some workers.[26, 27] This concept allows to present the actual pore radius, R_p, given as the sum of r and the thickness of the layer of nonfreezable water, β, which would depends on the surface chemistry of the pore wall. Eq 4.7 is then modified as

$$R_p = \frac{\alpha}{\Delta T} + \beta \qquad (4.8)$$

The assumptions put forward in the development of the model of the porous structure of water-swollen coal are:

(i) Pores are isolated from one another

(ii) All pores are cylindrical in shape as shown schematically in Figure 4.7.

(iii) Nonfreezable water exists exclusively at the interface between the core of ice from freezable bound water and pore wall.

(iv) β is independent of pore radius, temperature and w, and assumed to be 0.6 nm for YL and BZ coals and 0.3 nm for IL coal.

Although there is little information available for the determination of β values for coal at present, the following discussion may support the assumption (iv). Since water becomes nonfreezable when the molecular cluster is too small, nonfreezable water is likely to be dispersed on a molecular scale. It would bound to specific sites via specified interactions such as hydrogen bonds with hydrophilic sites in the coal matrix. The amounts of hydroxyl groups, determined by a hydrogen-deuterium exchange technique,[31] are 8.1 mmol/g-mf coal for YL, 8.4 for BZ, and 4.2 for IL coal. Thus, the numbers of nonfreezable water molecule per one mole of hydroxyl groups are 2.0 for YL, 2.0 for BZ, and 0.7 for IL coal, respectively. If it is assumed that the walls of pores where water condensed are covered thoroughly by hydroxyl groups as the most important hydrophilic sites, the number of monolayers of the nonfreezable pore water can be approximated to be two for YL and BZ coals while one for IL coal. The β values, are then supposed to be 0.6 nm for YL and BZ coals and 0.3 nm for IL coal, since the van der Waals radius of water molecule is about 0.3 nm. β determined here is within the range of that for porous silica, that has been hypothesized or experimentally determined to be one to three monolayers.[26, 40-46]

For the cyrindrical shaped pore model, the ratio of the entire volume

of pores, V_p, to the volume of the freezable pore water, V_{fp}, can be expressed by

$$\frac{V_p}{V_{fp}} = \frac{V_{fp} + V_{nf}}{V_{fp}} = \left(\frac{R_p(\text{ave})}{r(\text{ave})}\right)^2 = \left(1 + \frac{\beta}{r(\text{ave})}\right)^2 \tag{4.9}$$

where R_p(ave) and r(ave) are the volume averaged radius of the actual pore and the ice core, respectively. r(ave) can be given by

$$r(\text{ave}) = \frac{\alpha}{T_0 - T_c} \tag{4.10}$$

Then, α can be determined by combining eq 4.9 and 4.10

$$\alpha = \frac{\beta(T_0 - T_c)}{\sqrt{V_p/V_{fp}} - 1} \tag{4.11}$$

As listed in Table 4.6, α ranges from 45 to 57 (in nm K) depending on the samples, and is in good agreement with the values reported by Schmidt et al..[22] They estimated α to be about 50 for water confined in the regular mesoporous MCM-41 materials having pore radii ranging from 1 to 3 nm, by combining ^{1}H NMR and N_2 adsorption data.

It is possible to derive a function describing the pore size distribution (PSD), dV_p/dR_p, from FPD and the determined values of α and β by noting that

$$\frac{dV}{dR_p} = \frac{dV}{dX}\frac{dX}{dR_p} \tag{4.12}$$

and

$$X = \frac{10^3(R_p - \beta)}{(R_p - \beta)T_0 - \alpha} \tag{4.13}$$

By combining eqs 4.6, 4.12, and 4.13, the following formula is derived

$$\frac{dV}{dR_p} = \frac{10^3\alpha}{\{(R_p - \beta)T_0 - \alpha\}^2} \frac{V_p}{\sqrt{2\pi}\Delta} \exp\left(-\frac{X - X_c}{\sqrt{2}\Delta}\right)^2 \tag{4.14}$$

All symbols are previously defined. The PSD curves, dV_p/dR_p vs R_p are displayed in Figure 8. R_p distributes over the range of 1 - 3 nm. For YL coal, the distribution is seen to shift toward smaller R_p with decreasing w from 0.33 to 0 where the inherent nonfreezable water removed, while the change in the distribution is much less significant at greater w where the free and bound water removed. The mean pore radius, R_p(ave) (=r(ave)+β), were calculated and listed in Table 6. R_p(ave) reduced from 2.0 nm at w = 1.46 to 1.6 nm at w = 0. Thus the change in the PSD clearly demonstrates that the irreversible decrease in V_p can be explained by an irreversible shrinkage of pores with radii approximately 2 nm, abundant in the raw coal. For BZ coal, the PSD seems to shift slightly towards smaller R_p, with water removal while no meaningful changes were observed for IL coal, suggesting that the effect of drying on the irreversible change in the porous structure become less significant with increasing coal rank.

Finally we address how affect the drying on the surface area of coal. For the cylindrical shaped pores, the specific surface area of the water swollen coals, S_{H2O}, can be given by

$$S_{H_2O} = \frac{2V_p}{R_p(\text{ave})} \tag{4.15}$$

In Table 4.6, S_{H2O} are listed with the reported surface area of each dried coal evaluated by CO_2 gas adsorption technique, S_{CO2}.[2, 47] S_{H2O} estimated by the present method are 1 - 3 orders of magnitude greater than S_{CO2}. The magnitude seems to be more substantial with decreasing coal rank. This would be due to the swellable colloidal nature of coals. The lower rank coals are expanded by water to much extent because of their much hydrophilicity. In the expanded coal, the increase in the free volume of coal macromolecules would make the coals to have a large amount of surface.

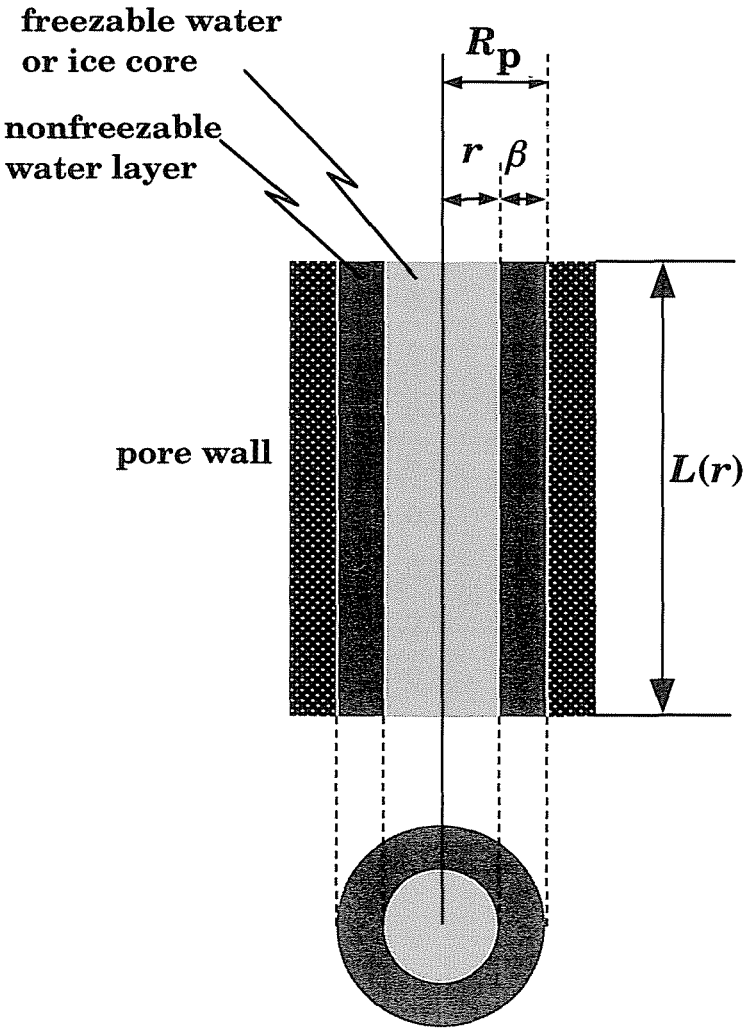

Figure 4.7. Schematic representation of cylindrical shaped pore.

Table 4.6. α, β, R_p(ave), S_{H2O} values, and the reported CO_2 surface areas.

coal	w [g/g of mf coal]	α [nm K]	β(fixed) [nm]	R_p(ave) [nm]	S_{H2O} [m^2/g]	S_{CO2} [m^2/g]
YL	1.46	57	0.6	2.0	633	
YL	0.33	58	0.6	2.0	617	
YL	0.25	45	0.6	1.6	730	
YL	0.13	46	0.6	1.5	711	
YL	0	52	0.6	1.6	664	270[a]
BZ	0.48	58	0.6	1.9	537	
BZ	0	48	0.6	1.7	494	274[b]
IL	0.11	53	0.3	1.7	224	
IL	0	50	0.3	1.5	213	132[b]

[a] ref. 2. [b] ref. 47

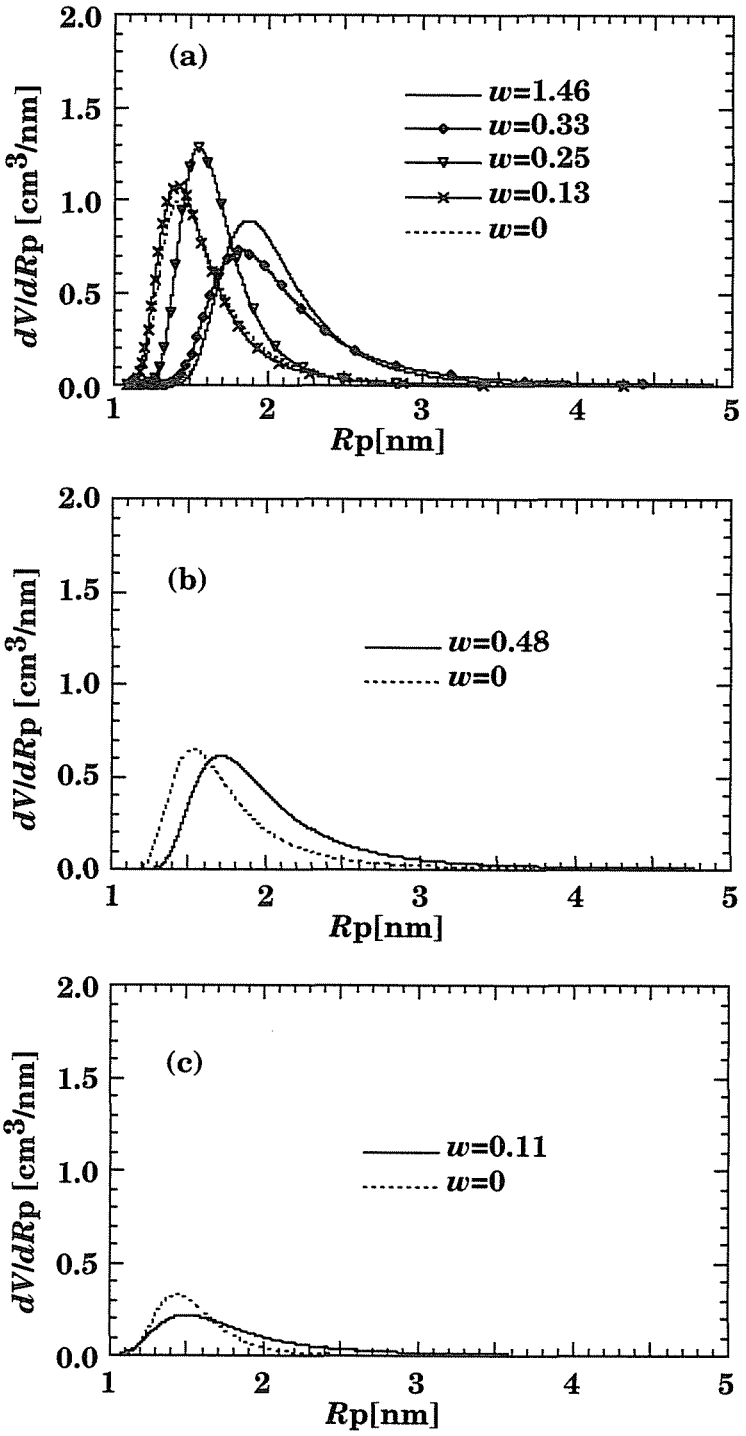

Figure 4.8. Pore size distribution for YL (a), BZ (b), and IL (c) coals.

4.4. CONCLUSIONS

The effect of pre-drying on the pore structure of water-swollen coal was evaluated on the basis of the freezing property of water condensed in pores. Within the limits of the present experimental conditions, the following conclusions can be drawn:

(1) In the course of pre-drying and subsequent swelling in water, the irreversible decrease in V_p and V_f take place when nonfreezable water is removed by the pre-drying. In contrast, V_{nf} is almost independent of the extent of the pre-drying. The reduction of V_p is thus explained by that of V_f.

(2) Gibbs-Thompson equation was used as a theoretical basis for converting FPD into pore size distributions (PSD) with employing a cyrindrical shaped pore model. The change in the PSD of YL coal clearly demonstrates that the irreversible decrease in V_p can be explained by an irreversible shrinkage of pores with radii approximately 2 nm, abundant in the raw coal without pre-drying.

(3) The specific surface area of the water swollen coals, S_{H2O}, are 1 - 3 orders of magnitude greater than that of each dried coal evaluated by CO_2 gas adsorption technique, S_{CO2}. This indicates that drying reduces considerably the internal porosity of coal.

References

(1) Deevi, S. C.; Suuberg, E. M. *Fuel* **1987**, *66*, 454.

(2) Woskoboenko, F.; Stacy, W. O.; Raisbeck, D. *The Science of Victorian Brown Coal*; Durie, R. A., Ed.; Butterworth-Heinemann Ltd.: Oxford, 1991; p152

(3) Evans, D. G. *Fuel* **1973**, *52*, 186.

(4) Gorbaty, M. L. *Fuel* **1978**, *57*, 796.

(5) Suuberg, E. M.; Otake, Y.; Yun, Y.; Deevi, S. C. *Energy Fuels* **1993**, *7*, 384.

(6) Allardice, D. J.; Evans, D. G. *Fuel.* **1971**, *50*, 236.

(7) Thompson, W. L. K. *Philos. Mag.* **1871**, *42*, 448.

(8) Mraw, S. C.; Naas-O'Rourke, D. F. *Science* **1979**, *205*, 901.

(9) Mraw, S. C.; Naas-O'Rourke, D. F. *J. Colloid Interface Sci.* **1982**, *89*, 268.

(10) Lynch, L. J.; Webster, D. S. *Fuel* **1979**, *58*, 429.

(11) Lynch, L. J.; Barton, W. A.; Webster, D. S. *Proceedings of 16th Biennial Low-Rank Fuels Symposium*; Groenewold, G. H., Ed.; Energy and Environmental Research Center: Montana, 1991, p 187.

(12) Barton, W. A.; Lynch, L. J. *Proceedings of 6th Australian Coal Science Conference* Newcastle, 1994, p 65.

(13) Barton, W. A.; Cheng, J. Y. *Proceedings of 7th Australian Coal Science Conference* Gippsland, 1996, p 521.

(14) Norinaga, K.; Kumagai, H.; Hayashi, J. i.; Chiba, T. *Energy Fuels* **1998**, *12*, 574.

(15) Defay, R.; Prigogine, I.; Bellemans, A.; Everett, D. H. *Surface Tension and Adsorption* New York: Wiley 1966.

(16) Jackson, K. A.; Chalmers, B. *J. Appl. Phys.* **1958**, *90*, 5420.

(17) Gibbs, J. W. *Collected Works.* New York: Longmans and Green 1928.

(18) Strange, J. H.; Rahman, M.; Smith, E. G. *Phys. Rev. Lett.* **1993**, *71*, 3589.

(19) Alnami, S. M.; Strange, J. H.; Smith, E. G. *Magn. Reson. Imaging*

1994, *12*, 257.

(20) Overloop, K.; Van Gerven, L. *J. Magn. Reson. Ser. A* **1993**, *101*, 179.

(21) Hansen, E. W.; Schmidt, R.; Stocker, M.; Akporiaye, D. *J. Phys. Chem.* **1995**, *99*, 4148.

(22) Schmidt, R.; Hansen, E. W.; Stocker, M.; Akporiaye, D.; Ellestad, O. H. *J. Am. Chem. Soc.* **1995**, *117*, 4049.

(23) Schmidt, R.; Stocker, M.; Hansen, E. W.; Akporiaye, D.; Ellestad, O. H. *Microporous Mater.* **1995**, *3*, 443.

(24) Akporiaye, D.; Hansen, E. W.; Schmidt, R.; Stocker, M. *J. Phys. Chem.* **1993**, *97*, 7743.

(25) Hansen, E. W.; Schmidt, R.; Stocker, M. *J. Phys. Chem.* **1996**, *100*, 11396.

(26) Ishikiriyama, K.; Todoki, M.; Motomura, K. *J. Colloid Interface Sci.* **1995**, *171*, 92.

(27) Ishikiriyama, K.; Todoki, M. *J. Colloid Interface Sci.* **1995**, *171*, 103.

(28) Rennie, G. K.; Clifford, J. *J. Chem. Soc. Faraday Trans. I* **1977**, *73*, 680.

(29) Vorres, K. S. *User's Handbook for the Argonne Premium Coal Sample Program*; Argonne National Laboratory: Argonne: IL, 1993.

(30) Green, T. K.; Kovac, J.; Larsen, J. W. *Fuel* **1984**, *63*, 935.

(31) Norinaga, K.; Kumagai, H.; Hayashi, J. i.; Chiba, T. *Energy Fuels* **1998**, *12*, 1013.

(32) Yang, X.; Garcia, A. R.; Larsen, J. W.; Silbernagel, B. G. *Energy Fuels* **1992**, *6*, 651.

(33) Jackson, C. L.; McKenna, G. B. *J. Chem. Phys.* **1990**, *93*, 9002.

(34) Skapski, A.; Billups, R.; Rooney, A. *J. Chem. Phys.* **1957**, *26*, 2754.

(35) Ketcham, W. M.; Hobbs, P. V. *Philos. Mag.* **1969**, *19*, 1161.

(36) Hardy, S. C. *Philos. Mag.* **1977**, *35*, 471.

(37) Brun, M.; Lallemand, A.; Quinson, J. F.; Eyraud, C. *Thermochim. Acta* **1977**, *21*, 59.

(38) Deodhar, S.; Lunner, P. in "*Water in Polymer*" ACS Symp. Ser. No. 127 (S.P. Rowland, Ed.) Am. Chem. Soc., Washington, DC, 1980.

(39) Homshow, L. G. *J. Colloid Interface Sci.* **1981**, *84*, 141.

(40) Antoniu, A. A. *J. Phys. Chem.* **1964**, *68*, 2745.

(41) Litvan, G. G. *Can. J. Chem.* **1966**, *44*, 2617.

(42) Drost-Hansen, W. *Ind. Eng. Chem.* **1969**, *61*, 10.

(43) Pearson, R. T.; Derbyshire, W. *J. Colloid Interface Sci.* **1974**, *46*, 232.

(44) Bruggeller, P. *J. Colloid Interface Sci.* **1983**, *94*, 524.

(45) Handa, Y. P.; Zakrzewski, M.; Fairbridge, C. *J. Phys. Chem.* **1992**, *96*, 8594.

(46) Overloop, K.; Van Gerven, L. *J. Magn. Reson. Ser. A* **1993**, *101*, 147.

(47) Larsen, J. W.; Hall, P.; Wernett, P. C. *Energy Fuels* **1995**, *9*, 324.

CHAPTER 5

Evaluation of Drying Induced Changes in the Molecular Mobility of Coal by Means of Pulsed Proton NMR

5.1. INTRODUCTION

During desorption of water from the bed moist state the coals shrink and on readsorption of water they swell.[1-3] The drying induced shrinkage would accompany the collapse of the gellike structure of coal, and thus, it could limit the accessibility of organic solvents[4] and mass transfer into coal matrix in aqueous media.[5] However, there have been few studies that examined the changes in the macromolecular structure of coal that are induced by drying. Moreover, there has been little information available on the relationship between the gel structure and the properties of water within the coal.

Generally, water sorbed in or on solid materials, such as coal, have properties that differ from those of bulk water in its normal thermodynamic states.[6-11] Norinaga et al.[11] classified water sorbed in coals (ranging from brown to bituminous coals) on the basis of its congelation characteristics, which were evaluated by a combination of differential scanning calorimetry (DSC) and proton magnetic resonance (^{1}H NMR) techniques as described in Chapter 3. Two different types of freezable water were observed; free water identical to bulk water and bound water that froze at around 226 K. These two types of water account for only 35-78% of the total water content, leaving nonfreezable water. Bound water has a lower freezing point and congelation enthalpy than bulk water. The differences in the properties of bulk and

bound water would be directly related to the size of a cluster of water molecules, that is, the size of the space in which they are condensed. Since nonfreezable water molecules occur in clusters smaller than the critical size for freezing[12], this water is likely to be dispersed on a molecular scale. It is expected to be condensed in micropores or bound to specific sites via specified interactions such as hydrogen bonds. Hence, changes in the properties of nonfreezable water must be explained not only in terms of macroscopic phenomena, such as porosity,[9, 10] but also molecular interactions between water and coal matrix.[6] The ^{1}H NMR technique may help to determine the nature of these molecular interactions.[13] The measured transverse relaxation can distinguish molecular structures/lattices on the basis of whether the molecular reorientation rates are below or above approximately 10^5 Hz. In the former and latter cases, the molecular structures are termed rigid or mobile, respectively. If the rate is below approximately 10^5 Hz, the molecular structures are deemed rigid, otherwise they are considered mobile. The mobile protons produce exponential decay in the observed free-induction decay curve, while rigid protons undergo a Gaussian decay. In the coal/water system, a portion of the hydrogen in the coal substrate was found to be mobile according to the ^{1}H NMR criteria.[6] This would be attributed to the local mobilization of coal structures that are initially stabilized by polar bonding between hydrophilic sites. This hypothesis is consistent with the observation that the fraction of mobile hydrogen in as-received coals increases as the rank of coal decreases from bituminous to brown.[11] This is because there is a greater abundance of oxygen functional groups (i.e., hydrophilic sites) in lower rank coal than in higher rank coal.

Transverse relaxation measurements have also been adopted to swollen coal in organic solvents.[14-19] Barton et al.[16] reported that when a bituminous coal swells in pyridine-d_5, as much as 50 % of the coal hydrogen is mobile, producing two exponential decays. The relaxation time constants (T_2) for more mobile and less mobile protons are ~400 μs and ~40 μs, respectively. They concluded that the more mobile protons are found in the extractable material. In coals there are methyl groups, aliphatic chains, hydrogen-bonding protons, and other easily mobilized structures present,[18] which are considered possible sources of the less mobile protons. Jurkiewicz et al. [20, 21] studied the

mobility of various types of hydrogen in untreated and pyridine-treated coals by a ^{1}H CRAMPS technique. The aromatic and aliphatic peaks are better resolved by saturation using deuterated pyridine. Pyridine has a great influence not only on the spectral resolution but also on the molecular dynamics of coal. They demonstrated that the dipolar dephasing experiment was useful for characterizing the molecular and macromolecular parts of coal separately. Therefore, the ^{1}H CRAMPS technique has the possibility of selectively evaluating the mobility of the different types of hydrogen in the coal structure swollen in a good solvent like pyridine. In coal-water systems, however, the chemical structure involving the mobile hydrogen has not been examined experimentally.

The goal of the study in this chapter was to evaluate the drying induced change in the macromolecular structure of coal using a pulsed ^{1}H NMR technique, focusing on molecular mobility. For several ranks of coal, the amount of the mobile hydrogen was systematically determined as a function of water content and the distribution of the three types of water. In addition, the chemical nature of mobile hydrogen was established experimentally.

5.2. EXPERIMENTAL SECTION

5.2.1. Coal samples

Three Argonne Premium Coal Sample Program (PCSP) coals (BZ, WY, and IL) and three brown coals (YL, MW, and SB) were studied. These coals with particle sizes finer than 150 μm were stored at 293 K in a gastight vessel filled with nitrogen gas saturated with water vapor for more than 2 weeks prior to use. The water content was determined from the fractional mass release by drying at 380 K under a nitrogen gas flow for 2 h in a thermobalance (TG-2000S, Mac Science Co. Ltd.). Literature values[22] were used for the water content of the PCSP coals. The PCSP coals were analyzed immediately after opening the ampules. For each coal, samples with different water contents were prepared by varying the relative humidity in the closed container from 0 to 97% using concentrated H_2SO_4 and aqueous solutions

saturated with selected inorganic salts.[2] The water content of the partially dried samples was determined in the same manner as described above. Hereafter, the water content will be referred to as w, the molar abundance of water per kilogram of moisture-free coal. From the DSC measurements of YL with different w, YL coal successively releases free, bound and nonfreezable water when dried under the experimental conditions.

5.2.2. ^{1}H NMR

The relaxation measurements were carried out at 298 K using a proton pulsed NMR spectrometer (JEOL Mu-25) operating at 25 MHz. A $90°_x$-τ-$90°_y$ solid-echo pulse sequence[23] was chosen to capture the entire free induction decays (FID). Typical values for the pulse width, pulse spacing, repetition time, and number of scans were 2.0 μs, 8.0 μs, 6 s, and 32, respectively. After measurement, the water content of the specimen was determined in the manner described above. FID after a single 90° pulse was also measured and compared with the solid-echo envelope. Details of the NMR measurement are described in Section 3.2.3.[11]

5.2.3. FT IR

As-received YL coal was dried in a vacuum oven at 333 K for 24 h. The predried YL coal and pulverized KBr were thoroughly mixed at a mass ratio of 1/100 with a mortar and pestle, and the mixture was then pelletized. The apparatus for the IR measurement is shown in Figure 5.1. The pellet was fixed in an IR cell equipped with CaF_2 windows, which was connected to an external vacuum system and dried at 333 K under a pressure of less than 1 Pa until no change in the absorption due to OH stretching (around 3400 cm^{-1}) was detected. After cooling to ambient temperature, the pellet was exposed to D_2O (Aldrich, 99.9 % atom D) vapor at 1.9 - 3.1 kPa for a prescribed time period and dried again in the same manner as described above. Then the spectrum was recorded on a JASCO FTIR-5300 at a resolution of 4 cm^{-1} at ambient temperature.

5.2.4. Deuteration

The apparatus for the deuteration is shown in Figure 5.2. A 0.3 g amount of the predried sample was placed in a glass tube that was connected to a vacuum system. After drying at 333 K for 2 h under a pressure of less than 1 Pa, the sample was exposed to D_2O vapor for a set period of time and dried again, and then ^1H NMR was used to determine the hydrogen content from the initial intensity of the FID. The sample was further exposed to D_2O vapor at 2.4-3.0 kPa for 1 month at ambient temperature, and then ^1H NMR measurements of the D_2O-swollen samples were made. The D_2O content was determined by using the thermobalance in the same manner as described above.

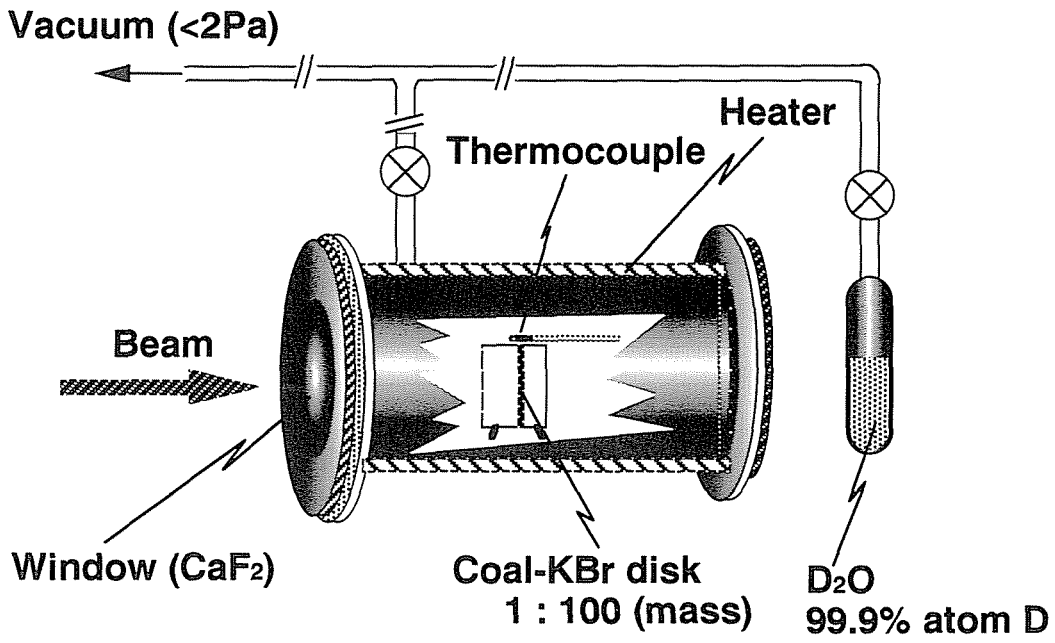

Figure 5.1. In-situ IR cell

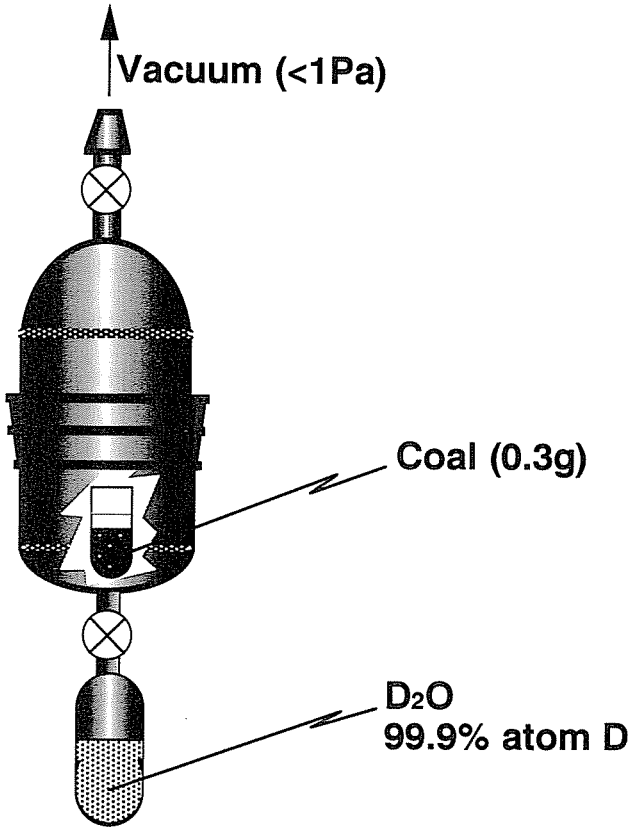

Figure 5.2. Apparatus for deuteration.

5.3. RESULTS AND DISCUSSION

5.3.1. Reliability of the NMR measurements

In this Chapter, the effect of drying on the amount of mobile coal hydrogen is discussed. Since the determination of the mobile hydrogen is based on the parameters obtained by the deconvolution of the ^{1}H NMR transverse relaxation signals, the reliability of the present NMR measurements should be substantiated. Figure 5.3 compares the ^{1}H NMR transverse relaxation signals of as-received samples obtained by two different pulse sequences at 298 K. The solid-echo signals coincide well with the free-induction decays after a single 90 degree pulse for all samples. Thus the solid-echo envelopes are correctly observed even for a mixed solid-liquid systems where the T_2 time constants differ from each other significantly. The advantage of using the solid-echo sequence is that it can avoid the loss of the information from the rapidly decaying free-induction decay (FID) signals encountered due to the dead time, and therefore, the entire transverse relaxation signal can be observed. Lynch et al.[16, 24] pointed out, however, that there is some deviation of the solid-echo signals from a true representation of the transverse relaxation for complex organic solids such as coal. The solid-echo signal component that arises from structures with lesser degrees of molecular mobility is attenuated as a result of multiple proton dipolar interactions, producing irreversible dephasing of the transverse magnetization. If the attenuation effects are significant, the initial amplitude of the slowly decaying components ($I_L(0)/I(0)$) obtained from the solid-echo envelope is larger than that from a 90 degree pulse. Under the present conditions, the difference in $I_L(0)/I(0)$ between the two different pulse sequences is within 3.5% as listed in Table 5.1. The attenuation is thus negligible. Further examination was made on the deconvolution of the relaxation decay into Gaussian and exponential functions. A sequential linear least-squares method was used for the deconvolution, in which a χ^2 value[25] was evaluated. The χ^2 values were defined as

$$\chi^2 \equiv \sum_i^N \left(\frac{y_i - f(x_i)}{\sigma_i} \right)^2 \qquad (5.1)$$

where σ_i and N are the standard deviation of each data point (x_i, y_i) and the total number of data points, respectively. The χ^2 values for three different combinations of fitting functions are listed in Table 5.2. For all cases, the χ^2 values are smallest when one exponential and two Gaussian functions are combined. Thus, the tail of the signal can be represented by a single exponential.

The effect of w on the solid-echo signals for BZ coal are shown in Figure 5.4. The slowly decaying components appear after 50 μs, and the amplitude decreases with decreasing w. On the basis of the data presented in Table 4, the following equations are used to fit the signal

$$I(t) = I_L(t) + I_G(t) \qquad (5.2)$$

$$I_L(t) = I_L(0) \exp [-t/T_{2L}] \qquad (5.3)$$

$$I_G(t) = I_{G1}(0) \exp [-t^2/2T_{2G1}{}^2] + I_{G2}(0) \exp [-t^2/2T_{2G2}{}^2] \qquad (5.4)$$

where $I(t)$ and $I_i(t)$ are the observed intensity at time t and that attributed to component i , respectively. The slowly decaying component was fitted by employing eq 6.3 to determine $I_L(0)$ and T_{2L} and then subtracting $I_L(t)$ from $I(t)$; the rest of the data, i.e., $I(t)$ - $I_L(t)$, was further described by eq 6.4 to obtain $I_{G1}(0)$, $I_{G2}(0)$, T_{2G1}, and T_{2G2}. In Figure 5.5, the observed and fitted $I(t)$ for as-received BZ coal were compared. The statistical errors of the fit and the corresponding time interval for fitting the slowly decaying components are listed in Table 5.3 for BZ coal. The error is generally small, less than 1%. We have examined the effect of the starting time, ranging from 30 μs to 90 μs, on $I_L(0)/I(0)$ and the goodness-of-fit for the as-received coal samples. The end time for the fitting was fixed at 300 μs. The difference in $I_L(0)/I(0)$ is within 1.5% relative to $I_L(0)/I(0)$ when the start time is 50 μs. A start time larger than 50 μs also gave a good fit. The exception is the slowly decaying component of dried coals, where the low signal-to-noise level leads to fluctuations of up to 15%. This is also the case for the other samples, though not shown. I finally

examined the overall accuracy of the results for one as-received and one dried BZ coal by independent measurements for three individual samples under the same experimental conditions. The result is shown in Table 5.4. The errors in the determination of $I_L(0)/I(0)$ and w for as-received BZ coal are only 0.3% and 1%, respectively. These data demonstrate the accuracy level of the results reported in the present work.

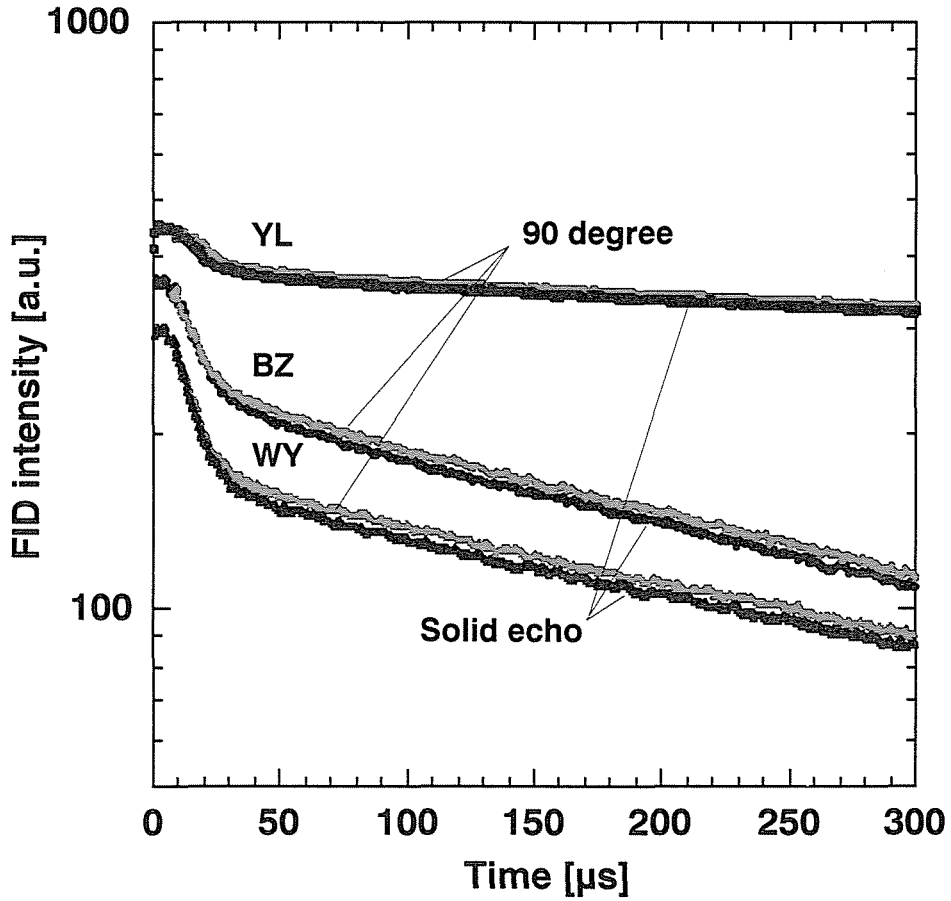

Figure 5.3. Comparison of ^{1}H NMR transverse relaxation signals obtained by different pulse sequences.

Table 5.1. Comparison of the Initial Amplitude and T_2 of the Slowly Decaying Component Obtained by Two Different Pulse Sequences.

coal	90°		solid-echo	
	$I_L(0)/I(0)$[a] [-]	T_{2L}[a] [μs]	$I_L(0)/I(0)$[a] [-]	T_{2L}[a] [μs]
YL	0.863	1870	0.845	1840
SB	0.541	482	0.558	500
BZ	0.640	461	0.636	459
WY	0.570	463	0.551	462
IL	0.240	332	0.232	336

[a] see eq 5.2-5.4

Table 5.2. χ^2 Values for Different Fitting Functions.

	χ^2 [a.u.]		
	YL	BZ	WY
1G[a]+1E[b]	2.11	2.37	2.28
1G+2E	1.10	1.73	1.65
2G+1E	1.09	1.59	1.56

[a] Gaussian, [b] exponential

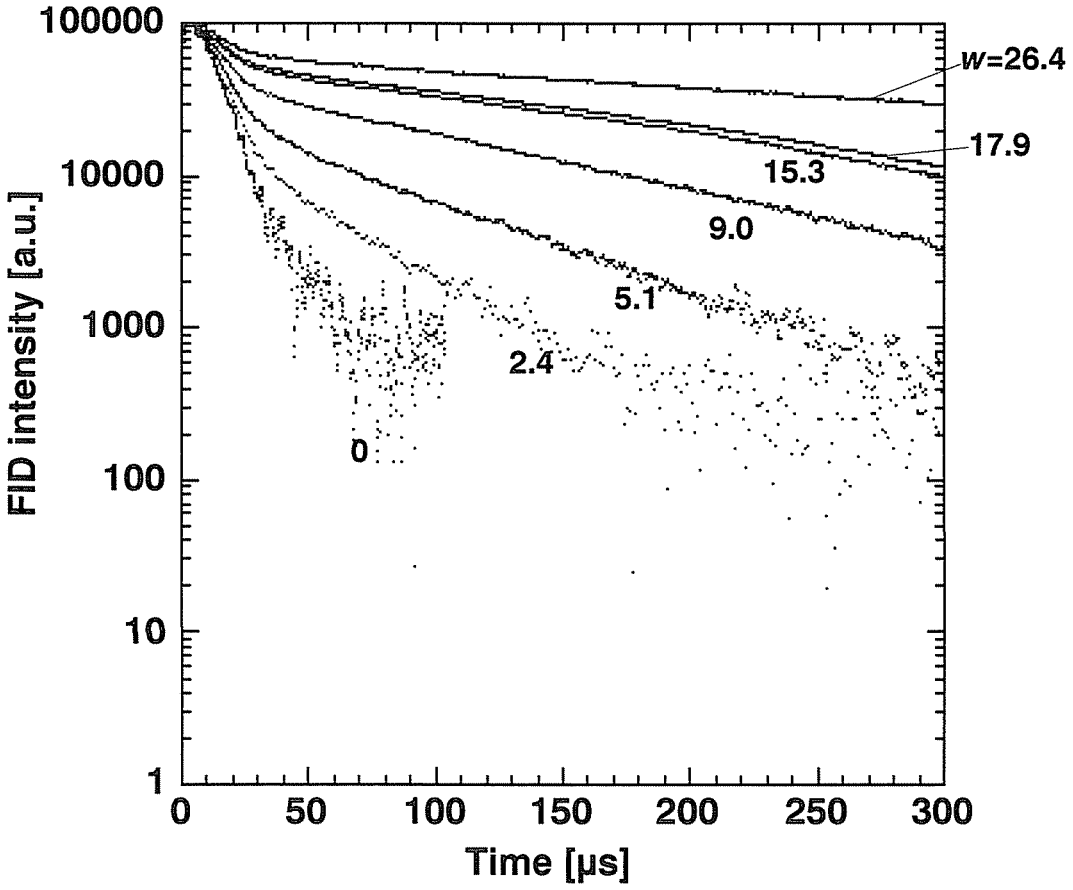

Figure 5.4. Change in ^{1}H NMR transverse relaxation signals with w for BZ.

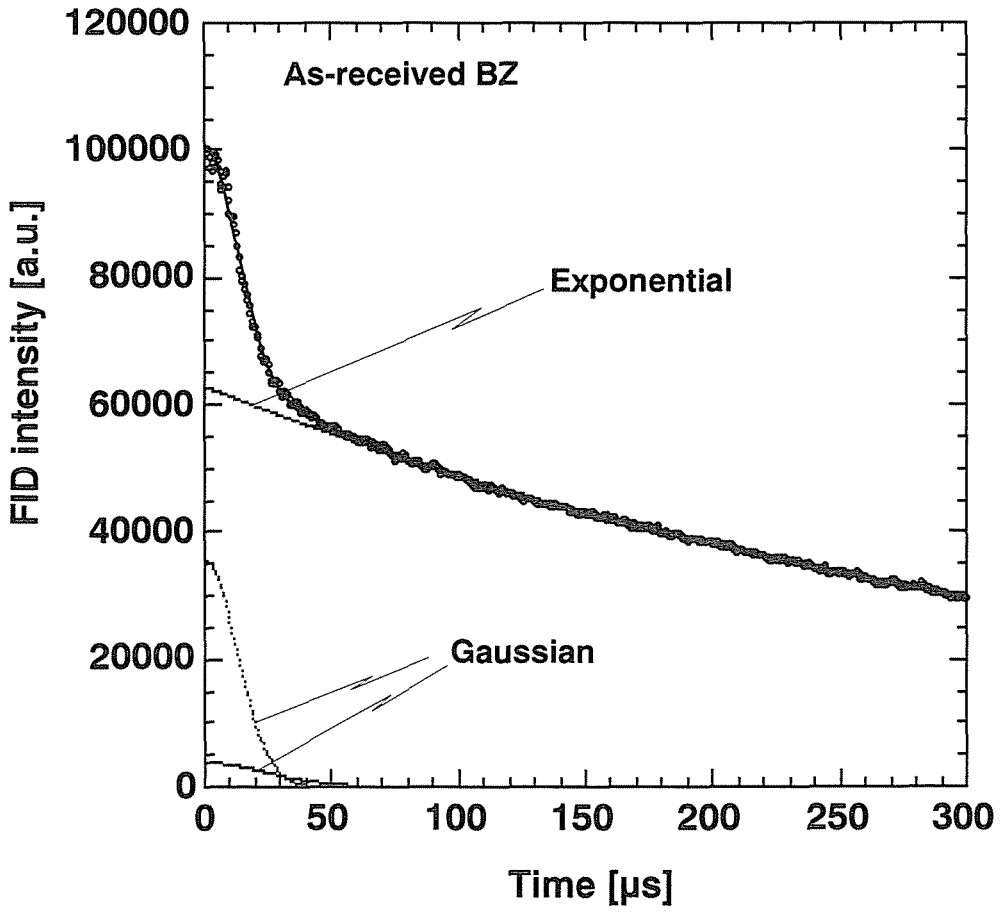

Figure 5.5. ^{1}H NMR transverse relaxation signal of as-received BZ approximated by two Gaussian and a slowly decaying components.

Table 5.3. Error in $I_L(0)$ Value for BZ Samples with Different w.

w [mol/kg-mf coal]	error in determination $I_L(0)$ ±[%]	time interval initial [μs]	end
26.4	0.10	50	300
17.9	0.21	50	300
15.3	0.24	50	300
9.0	0.12	50	300
5.1	0.40	50	300
0	12.3	70	150

Table 5.4. Reproducibility of $I_L(0)/I(0)$ and T_{2L} for BZ.

	$I_L(0)/I(0)$ [-]	T_{2L} [μs]	w [mol/kg-mf coal]
as-received			
Run 1	0.636	459	26.7
Run 2	0.632	464	26.4
Run 3	0.634	453	26.5
Relative error [%]	0.3	1.2	1.0
dried			
Run 1	0.060	42	-
Run 2	0.070	49	-
Run 3	0.052	45	-
Relative error [%]	17	19	-

5.3.2. Proton spin-spin relaxation characteristics

An FID curve for the as-received YL coal is drawn as a function of time in Figure 5.6. Since the attenuation of the Gaussian component[16, 24] is negligible under the present condition, the intensity at 0 μs corresponds to the total amount of hydrogen in the specimen. Assuming that all the hydrogen present as water belongs to the slowly decaying component at 298 K, the temperature used for the measurements, the total amount of hydrogen in this component is larger than that present as water. In other words, a portion of the coal hydrogen is mobile, producing the exponential decays. This result agrees with the findings of Lynch et al.[6] who hypothesized that such mobile hydrogen is located in the part of the coal structure that has been plasticized by water. They examined the change in the amount of the "mobile coal hydrogen" with water content for an Australian coal (82.6 C wt%, daf). The amount increased steadily up to 10 wt% of water content. At least 8% of hydrogen to the total coal hydrogen was found to be destabilized by the interaction with water. The amount of mobile, moisture-free coal hydrogen was defined as C_{MH} Changes in C_{MH} with w are shown in Figure 5.7 for YL (Figure 6.7a) and for BZ and WY coals (Figure 6.7b). For YL coal, C_{MH} is 15 mol of H/kg of moisture-free coal in the as-received state. C_{MH} remains almost unchanged as the value of w drops from 77 to 20 mol and decreases at lower values of w, reaching a level of 3 mol of H/kg at w = 5.1 mol. This result indicates that the release of nonfreezable water leads to the conversion of the slowly decaying component of mobile coal hydrogen into the immobile, Gaussian component. The release of free and bound water plays a negligible role on this conversion. For BZ and coals containing no free water, C_{MH} also decreases with a decrease in the amount of nonfreezable water. The release of 2 mol of nonfreezable water reduces approximately 1 mol of C_{MH} for YL, BZ, and WY coals. In Chapter 2, the effects of drying on the physical structure of coal were examined on a molecular scale for a model molecule using a computer-aided molecular design (CAMD) technique.[26] The conformation of the model molecule was changed from an expanded to a contracted state by decreasing the number of water molecules in the vicinity of the model molecule. This contraction was caused mainly by the formation of intramolecular hydrogen bonds and was due to

the removal of water molecules directly interacting with oxygen moieties in the model molecule. Nakamura et al.[27] reported that the glass transition temperature of a polyhydroxystyrene varied inversely with the amount of sorbed water and postulated that water sorbed in the polymer acts as a hydrogen-bond-breaking agent, thereby plasticizing it. Thus, the reduction of C_{MH}would be a result of the stabilization of intra- and intermolecular hydrogen-bonding interactions induced by the release of nonfreezable water.

Another possible interpretation of our results is as follows: The chemical exchange between the water protons and the labile protons of the coal substrate can be detected through its influence on the spin-spin relaxation seen in hydrated materials such as keratin[28] and silica gel.[29, 30] The labile protons attached to O, N, or S atoms are capable of hydrogen bonding with the nonfreezable water molecules, and these bonds provide the pathway for proton exchange. The removal of the nonfreezable water thus reduces the probability of a chemical exchange and leads to the reduction in C_{MH}. However, at present, it is difficult to quantitatively evaluate the proton exchange rate because of the unknown heterogeneity of the system. Regardless of which of these hypothesized mechanisms in fact occurs, the immobilization of the protons that are attached to O, N, or S atoms (e.g., hydroxylic hydrogen) plays a dominant role in the reduction of C_{MH}.

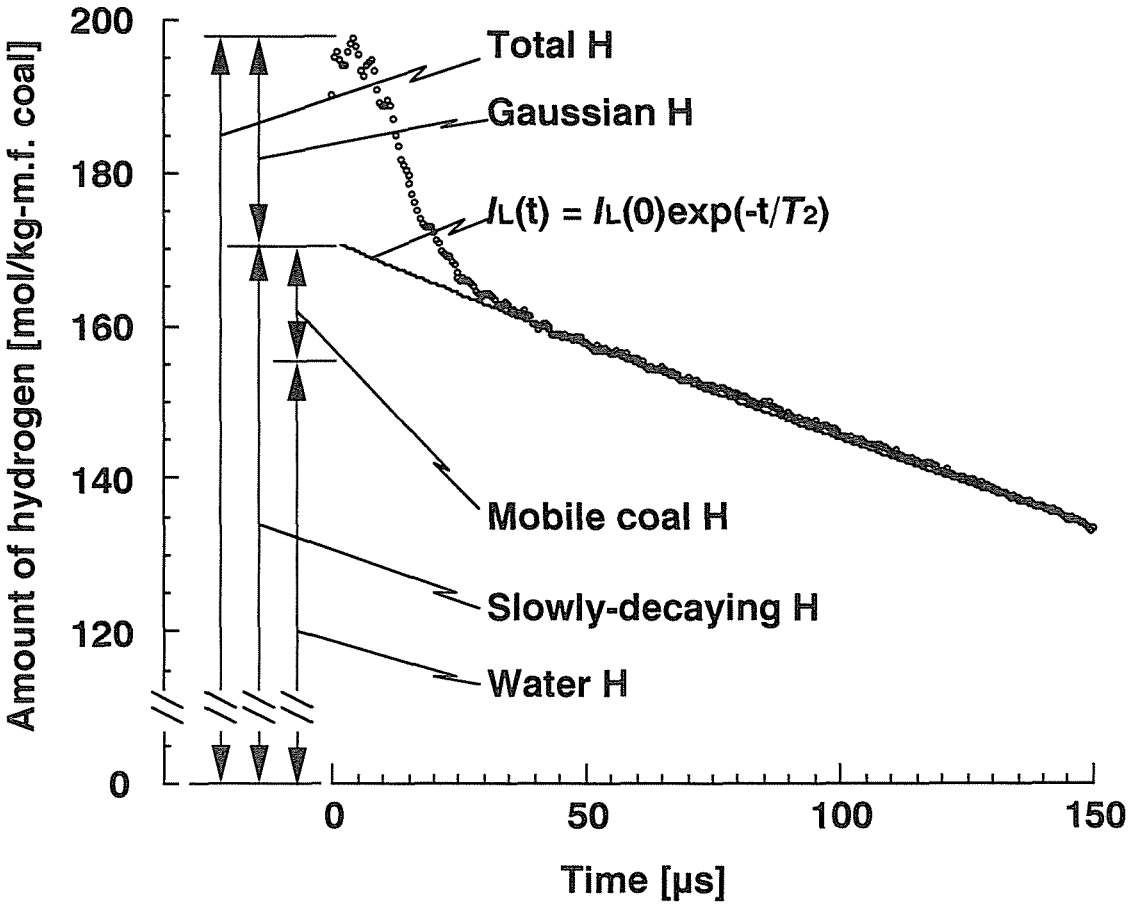

Figure 5.6. ^{1}H NMR transverse relaxation signal of as-received YL at 298 K. The solid line represents the fit of the data points for the slowly decaying components using an exponential function.

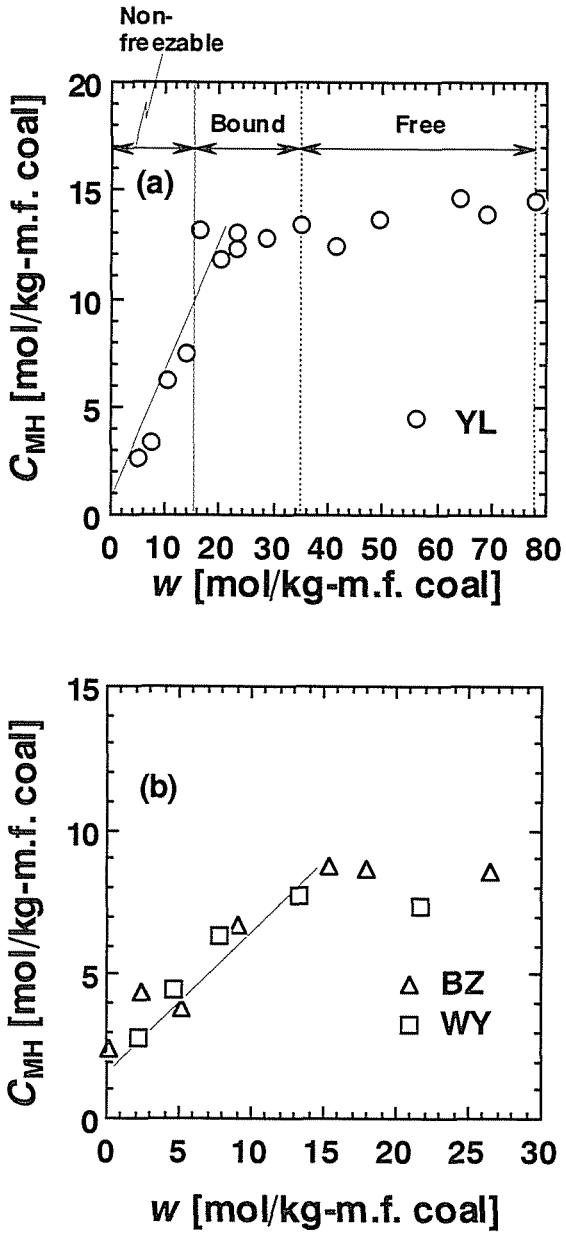

Figure 5.7. Change in C_{MH} for YL, BZ, WY, and IL with water removal.

5.3.3. Nature of mobile coal hydrogen

It is a well-established fact that exposing hydroxyl groups in coal to liquid or gaseous D_2O can deuterate them.[31-34] Figure 5.8 shows the change in the IR spectra of deuterated YL coal. The peak around 2500 cm^{-1} grows with the length of exposure, while the peak due to OH groups around 3400 cm^{-1} diminishes in size. The difference in the wavenumber between the centers of these peaks, approximately 900 cm^{-1}, agrees well with the theoretically predicted shift[35] caused by the deuteration of OH groups. Furthermore, note that there are no remarkable changes in the intensity of the two peaks arising from C-H bond stretching. The hydroxyl groups are completely and exclusively deuterated under these reaction conditions. The extent of deuteration of YL coal is shown in Figure 5.9 as a function of the time period of exposure. The extent of deuteration is determined by the change in the initial intensity of FID. The complete deuteration of YL coal requires an exposure of more than 80 h. Although not shown, the extent of the deuteration also leveled off at 80 h for the other coals. The amounts of hydroxyl groups were also quantified for the present coal samples by employing other methods such as acetylation,[36] solid state ^{13}C NMR,[37] or tritiation by tritium oxide.[34] As displayed in Figure 5.10, the reported values of hydroxyl groups are nearly consistent with the amount of deuterated hydrogen in the individual coal samples prepared by 128 h of deuteration, hereafter referred to as C_{DH}. In Figure 5.11, C_{MH} of the as-received coal is plotted against C_{DH} For SB, BZ, WY, and IL, the value of C_{DH} is in good agreement with that of C_{MH} while C_{MH} is larger than C_{DH} for YL and MW coals. This suggests that hydroxylic hydrogen loses its mobility when the nonfreezable water is removed, as predicted above, and that other types of hydrogen also lose their mobility in YL and MW coals. If this is correct, then C_{MH} should not change for coals other than YL and MW coals when the deuterated coals are swollen in D_2O.

To determine the structural nature of the mobile hydrogen, the deuterated samples were swollen with D_2O vapor and proton transverse relaxation measurements were made. Figure 5.12 shows the amounts of mobile and immobile hydrogen in as-received, dried, deuterated, and then D_2O-vapor swollen samples. The dried samples were prepared under a pressure

of less than 1 Pa, at 333 K, for 12 h. The initial intensities of the FID for the D_2O swollen samples were 1-5%/H larger than those of the individual dry-deuterated samples because of contaminants such as HDO and H_2O in the D_2O used. The hydrogen from these contaminants is observed as a slowly decaying component. To evaluate the net increase in C_{MH} induced by D_2O swelling, the observed amount of increased hydrogen in each case was subtracted from the amount of slowly decaying hydrogen. For YL coal, drying reduces C_{MH} from 15 to 1 mol of H/kg and the subsequent deuteration replaces 8 mol of hydrogen with deuterium, reducing C_{MH} to zero. In the other dried coals, 2-5% of the total hydrogen remains mobile after drying, and this disappears with deuteration. Since the results shown in Figure 5.8 demonstrate that the present deuteration is exclusive for hydroxyl groups and also complete, the hydroxylic hydrogen is selectively labeled by deuterium. Thus, the mobile hydrogen remaining after drying consists entirely of hydroxylic hydrogen, although it is easily expected that the different kinds of coal fragments possess different mobility due to their chemical and physical nature. Water so strongly bonded,[38] hydroxyl groups of the substrate (coal matrix), or both would contribute to the hydrogen remaining mobile even after drying under vacuum. When the deuterated YL coal is swollen in D_2O vapor, C_{MH} increases to 7 mol and no hydroxylic hydrogen is involved. Therefore, the increase is due to the mobilization of other types of hydrogen. Thus, the reduction in C_{MH} for YL coal cannot be interpreted only in terms of the chemical exchange of protons between water and hydroxyls in the coal substrate. Considerable numbers of nonexchangeable protons are also mobilized in the interaction between water and brown coals. For other coals, since non-hydroxylic hydrogen is never mobilized independently of the water content, the C_{MH} remains close to zero, even after swelling.

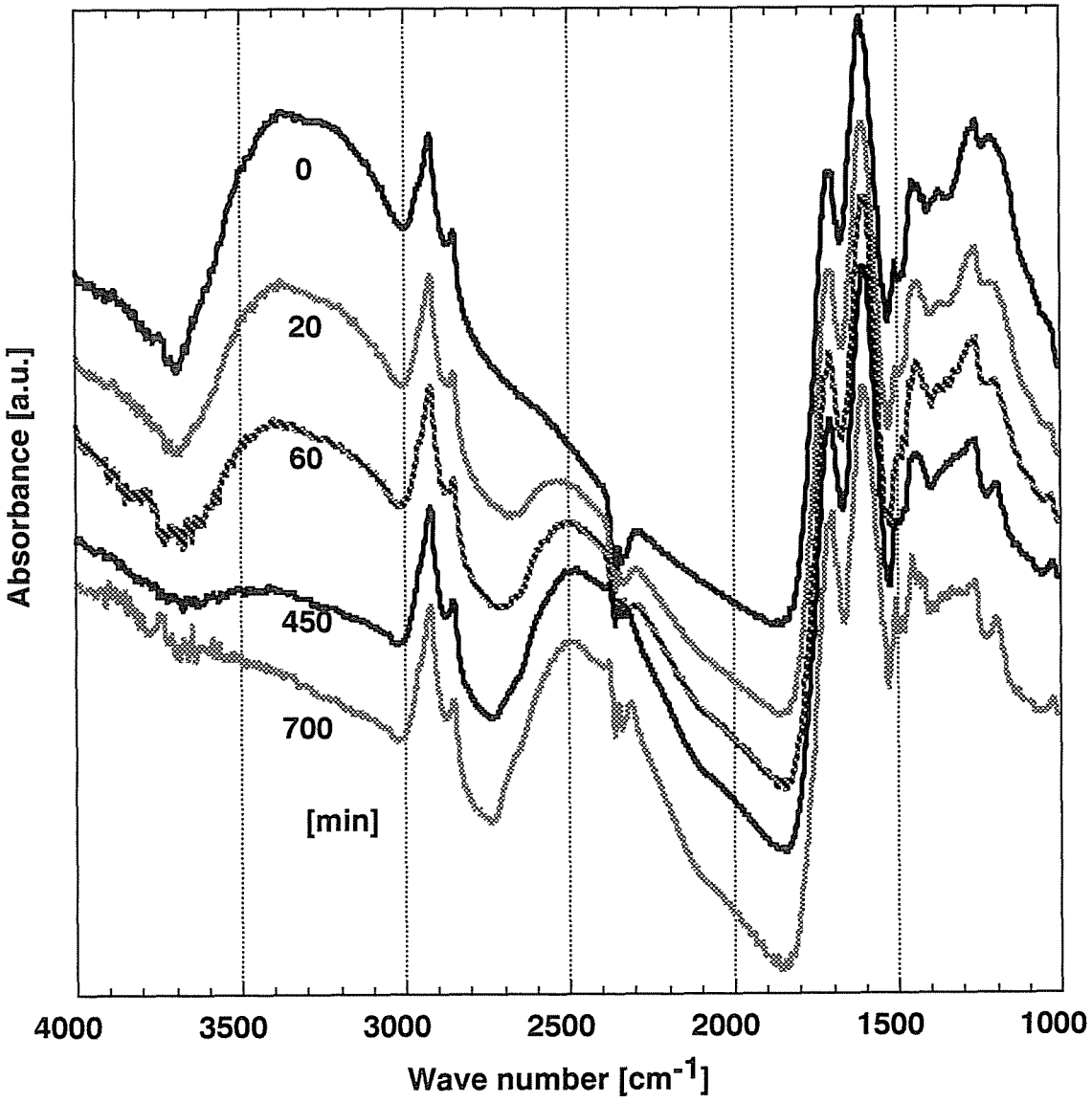

Figure 5.8. Changes in the IR spectra of deuterated YL with time period of exposure to D_2O vapor.

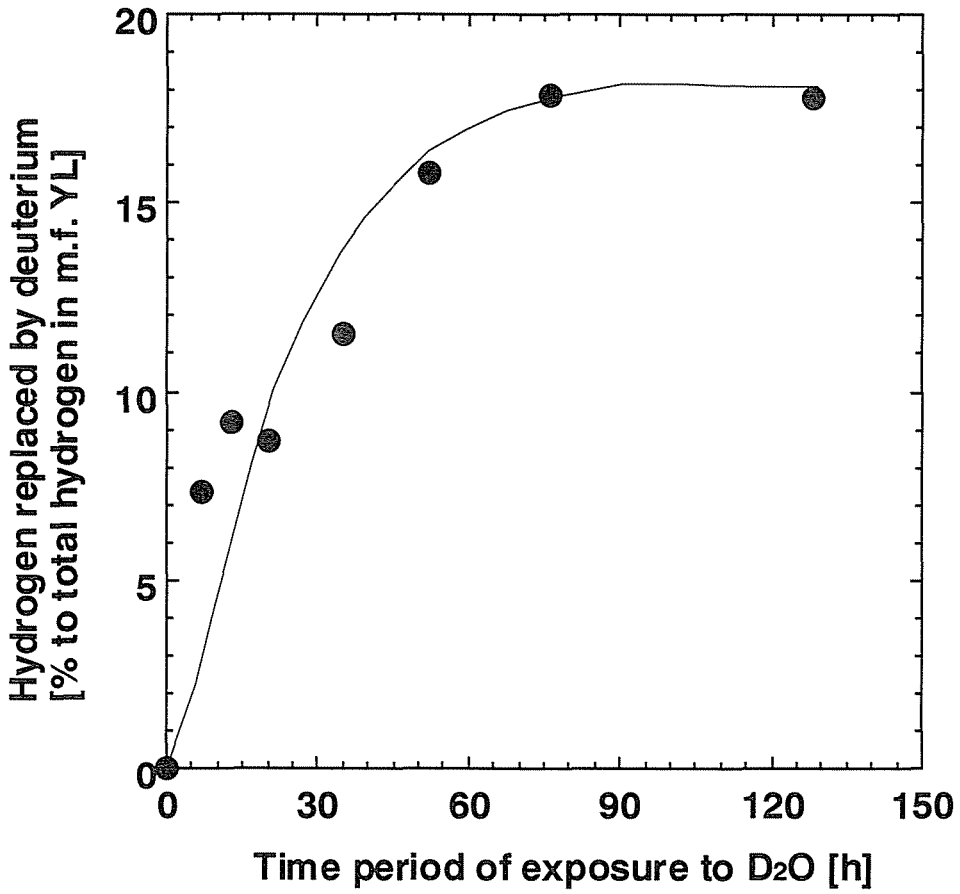

Figure 5.9. Percentage of the total hydrogen replaced by deuterium in mf YL versus time period of exposure to deuteration.

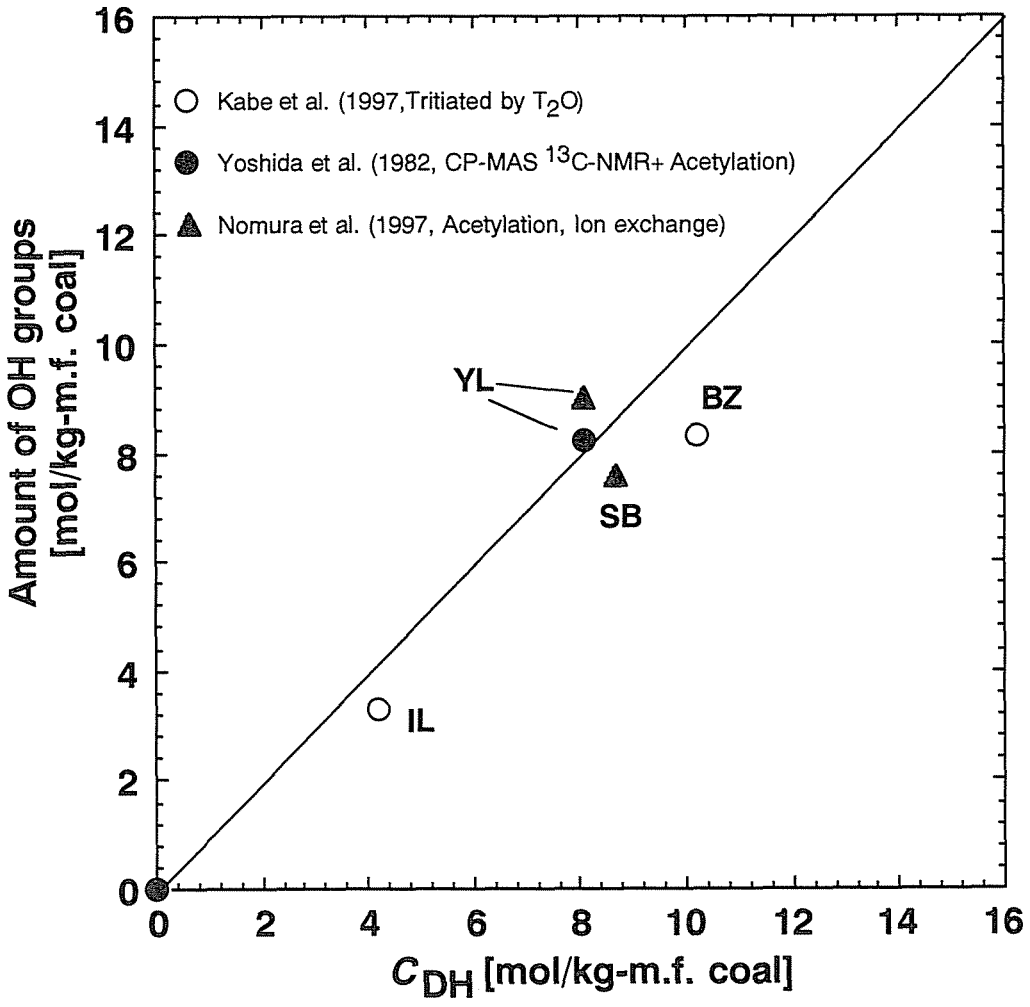

Figure 5.10. Comparison of amount of hydroxyl group with C_{DH}

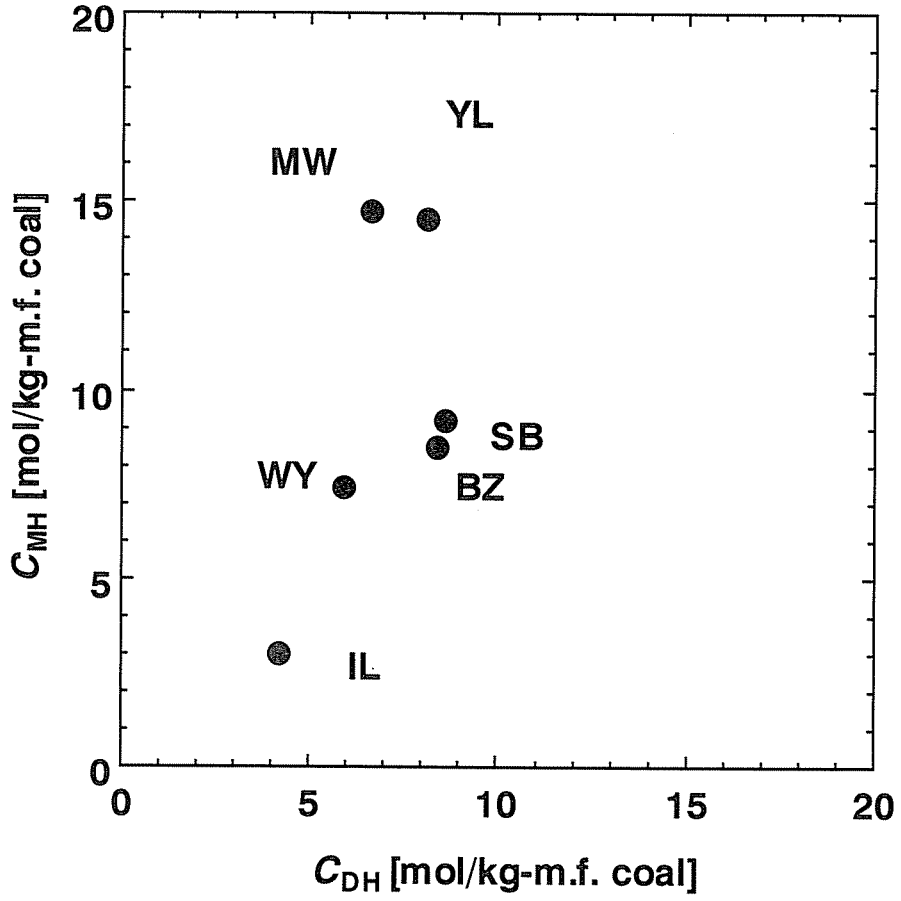

Figure 5.11. Relationship between C_{MH} and C_{DH}

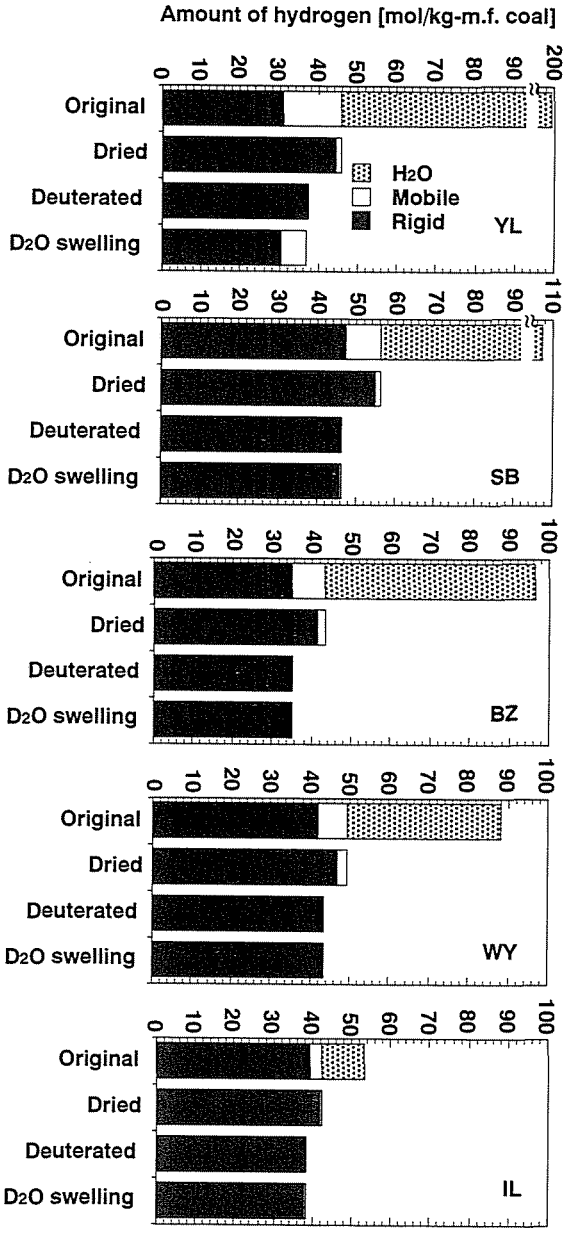

Figure 5.12. Changes in the distribution of hydrogen induced by drying, deuteration, and subsequent swelling in D_2O. Drying is achieved under a pressure of less than 1 Pa at 333 K. The D_2O contents of the swollen samples are 16.2, 19.1, 14.4, and 7.3 mol/kg of dry deuterated coal for YL, BZ, WY, and IL, respectively.

5.4. CONCLUSIONS

The changes in the hydrogen mobility in six different coals induced by drying at 303 K were studied by means of the pulsed ^1H NMR technique. Given the experimental conditions, the following conclusions were made:

(1) A portion of the coal hydrogen appears to be mobile in the NMR sense, and this amount, C_{MH} varies inversely with the amount of nonfreezable water. The release of 2 mol of nonfreezable water reduces C_{MH} by approximately 1 mol for YL, BZ, and WY coals.

(2) For the as-received coals other than YL and MW, the value of C_{MH} agrees closely with the amount of hydroxylic hydrogen, C_{DH}, that is quantitatively replaced with deuterium, while as-received YL and MW coals contain more C_{MH} than C_{DH}.

(3) C_{MH} of deuterated YL coal increases with swelling in D_2O vapor, indicating that a portion of the non-exchangeable hydrogen is also mobilized by water. On the other hand, with the other deuterated coals, C_{MH} remains nearly zero after D_2O swelling. This identifies the mobile hydrogen as hydroxylic.

References

(1) Evans, D. G. *Fuel* **1973**, *52*, 186.

(2) Deevi, S. C.; Suuberg, E. M. *Fuel* **1987**, *66*, 454.

(3) Woskoboenko, F.; Stacy, W. O.; Raisbeck, D. *The Science of Victorian Brown Coal*; Durie, R. A., Ed.; Butterworth-Heinemann, Ltd.: Oxford, 1991; p 152

(4) Suuberg, E. M.; Otake, Y.; Yun, Y.; Deevi, S. C. *Energy Fuels* **1993**, *7*, 384.

(5) Gorbaty, M. L. *Fuel* **1978**, *57*, 796.

(6) Lynch, L. J.; Barton, W. A.; Webster, D. S. *Proceedings of 16th Biennial Low-Rank Fuels Symposium*; Groenewold, G. H., Ed.; Energy and Environmental Research Center: Montana, 1991, p 187.

(7) Lynch, L. J.; Webster, D. S. *Fuel* **1979**, *58*, 429.

(8) Barton, W. A.; Lynch, L. J. *Proceedings of 6th Australian Coal Science Conference,* Newcastle, Australia, 1994; p 65.

(9) Mraw, S. C.; Naas-O'Rourke, D. F. *Science* **1979**, *205*, 901.

(10) Mraw, S. C.; Naas-O'Rourke, D. F. *J. Colloid Interface Sci.* **1982**, *89*, 268.

(11) Norinaga, K.; Kumagai, H.; Hayashi, J. i.; Chiba, T. *Energy Fuels* **1998**, *12*, 574.

(12) Sheng, P.; Cohen, R. W.; Schrieffer, J. R. *J. Phys. C: Solid State Phys.* **1981**, *14*, 565.

(13) Lynch, L. J. *Magnetic Resonance and Biology*; Cohen, J. S., Ed.: John Wiley & Sons, New York, 1983, p 248.

(14) Jurkiewicz, A.; Marzec, A.; Idziak, S. *Fuel* **1981**, *60*, 1167.

(15) Jurkiewicz, A.; Marzec, A.; Pislewski, N. *Fuel* **1982**, *61*, 647.

(16) Barton, W. A.; Lynch, L. J.; Webster, D. S. *Fuel* **1984**, *63*, 1262.

(17) Kamienski, B.; Pruski, M.; Gerstein, B. C.; Given, P. H. *Energy Fuels* **1987**, *1*, 45.

(18) Yang, X.; Larsen, J. W.; Silbernagel, B. G. *Energy Fuels* **1993**, *7*, 439.

(19) Yang, X.; Silbernagel, B. G.; Larsen, J. W. *Energy Fuels* **1994**, *8*, 266.

(20) Jurkiewicz, A.; Bronnimann, C. E.; Maciel, G. E. *Fuel* **1990**, *69*, 804.

(21) Jurkiewicz, A.; Bronnimann, C. E.; Maciel, G. E. High-Resolution ^{1}H NMR studies of Argonne premium coals. In *Magnetic Resonance in Carbonaceous Solids*; Botto, C. E., Sanada, Y., Eds.; Advances in Chemistry Series 229; American Chemical Society: Washington, DC, 1993; p 401.

(22) Vorres, K. S. *User's Handbook for the Argonne Premium Coal Sample Program*; Argonne National Laboratory: Argonne IL, 1993.

(23) Powles, J. G.; Mansfield, P. *Phys. Lett.* **1962**, *2*, 58.

(24) Lynch, L. J.; Webster, D. S.; Barton, W. A. *Adv. Magn. Reson.* **1988**, *12*, 385.

(25) Press, W.; Flannery, B.; Teukolsky, S.; Vetterling, W. *Numrical Recipes* ; Cambridge University Press: New York 1987.

(26) Kumagai, H.; Nakamura, K.; Sasaki, M.; Yoneda, J.; Sanada, Y. *Proceedings of International Conference on Coal Science,* Banff, Canada, 1993; Vol. I, p 136.

(27) Nakamura, K.; Hatakeyama, T.; Hatakeyama, H. *Polymer* **1981**, *22*, 473.

(28) Lynch, L. J.; Marsden, K. H. *J. Colloid Interface Sci.* **1973**, *42*, 209.

(29) Resing, H. A. *J. Phys. Chem.* **1974**, *78*, 1279.

(30) Zimmerman, J. R.; Brittin, W. E. *J. Phys. Chem.* **1957**, *78*, 1328.

(31) Blom, L.; Edelhausen, L.; van Krevelen, D. W. *Fuel* **1959**, *38*, 537.

(32) Yokoyama, S. Doctoral Thesis, Hokkaido University, 1972.

(33) Gethner, J. S. *Fuel* **1982**, *61*, 1273.

(34) Qian, W.; Ishihara, A.; Fujimura, H.; Saito, M.; Godo, M.; Kabe, T. *Energy Fuels* **1997**, *11*, 1288.

(35) Pimentel, G. C.; Mcclellan, A. L. *The Hydrogen Bond*; W. H. Freeman and Company: San Francisco and London, 1960.

(36) Nomura, M.; Muratani, T.; Murata, S.; Maeda, S.; Ohki, A. *Am. Chem. Soc. Div. Fuel Chem. Prepr.* **1997**, 40(1), 168.

(37) Yoshida, T.; Nakata, Y.; Toshida, R.; Ueda, S.; Kanda, N.; Maekawa, Y. *Fuel* **1982**, *61*, 824.

(38) Yang, X.; Garcia, A. R.; Larsen, J. W.; Silbernagel, B. G. *Energy Fuels* **1992**, *6*, 651.

CHAPTER 6

Summary of Findings

As-mined coals hold more or less residual water. In particular, low-rank coals contain a number of oxygen functional groups resulting in material with hydrophilicity, and this is the primary reason for their water content being as much as 30-60 wt% on a wet basis. Such substantial water content necessitates drying prior to use. The present thesis is a summary of series of fundamental studies which have been conducted in an effort to make clear the drying induced changes in the molecular interaction between coal and water. The results are summarized in the following.

In Chapter 2, a computer-aided molecular design technique was utilized to evaluate the change in conformation of a model molecule of brown coal along with a progress of moisture release. The model molecule was constructed based on the data from elemental composition and solid state ^{13}C NMR of a brown coal. It was found that the interaction between model molecule and water molecules became more significant than that between water molecules in lower water content. The nonbonding interaction energy and the excluded volume of the model molecule dropped significantly when the water removal exceeds 80% and it never regained their original values even when again surrounded by the same number of water molecules. The hydrogen bonding interaction contributed more significantly to the conformational stabilization than the electrostatic and van der Waals interactions did.

In Chapter 3, water sorbed in the eight different coals were classified by a combination of DSC and NMR techniques on the basis of congelation

characteristics. Two different types of freezable water, namely, free water and bound water were found in DSC, and these two types were quantified from their experimental heat of congelation. Their fractions account for 35-78% of the total, with the balance defined as nonfreezable water. The congelation of freezable water was also observed in NMR, as the conversion of the slowly decaying components into Gaussian one at 213-273 K. The amounts of the freezable water determined by NMR were in good agreement with those determined by DSC. The nonfreezable water was determined to be mobile in the NMR sense, i.e., with molecular reorientation rates above 10^5 Hz even at 213 K, and it was thus observed independently from the other types of water.

In Chapter 4, the effect of pre-drying on the porous structure of water-swollen coal was evaluated on the basis of the freezing property of water condensed in pores. Coal samples were pre-dried to the different extents at 303 K, and subsequently immersed in excess amount of water. The freezing properties of water condensed in pores of the swollen coals were measured by ^{1}H NMR in the temperature range from 170 to 294 K. The total volume of pores filled with water (V_p) was defined as the amount of water that was not frozen at 260 K. Removal of nonfreezable water from the coal samples by the pre-drying resulted in decrease of V_p while that of the other types of water little changed V_p. The freezing point distribution (FPD) was obtained by the NMR for pore condensed water that froze at 213 - 260 K and also numerically simulated using a Gaussian function. A modified Gibbs-Thompson equation, which relates the freezing point depression to the pore dimension, was applied to the conversion of FPD into pore size distribution (PSD) employing a cyrindrical shaped pore model. PSD was found to be in the range from 1 to 3 nm as pore radius and suggested that the reduction of V_p for a brown coal was mainly owing to the collapse or shrinkage of pores with radii around 2 nm, abundant in the coal without pre-drying. The specific surface area of the water swollen coals were 1 - 3 orders of magnitude greater than that of each dried coal evaluated by CO_2 gas adsorption technique.

In Chapter 5, the changes in the hydrogen mobility in six different coals induced by drying at 303 K were studied by means of the pulsed ^1H NMR technique. A portion of the coal hydrogen appears to be mobile in the NMR sense, and this amount, C_{MH}, varies inversely with the amount of nonfreezable water. The release of 2 mol of nonfreezable water reduces C_{MH} by approximately 1 mol. For the as-received coals other than brown coals, the value of C_{MH}agrees closely with the amount of hydroxylic hydrogen, C_{DH}, that is quantitatively replaced with deuterium, while as-received brown coals contain more C_{MH}than C_{DH}. C_{MH} of deuterated brown coal increases with swelling in D_2O vapor, indicating that a portion of the non-exchangeable hydrogen is also mobilized by water. On the other hand, with the other deuterated coals, C_{MH}remains nearly zero after D_2O swelling. This identifies the mobile hydrogen as hydroxylic.

List of Symbols

α	: constant in eqs (4.7) and (4.8)	[nm K]
β	: thickness of the layer of nonfreezable pore water	[nm]
χ^2	: value determined by eq (5.1)	[-]
C_{DH}	: amount of deuterated hydrogen	[mol/kg mf coal]
C_{MH}	: amount of mobile coal hydrogen	[mol/kg mf coal]
Δ	: width of transition curve	[K^{-1}]
ΔH	: enthalpy of fusion or congelation	[J/g]
ΔT	: freezing point depression	[K]
E_c(b)	: bonding energy	[kcal/mol]
E_c (nb)	: nonbonding energy	[kcal/mol]
E_c (el)	: electrostatic energy	[kcal/mol]
E_c (hb)	: hydrogen bonding energy	[kcal/mol]
E_c (vdW)	: van der Waals energy	[kcal/mol]
f_V	: V_c of swollen coal at $w = 0$ relative to that at raw state	[kcal/mol]
$\gamma_{s,l}$	: surface energy at liquid-solid interface	[N m^{-1}]
H_L	: amount of hydrogen demonstrating exponential decay normalized by amount of hydrogen present as water	[%]
H_w	: height of bed of water-swollen coal	[mm]
H_w^n	: height of coal particle bed per unit mass of coal on a dry basis	[mm/g]
I_T	: transverse magnetization at 40 μs at given temperature, T	[-]
$I(0)$	: initial amplitude of transverse relaxation signal	[-]
$I_L(0)$	: initial amplitude of the slowly decaying components	[-]
$I_G(0)$	: initial amplitude of Gaussian components	[-]
k	: constant value in eq (4.5)	[-]

m	: mass of coal samples	[g]
N	: number of data points	[-]
r	: linear dimension of ice crystal	[nm]
r(ave)	: volume averaged radius of ice core	[nm]
R_p	: pore radius	[nm]
R_p(ave)	: volume averaged radius of actual pore	[nm]
ρ	: density	[g/cm^3]
ρ_c	: coal density measured by water pycnometry	[g/cm^3]
S_{H2O}	: specific surface area determined by eq (4.15)	[m^2/g]
S_{CO2}	: specific surface area determined by CO_2 adsorption	[m^2/g]
σ_i	: standard deviation	[-]
T_0	: normal bulk melting point	[K]
T_c	: phase transition temperature	[K]
T_2	: ^{1}H NMR transverse relaxation time	[μs]
T_{2L}	: ^{1}H NMR transverse relaxation time of slowly decaying components	[μs]
T_{2G}	: ^{1}H NMR transverse relaxation time of Gaussian components	[μs]
τ	: pulse spacing in solid echo sequence	[μs]
V	: volume of water in swollen coal	[cm^3/g]
V_c	: coal volume including volumes of dense and porous parts	[cm^3/g]
V_m	: excluded volume of model molecule	[-]
V_s	: excluded volume of whole system	[-]
V_p	: pore volume	[cm^3/g]
V_f	: volume of freezable pore water	[cm^3/g]
V_{nf}	: volume of nonfreezable pore water	[cm^3/g]
W	: water content of water swollen coal	[g/g mf coal]
w	: water content	[g/g mf coal]
X	: inversed temperature (=1000/T)	[K^{-1}]
X_c	: =1000/T_c	[K^{-1}]

Acknowledgment

I would like to give my special thanks to Professor T. Chiba who supervised this study, for his constant guidance and encouragement. I am also grateful to Associate Professor J.-i. Hayashi for his useful advise and wholehearted encouragement. Dr. H. Kumagai, who introduced me the research theme on "water in coal" and carried out the simulative works, is gratefully acknowledged.

This thesis would not be complete without the appreciable efforts of the examining committee consisting of Prof. T. Chiba, Prof. H. Hattori, Prof. H. Ito, and Associate Prof. J.-i. Hayashi. I sincerely thank the committee for their constructive comments and advises.

I am also very grateful to Drs. T. Yoshida and M. Sasaki of the Hokkaido National Industrial Research Institute for their useful advise on the NMR experiments and allowing me to use their facilities.

A special note of thanks goes to Mr. N. Kudo who carried out portions of experimental works in Chapter. 4, and to Messrs. R. Moriyama, and N. Kashimura for their help on numerical analysis in the Chapter.

I would not forget to thank Dr. M. Satou for all the help he availed to me.

I can not finish without expressing my gratitude to the colleague; Messrs. T. Yamashita, R. Kato, M. Morita, and other members of Prof. Chiba's and Prof. Hattori's Laboratories, for their kindly help and support.

Finally I wish to express my thanks to my parents and sisters for their understanding and thoughtful encouragement.